Energy-efficient Human Activity Recognition for Self-powered Wearable Devices

Author:

Khalifa, Sara

Energy-efficient Human Activity Recognition for Self-powered Wearable Devices

THE UNIVERSITY OF NEW SOUTH WALES

SYDNEY · AUSTRALIA

Dissertation submitted in fulfilment

of the requirements for the degree of

Doctor of Philosophy

in

Computer Science and Engineering

Sara Khalifa

Supervisor: Professor Mahbub Hassan

Co-supervisor: Professor Aruna Seneviratne

November 2015

ORIGINALITY STATEMENT

'I hereby declare that this submission is my own work and to the best of my knowledge it contains no materials previously published or written by another person, or substantial proportions of material which have been accepted for the award of any other degree or diploma at UNSW or any other educational institution, except where due acknowledgement is made in the thesis. Any contribution made to the research by others, with whom I have worked at UNSW or elsewhere, is explicitly acknowledged in the thesis. I also declare that the intellectual content of this thesis is the product of my own work, except to the extent that assistance from others in the project's design and conception or in style, presentation and linguistic expression is acknowledged.'

Signed   …………………………………………….................

Date   ………………………………………….................

ABSTRACT

Advances in energy harvesting hardware have created an opportunity to realise self-powered wearables for continuous and pervasive Human Activity Recognition (HAR). Unfortunately, the power requirements of continuous activity sensing using accelerometer sensors and burdensome on-node classification are relatively high compared to the amount of power that can be practically harvested, which limits the usefulness of energy harvesting.

This thesis makes three fundamental contributions. First, we propose HARKE, Human Activity Recognition from Kinetic Energy, a novel approach to HAR that does not use an accelerometer. Instead, HARKE employs and infers human physical activities directly from the Kinetic Energy Harvesting (KEH) patterns generated from a device that harvests kinetic energy to power the wearable device. We also show the ability of HARKE to detect related details such as the steps taken by the user in a walking activity. By not using an accelerometer, a significant percentage of the limited harvested energy can be saved. Second, we introduce a novel framework that reduces the on-node classification overhead and guarantees energy neutrality. The proposed framework transmits an unmodulated signal, called an activity pulse, and uses only the received signal strength of the activity pulse to classify human activities. Neither accelerometer nor classifier is required on the wearable device, which therefore, guarantees energy neutrality. Finally, we validate the feasibility of using KEH patterns generated from human speech as a potential new source of information for detecting hotwords, such as "OK Google", which are used by voice control applications to differentiate user commands from background conversations. Unlike methods that use existing sensors like microphones or accelerometers, our proposal enables pervasive voice control and HAR at minimum energy cost.

We believe that the findings in this thesis will open the door for a new direction of research and development to realise the vision of pervasive self-powered HAR, moving us closer towards self-powered autonomous wearables.

I dedicate this thesis to
my husband, Moustafa, my beloved children, Faris and Adel,
my parents, my sister, my mother-in-law and my sister-in-law
for their constant support and unconditional love.

I love you all!

ACKNOWLEDGEMENTS

These past several years have not been an easy ride, either academically or personally. I express my gratitude to all the people who have contributed to my life, now and in the past. I appreciate all the people who have directly or indirectly helped me accomplish this work.

In the first place, I express deep gratitude to my supervisor, Professor Mahbub Hassan, for giving me the opportunity to pursue my PhD with him. He has not only helped me accomplish this work in many ways, but truly supported me through many difficulties I had during my PhD period. He always had time for me and promptly responded to my questions and queries. He has also given me fantastic opportunities in my academic career and opened doors to prospects that I never dreamt of. He is really an exceptional advisor and I am greatly indebted to him for the difference he has made to my life.

I also express my sincere appreciation to my co-supervisor, Professor Aruna Seneviratne, for his boundless support. He has been always available to provide guidance, encouragement and valuable feedback. I have been extremely lucky to have such a supportive co-supervisor.

My sincere thanks go to Professor Sajal K. Das (Missouri University of Science and Technology, Missouri, USA) for his great collaboration and constructive suggestions. It was an honour for me to work closely with such a great professor. Special thanks go also to Professor Per Gunningberg, (Uppsala University, Sweden) for valuable discussions contributing to my thesis. I was very lucky to meet him on his sabbatical leave at National ICT Australia (NICTA) while I was writing my thesis.

Truthful thanks go to Rodney Berriman and Tarik Abbasi for helping me build the hardware prototype I used in this thesis. I also thank Guohao Lan for his help with the Bluetooth experiment testbed described in Chapter 5. I highly appreciate

the efforts and the patience of all the volunteers who helped me to collect the data used in this thesis.

My appreciation also goes to Prashanthi Jayawardhane (the coordinator of Mobile System Research Group (MSRG), NICTA) for her help in many administrative aspects, from travel arrangements to research equipment purchases.

My gratitude is extended to my fellow students, Syed Arshad, Ayub Bokani and Eisa Zarepour for their great support in discussing challenges and sharing experiences. I also thank my friend, Nipa Chowdhury, for her encouragement and support at all times. Moreover, I thank all students at the School of Computer Science and Engineering (CSE), University of New South Wales (UNSW) and NICTA who have helped me in numerous ways.

I must acknowledge, with great gratitude, the financial support extended to me by UNSW and NICTA during the course of my PhD work. I must also mention the support and the help given by Alman Yeung (UNSW-NICTA Research Student Administrator) in applying the maternity leave condition to my International Postgraduate Research Scholarship (IPRS). I warmly appreciate the generosity and understanding of my extended family.

Special and unique thanks go to Professor Abdel-Hadi Ahmed (Cairo University), the first person who taught me what mathematics and statistics are. He was always ready to help me and always had encouraging words that were highly reflected positively on me. I am really grateful to him.

None of this would have been possible without the unconditional love and boundless support of my family. My heartfelt gratitude goes to my parents and my sister, Marwa, for all what they have done for me. Good upbringing, education, and unconditional love, these were the greatest gifts they could give me. My appreciation, love and gratitude also go to my mother-in-law and sister-in-law, Mai, for their endless support and encouragement. I am greatly indebted to all of them for what I am today.

Finally and most importantly, I thank my best friend, soul-mate, and husband, Moustafa, and my beloved children, Faris and Adel. They have been a true and great support and have unconditionally loved me. They are the wind beneath my wings; and mere words cannot articulate my gratitude and love to them.

Sara Khalifa

Sydney, Australia

November 2015

Contents

List of Figures

List of Tables

PUBLICATIONS

Journal Papers

1. **S. Khalifa**, M. Hassan, A. Seneviratne, and S. K. Das, Energy harvesting wearables for activity-aware services, IEEE Internet Computing, vol. 19, no. 5, pp. 8 - 16, September/October, 2015. (Impact factor ≈ 2.000)

Conference Papers

1. **S. Khalifa**, M. Hassan, and A. Seneviratne, "Step detection from power generation pattern in energy-harvesting wearable devices", in proceedings of the 8th IEEE International Conference on Internet of Things (iThings 2015), Sydney, Australia, December 11 - 13, 2015.

2. G. Lan, **S. Khalifa**, M. Hassan and W. Hu, "Estimating Calorie Expenditure from Output Voltage of Piezoelectric Energy Harvester - an Experimental Feasibility Study", in proceedings of the 10th EAI International Conference on Body Area Networks (BodyNets 2015), Sydney, Australia, September 28 - 30, 2015.

3. **S. Khalifa**, M. Hassan, and A. Seneviratne, "Pervasive Self-powered Human Activity Recognition without the Accelerometer", in proceedings of the IEEE International Conference on Pervasive Computing and Communications (Percom 2015), St Louis, Missouri, USA, March 23 - 27, 2015. (Acceptance rate ≈ 15%)

4. **S. Khalifa**, M. Hassan, and A. Seneviratne, "Feature Selection for Floor-changing Activity Recognition in Multi-Floor Pedestrian Navigation", in proceedings of the seventh International Conference on Mobile Computing and Ubiquitous Networking (ICMU2014), Singapore, January 6 - 8, 2014.

5. **S. Khalifa**, M. Hassan, and A. Seneviratne, "Adaptive Pedestrian Activity Classification for Indoor Dead Reckoning Systems", in proceedings of the Inter-

national Conference on Indoor Positioning and Indoor Navigation (IPIN2013), Montbeliard-Belfort, France, October 28 - 31, 2013.

6. **S. Khalifa**, "Converting context to indoor position using built-in smartphone sensors". An extended abstract in the PhD forum of PerCom Conference, San Diego, California, March 18 - 22, 2013.

7. **S. Khalifa** and M. Hassan, "Evaluating Mismatch Probability of Activity-based Map Matching in Indoor Positioning", in proceedings of the International Conference on Indoor Positioning and Indoor Navigation (IPIN2012), Sydney, Australia, November 15 - 17, 2012.

Technical Reports

1. **S. Khalifa**, M. Hassan, and A. Seneviratne, "Human Activity Recognition for Indoor Positioning using Smartphone Accelerometer", UNSW-CSE-TR-201303, January 2013, [Online accessed 6-October-2015], URL: ftp:// ftp. cse.unsw.edu.au /pub/doc/papers/UNSW/201303.pdf.

AWARDS

1. Winner of the 2015's CISRA Best Research Paper Prize for the paper titled: "Pervasive Self-powered Human Activity Recognition without the Accelerometer", November 2015. The prize is valued $2000 and a certificate from the dean. This prize was available to all PhD students who are enrolled in a CSE research program. The prize was given at the annual CSE Prizes Reception in April 2016.

2. Winner of the Best Presentation Prize over School of Computer Science and Engineering in the UNSW Engineering Postgraduate Research Symposium (EPRS2015). The prize is valued $500 and a certificate from the Dean. The presentation was titled "Energy Efficient Human Activity Recognition for Wearable Devices". The event included 100 PhD students from all schools of the faculty of Engineering in UNSW, including 11 students from School of Computer Science and Engineering. The presentations were held on 9-10 November and the awards ceremony on 11 November, 2015.

3. Winner of the Best Poster Award under the category of "Signal processing, imaging, and embedded systems" in IEEE technology of the Future (ITOF 2015) competition. The prize is valued $500 and a certificate from the main chair. The poster was titled "Enabling Battery-less Wearables: Tracking Activities from Bodys Kinetic Energy". The competition was open for participants of the Faculty of Engineering from ALL universities in NSW. The poster presentation and the award ceremony were held on the 29th of October, 2015.

4. Engineering Research Excellence Award (EREA), UNSW, from January 2014 to November 2015.

5. Australian Postgraduate Award (APA), from January 2014 to November 2015.

6. NICTA Research Project Award (NRPA), from March 2012 to November 2015.

7. International Postgraduate Research Scholarship (IPRS), UNSW, from February 2012 to January 2014.

Chapter 1

Introduction

Rapid growth in aging population is currently a big challenge for the community and economy of the world. According to the 2015 Revision of World Population Prospects report by the United Nations, the population aged 60 and over comprises 12% of the global population in 2015 and it is the fastest growing with a rate of 3.26% per year [1]. By 2050, the aging population in Australia is projected to increase to 21% (8.4 million people) than 15% of the population (3.5 million people) in 2014 [2]. Similarly by 2030, more than 20% of U.S. residents are expected to be aged 65 and over, compared to 13% in 2010 [3]. This is due to the substantial improvements in life expectancy that have occurred in recent years. Globally, life expectancy at birth has increased from 65 years for men and 69 years for women in 2000-2005 to 68 years for men and 73 years for women in 2010-2015 [1]. Consequently, a higher demand for health services is placed, leading to a significant rise in healthcare costs. For example, in 2014, the U.S. healthcare expenditure has increased by 5.3% to reach $3.0 trillion. Similarly, the overall healthcare expenditure in Australia has significantly increased from $68.7 billion in 2002-03 to $147.4 billion in 2012-13 (1.6 times higher) [4].

One possible path to more affordable and scalable healthcare systems is human activity recognition (HAR). Automatic recognition and analysis of a patient's physical activities through HAR [5, 6] can enable the healthcare authorities to continuously monitor the current status of a patient from a remote location as shown
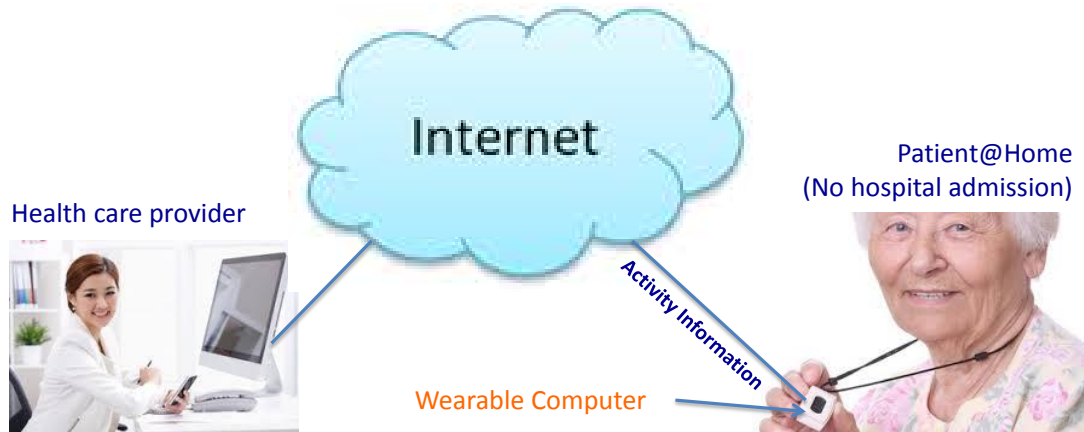
Figure 1.1: An example of remote health care services using wearable devices and HAR.

in Figure 1.1. HAR is expected to play an important role in reducing healthcare costs by reducing the need for hospital admissions.

HAR enables a wide range of activity-aware services in various domains, including fitness management [7], smart living [8], military [9], security, and indoor positioning [10]. For example, a system that can recognise various ambulation activities, such as walking, running, jogging, can help individuals to monitor their fitness level and improve well being. Similarly, a smartphone capable of detecting activities such as climbing a stair, riding a lift, or moving up a ramp, may infer the position of a pedestrian in a complex indoor environment by matching the activities to an indoor map that shows the precise locations of stairs, lifts, and ramps [11]. It is clear that HAR has the potential to improve the user's experience and quality of life.

There are two fundamentally different approaches to HAR, using *infrastructure sensors* [12, 13] and *wearable sensors* [14]. In the former, the sensors are installed at fixed locations to detect human activity when a user visits these locations and interacts with the sensors. For example, cameras installed at fixed locations can help detect user activity whenever the user comes within their vicinity [15, 16]. However, deployment and maintenance of infrastructure sensors are costly. On the other hand, wearable sensors provide an alternative option by placing various types of sensors on the human body. For example, an accelerometer in a wristband can help identify

different activities by simply collecting and analysing the time series acceleration data. Consequently, wearable sensors can help achieving pervasive HAR without the need to deploy infrastructure sensors.

Almost all existing wearable products are powered by batteries. While battery technology has improved over the years, battery-powered devices cannot provide sustained operation. To achieve sustained operation, we either need to instrument the wearables with large batteries or be prepared to manually replenish the batteries when they die. Neither of these options is desirable because large batteries make the wearables heavy and less convenient to wear, while manual replacement is inconvenient and not a practical option for many elderly users, who may have to critically depend on such systems. Due to this, researchers are now investigating energy harvesting solutions to power these wearable sensors [17, 18, 19], which will allow continuous and permanent operation of these sensors without any need for battery recharge or replacement. Energy harvesting or scavenging is a process of converting various forms of ambient energy sources, such as kinetic, thermal, radio frequency, solar or light, into electrical energy, which can then be used to power a small electronic device making it self-powered.

However, there is a caveat. Energy harvesting generally suffers from low power output, which may challenge the power requirement of the wearable sensor's components, such as the accelerometer used for sampling human motion. Given that the sensor will also have to turn on its radio for occasional communications with a nearby sink, the power generated from energy harvesting is clearly too small to simply port the existing accelerometer-based HAR techniques into an energy-harvesting wearable. How to achieve HAR using energy-harvesting wearables is indeed an extremely challenging problem that requires new solutions. A recent survey [20] on HAR using wearables has revealed that although significant research has been carried out for battery-powered wearables, there exists very limited literature on energy-harvesting wearables for HAR. The aim of this thesis is to study the limitations of energy harvesting wearables for HAR and propose new solutions to overcome these limitations and therefore enabling self-powered wearable devices.

The remainder of this chapter is as follows. The motivation behind this research

is explained in Section 1.1. Section 1.2 describes the research issues including a critical examination of energy-harvesting wearables and their limitations in the context of HAR. The research objective of this thesis is stated in Section 1.3, followed by the contributions made towards this objective. Finally, Section 1.4 shows the organisation of the dissertation.

1.1 Research Motivation

Over the past few years, a research trend in Energy Harvesting (EH) has emerged and gained the attention of the research community [21, 22]. EH is commonly defined as the conversion of ambient energy such as vibrations, heat, wind, or light into electrical energy. EH devices can eliminate the need for battery replacement and significantly enhance the versatility of consumer electronics. In fact, considerable advancements have recently been made in EH hardware technology, leading to many off-the-shelf products available at low cost. These developments point to future wearable devices that will be equipped with some sort of EH hardware to ease the dependence on batteries [23].

This means that it is conceptually possible to replace the battery of a wearable sensor with an EH unit to achieve perpetual sensing in many applications including HAR. Of all the ambient energy options, kinetic energy harvesting (KEH) is the most relevant for wearables because it can power the wearable directly from human motion. Advances in KEH hardware have motivated us to consider the concept of self-powered wearables for continuous and pervasive human activity recognition (HAR), where numerous tiny wearable devices sense and monitor the human continuously.

1.2 Research Issues

The most fundamental issue with KEH is the low power output [24]. The power that can be practically harvested from human motion is too small to power all necessary functions of a wearable sensor. A typical wearable sensor will need power
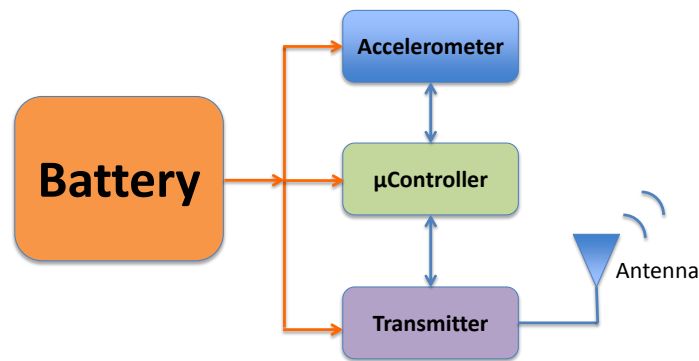
Figure 1.2: A block diagram of a conventional battery-based wearable sensor for HAR.

for accelerometer measurements at a high sampling rate and classification processing in which the classifier detects human activities by analysing the features extracted from the accelerometer data. A radio transmitter is also required for occasional communication with a nearby sink.

1.2.1 Power Requirement of Wearable Devices

Figure 1.2 shows a simplified block diagram of a conventional battery-powered accelerometer-based HAR. In this diagram, a battery is used to power three main components: an accelerometer, a micro-controller, and a radio communication transmitter. The power consumption of a wearable device is mainly due to three functions: accelerometer sampling, activity classification and radio communication. The accelerometer sampling and activity classification functions constitute the power consumption of the HAR process. The radio communication is used to pass the detected activity information to the base station, if the classification function is done onboard the wearable platform. Otherwise, the classification function can be done at the base station or a server outside the wearable, in which case the transmitter needs to transmit the accelerometer data to the base station.

- Accelerometer sampling

  Typically a triaxial accelerometer is used to measure human acceleration in three dimensions. Generally, the more frequent the measurements, the more
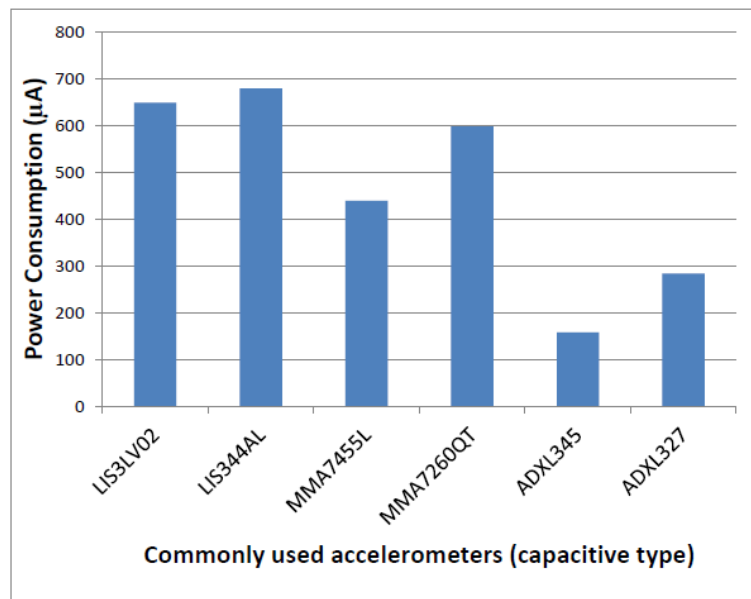
Figure 1.3: The mean power consumption of 6 commonly used accelerometers.

information is available to enable more accurate classification. The frequency of measurement is called the sampling rate of the accelerometer, which is expressed in Hertz or the number of measurements per second. To perform a measurement, an accelerometer must be turned on for a few milliseconds. Since the accelerometer consumes power when it is active, it is turned off when it is not measuring. Therefore, an accelerometer is continuously turned on and off, at a frequency dictated by the sampling rate.

Considering that capacitive accelerometers are the most widely used in wearable and mobile devices, Figure 1.3 compares the power consumption of six commonly used capacitive accelerometers. The values presented in Figure 2.6 have been tested and verified by the authors in [25] using a 3.3 v power supply and a 50 Hz sampling rate. These results confirm that accelerometers consume hundreds of microwatts. Moreover, Figure 1.4 plots the power consumption of three widely used accelerometers: ADXL150 (used in wearable sensors), SMB380 (used in Samsung Galaxy smartphones), LIS302DL (used in IPhone smartphones) as a function of the sampling rate.

We can see that the power consumption increases significantly with rising the sampling frequency; moreover, the average power consumption of the ac-
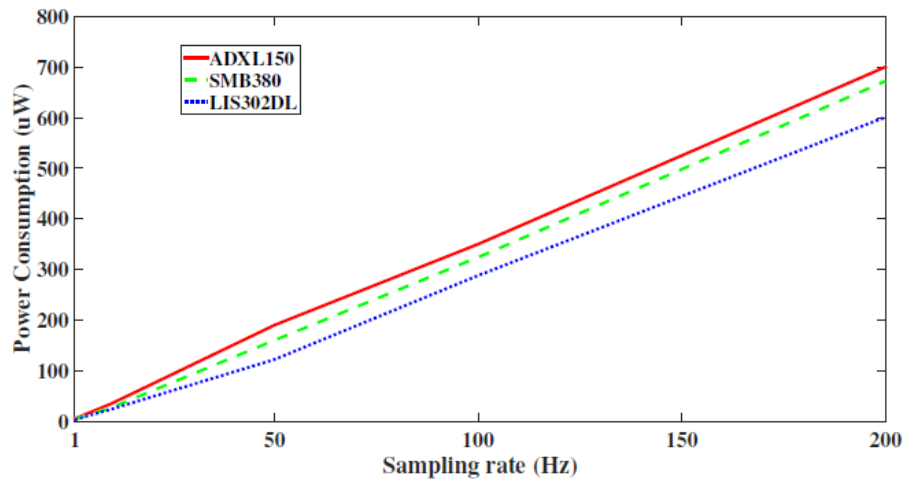
Figure 1.4: Power consumption of popular accelerometers as a function of the sampling rate.

celerometer is nearly a linear function of the sampling rate [26]. For example, the data sheet of an ADXL150 accelerometer [27] shows that the accelerometer consumes about 5 μW on average per Hz, which means that it would require 250 μW if a sampling rate of 50 Hz were required for a given activity set. The required sampling rate depends on the set of monitored activities and typically ranges from 1-50Hz [28, 29, 30, 31]. This means the battery must supply between 5-250 μW to the accelerometer. This is not a major issue for battery-powered wearable devices. However, it is an issue for energy harvesting wearable devices.

- Activity classification

  Typically, a classifier is trained with a number of informative features extracted from a large number of acceleration samples collected during various activities, such as walking, running, or standing. Later, when new acceleration samples are presented to the classifier, it can recognise the activity using the trained model. A detailed measurement study in [32] indicates that the average power consumption of an accelerometer running at 20 Hz is four times as much as the average power consumption for extracting features and executing a classifier. Consequently, the activity classification is responsible for 20% of the total HAR power consumption.
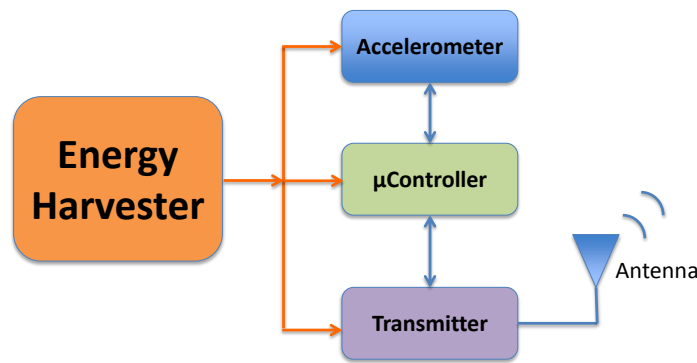
Figure 1.5: A block diagram of energy harvesting wearable sensor for HAR.

1.2.2   Power Generation of Energy Harvesting Devices

Let us now consider the future energy harvesting wearables that could be used in HAR. If we simply port the conventional battery-powered HAR design to the energy harvesting domain, we will end up with the wearable architecture shown in Figure 1.5. The battery is simply replaced by a kinetic energy harvesting unit which converts the kinetic energy generated from human activity into electrical energy. Then the generated electrical energy is used to power the HAR system components. However, we immediately face two major problems.

- We may not be able to supply enough power to the accelerometer for accurate HAR. Accelerometers are usually considered low-power electronics drawing only about a few μW per sample per second (Hz). However, when used in kinetic-powered devices, the accelerometer power requirements is considered relatively high compared to the total kinetic power available, which is also measured in μW. Table 1.1 shows the amount of power that could be generated using a commercial kinetic energy harvester for different activities [33]. It shows that some activities generate only a few μW, which is much lower than what is required to sample the accelerometer at a rate sufficiently high for accurate activity classification. Clearly this will force the sensor to cut down the power to the accelerometer, i.e., use a lower sampling rate and accept lower activity classification accuracy, each time the user switches to one of those activities that produce small amounts of power.

Table 1.1: The average Harvested Power for different activities when the device is attached to the shank.

Activity	Average Harvested Power (μW)
Walking	10.30
Running	28.74
Cycling	0.36
Sitting	0.02
Lying	0.36

- Even if the harvested power is enough to operate the accelerometer at the required sampling rate, it reduces the amount that could be accumulated in the capacitor for future radio communications. Insufficient stored energy in the capacitor will force more aggressive duty cycling of the radio or more drastic reduction in transmission power. In summary, when the power supply is limited by energy harvesting, powering the accelerometer trades off the quality of radio communication.

In fact, using energy harvesting to provide a self-powered HAR is a very challenging problem that requires innovative sensing and communication solutions.

1.3 Research Contributions

This dissertation aims to provide a new paradigm for HAR that overcomes the power limitations of energy harvesting, towards self-powered autonomous wearabales. The main contributions towards our objective are summarised in this section.

1.3.1 HARKE: Human Activity Recognition from Kinetic Energy

We propose HARKE, a novel approach for realising HAR in a kinetic-powered device. Our approach employs kinetic energy harvesting and infers human activity directly from the kinetic energy harvesting (KEH) patterns without using an accelerometer. The proposed use of KEH patterns to classify human activities is based on the

observation that different activities produce kinetic energy in different ways leaving their signatures in the harvested power signal. Since no accelerometer is used in the HARKE architecture, a significant amount of the harvested power can be saved.

We use both mathematical modelling and a real hardware prototype to examine the generated patterns of a kinetic energy harvester. Our examinations show that the generated KEH signal switches to clearly distinguishable patterns as the user changes activities. By applying information theoretic measures on the estimated KEH data, we confirmed that KEH patterns contain rich information for discriminating many typical activities of daily life. Using extensive data collected from ten different subjects, for five common daily activities, we demonstrate the effectiveness of KEH patterns as a new source of information for HAR. We further analyse the energy savings of HARKE due to the removal of the accelerometer and we show that HARKE saves up to 72% of HAR power consumption in a kinetic-powered wearable, given that 80% of HAR power consumption is due to the accelerometer.

The details of this contribution are presented in Chapter 3 and Chapter 4. Chapter 3 introduces the novel concept of HARKE and uses a mathematical model to evaluate the performance of HARKE. Chapter 4 presents the ultimate validation of HARKE using a commercially available piezoelectric KEH transducer.

1.3.2   Energy Neutral Self-powered Wireless HARKE

Although HARKE provides an important step forward for realising self-powered HAR by eliminating the accelerometer's power consumption, it still cannot guarantee system energy-neutrality. Activity classification using KEH patterns would still consume significant power in the device or, if the classification is done in the server, then energy consumption due to communication of a massive amount of KEH voltage data would challenge energy-neutrality. In Chapter 5 we propose a new framework based on Bayesian Decision Theory that guarantees energy neutrality for HARKE. The proposed Bayesian framework utilizes a capacitor to store the incoming energy harvested for a fixed-length time window and then uses all the stored energy to transmit an unmodulated signal, called an *activity pulse*.

Since different activities generate power at different rates, the transmission and receiving signal strengths also differ among different activities. Thus those signal strengths can be used to classify the activities. Energy neutrality is guaranteed because the transmission power of the activity pulse only uses the amount of energy harnessed in the last time window, and no additional energy is required to power any sensing or classification components in the wearable device. Using a real dataset collected from a kinetic energy harvester coupled with a Bluetooth prototype, an overall accuracy of 91% is achieved when the distance between the transmitter and the receiver is set to 30 cm. We also point out that the overall accuracy falls to 85% and 65% when the distance is increased to 60 cm and 100 cm, respectively.

1.3.3 Step Detection from Piezoelectric Energy Harvesting Patterns

Step detection is increasingly being used in health and fitness monitoring and indoor positioning applications. In Chapter 6 we show that the generated patterns of a Piezoelectric Energy Harvesting (PEH) transducer are not only informative for recognising a user's activity (e.g. walking) but can also identify each step the user has taken. To validate the concept of PEH-based step detection, we collected the generated patterns of a PEH wearable device from four subjects under different walking scenarios, including walking along straight and turning paths as well as descending and ascending stairs, covering a total of 570 steps. We found that, like acceleration, the generated PEH traces also exhibit distinctive peaks for steps, which can be detected accurately using widely used peak detection algorithms. We demonstrated that widely used peak detection algorithms can detect steps from PEH power generation patterns with an accuracy of 96%.

1.3.4 Hotword Detection from Vibration Energy Harvesting Patterns

Finally, we apply the novel concept of HARKE in a slightly different application. Here, we conduct the first experimental study to validate the feasibility of using the Vibration Energy Harvesting (VEH) patterns generated from human speech as a potential new source of information for detecting hotwords, such as "OK Google", which are used by voice control applications to differentiate user commands from background conversations. Pervasive hotword detection requires continuous sensing of audio signals, which results in significant energy consumption when a microphone is used as an audio sensor. How to reduce audio sensing energy costs using other low-power sensors that can also register voice signals is a recent research trend. For example, researchers have shown that, instead of microphones, gyroscopes [34] or even accelerometers [35] can be used to detect hotwords at a fraction of the energy consumption. Unlike gyroscopes and accelerometers, our proposal enables pervasive voice control at minimum energy cost.

This contribution is demonstrated in Chapter 7. Using piezoelectric energy harvesting circuits, we conduct a comprehensive experimental study involving 8 subjects. Our experiments involve the analysis of two possible usage scenarios, indirect and direct. In the first, the VEH is only expected to pick up the *ambient* vibrations caused by user speech in the vicinity of the device. In the second, the user talks directly to the surface of the piezoelectric beam. For both usage scenarios, we evaluate two types of hotword detection, speaker-independent, which does not require speaker-specific training, and speaker-dependent, which relies on speaker-specific training. Our analysis illustrates that hotwords can be detected from the power generation patterns of VEH circuits with up to 85% accuracy, which is comparable to accelerometer-based hotword detection.

1.4 Thesis Organisation

The rest of the thesis is organised as follows.

Chapter 2 reviews the related work of accelerometer-based HAR and presents recent advancements in energy harvesting hardware.

Chapter 3 introduces HARKE as a novel architecture of *Human Activity Recognition from Kinetic Energy.*

Chapter 4 provides the experimental validation of HARKE using a commercially available piezoelectric energy harvesting transducer.

Chapter 5 proposes a new framework based on Bayesian Decision Theory that guarantees the energy neutrality of HARKE.

Chapter 6 presents the first experimental study to validate the concept of step detection from the generated patterns of PEH wearable devices.

Chapter 7 investigates vibration energy harvesting as a potential new source of information for detecting hotwords, such as "OK Google", which are used by voice control applications to differentiate user commands from background conversations.

Chapter 8 concludes the thesis by summarising the main outcomes and also discuss possible future directions of this research.

Chapter 2

Related Work

Human activity recognition (HAR) has been an area of significant research in the literature over the past decade [36]. Figure 2.1 shows the number of scientific papers per year given by searching for "Human activity recognition" on Google Scholar. These results confirm that HAR has attracted a large section of the research community with approximately 5690 citations between 2005 and 2014. Figure 2.2 shows the basic process of HAR, which aims at recognising human activities by sensing (measuring) and understanding the natural phenomena of human activity through context modeling and reasoning [37, 38]. Existing HAR systems can be broadly classified into two different approaches, as shown in Figure 2.3, using infrastructure sensors and wearable sensors. In the former, sensors that can detect motion, pressure, temperature, and so on, are installed at specific locations and in furniture to detect activity when a user visits these locations and interacts with the sensors [12, 13]. For example, a pressure sensor installed beneath a sofa could detect sitting activity from the pressure change whenever a user sits there. Cameras installed at fixed locations can help detect user activities whenever a user comes within their vicinity. However, deployment and maintenance of infrastructure sensors are costly.

Wearable sensors, on the other hand, provide an alternative option [39, 14]. By placing various types of sensors on the human body, accurate and pervasive HAR can be achieved without the need for deploying significant infrastructure. For example, an accelerometer in a wristband can help detect different activities by
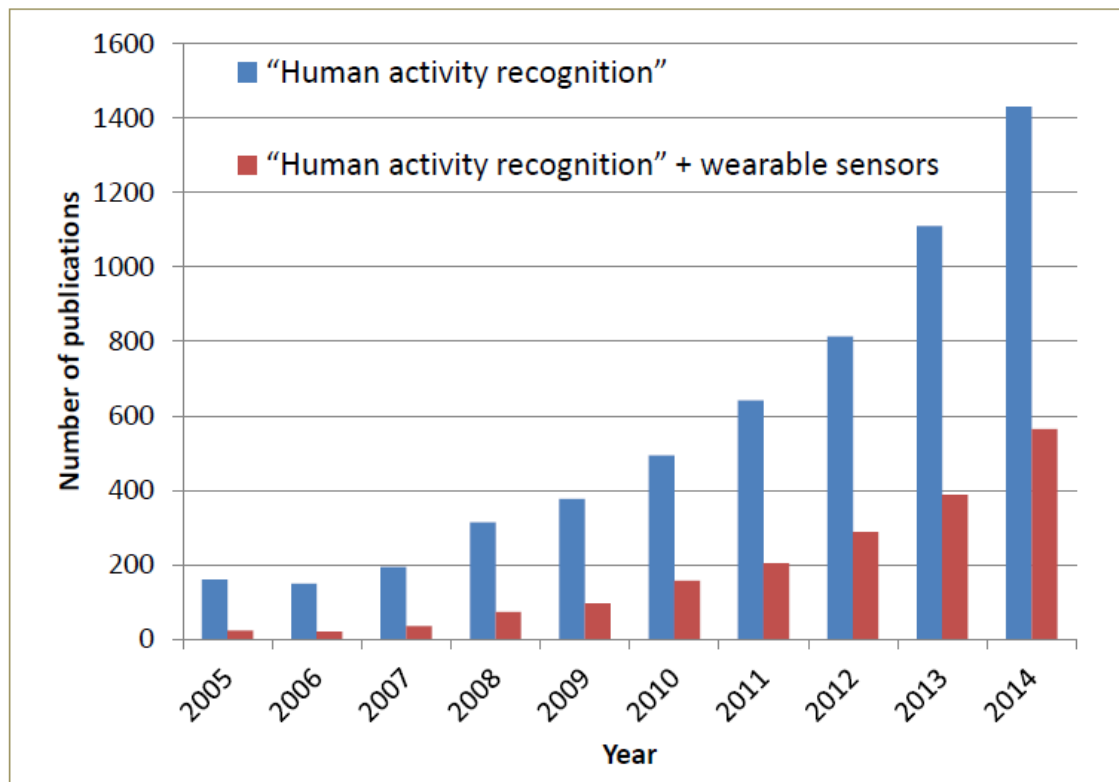
Figure 2.1: Number of scientific papers per year according to Google Scholar as of November 12, 2015.

simply collecting and analysing time series acceleration data. Because wearables can continuously monitor user activities at all times and locations, they provide a more pervasive HAR solution compared to the infrastructure-based approach that requires the user to be within the sensing range for effective activity recognition.

Consequently, wearable sensor-based HAR has recently become the focus of intense research and development [20], producing a wealth of tools and algorithms to accurately detect human activities from data collected by wearables. Figure 2.1 confirms the attraction of wearable sensor-based HAR in the research community. By adding the term "wearable sensors", we can see that between 30% and 40% of the scientific papers published in the last four years refer to wearable sensors instead of infrastructure sensors. In fact, deployments of such systems have already begun, such as Fitbit, iWatch, and Google Glass. It is predicted that the market for wearable health and fitness monitoring will grow to $70 billion by 2025 [40].

Almost all existing wearable products are powered by batteries. While battery
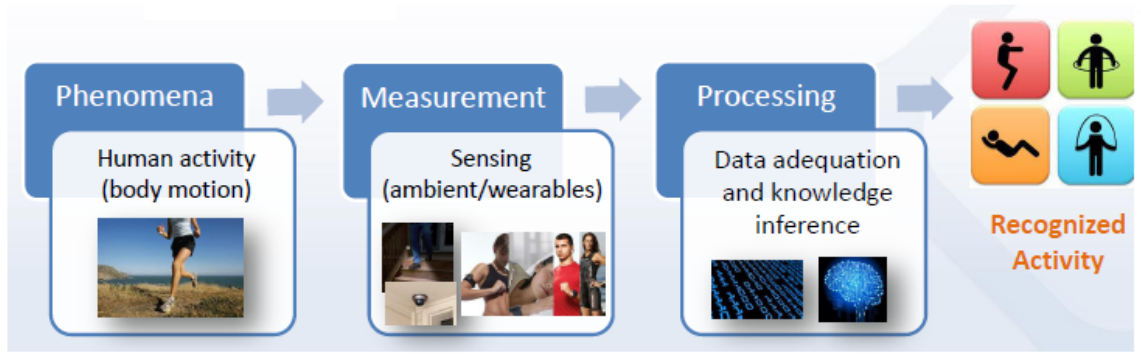
Figure 2.2: The basic process of human activity recognition (HAR).

technology has improved over the years, battery powered devices cannot provide sustained operation. To achieve sustained operation, we either need to instrument wearables with large batteries or be prepared to manually replenish batteries when they die. Neither of these options is desirable because large batteries make wearables heavy and less convenient to wear, while manual replacement is not practical for many elderly users, who may be critically dependent on such systems. Due to this, researchers are now investigating energy harvesting solutions [17, 18, 19], which will allow continuous and permanent operation of these wearables with no need for battery recharge or replacement.

In this chapter, we first review some of the studies related to wearable sensor-based HAR in Section 2.1. We then focus on the studies concerned with providing energy efficient HAR to extend the battery life of wearables in Section 2.2. A brief overview of kinetic energy harvesting, including the technological advancements in hardware, is presented in Section 2.3. Finally, we discuss the opportunities and challenges of using KEH to provide self-powered HAR in Section 2.4.

2.1 Wearable Sensor-based HAR

Typically, wearable sensor-based HAR relies on accelerometers to frequently sample human motion. Typically a triaxial accelerometer is used to measure the acceleration of a subject in three dimensions while performing different activities. Informative features are then extracted from the acceleration data and used to train a classifier,
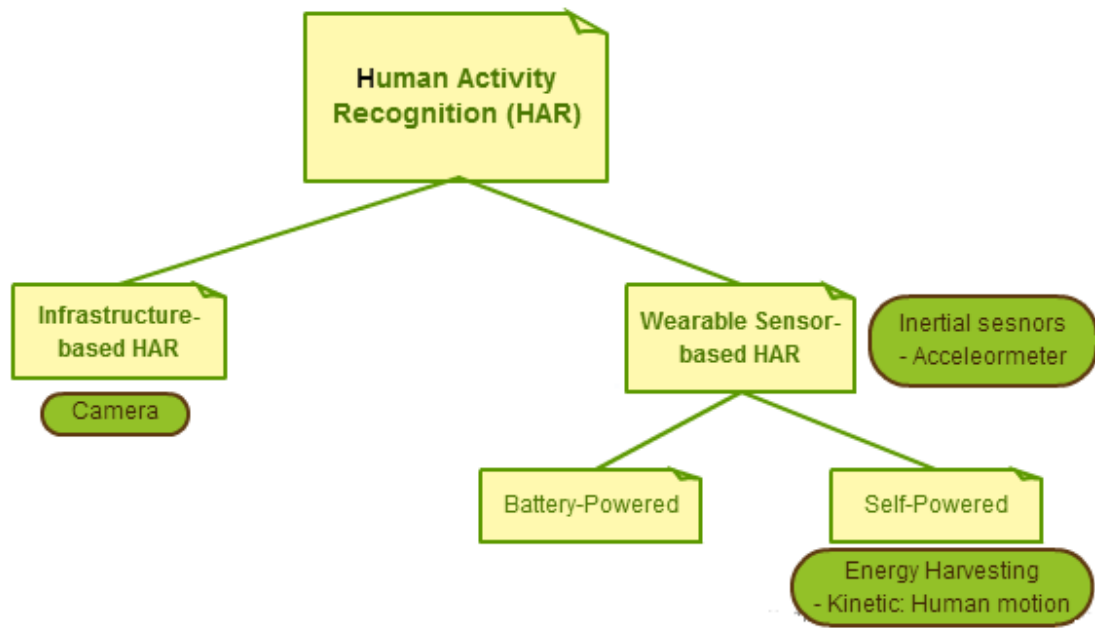
Figure 2.3: The existing approaches of human activity recognition (HAR).

which is used later to detect activities from a given sample of acceleration values. Therefore, the available approaches for accelerometer-based HAR share 3 basic components, accelerometer data collection, feature extraction, and classification. In the data collection phase, most published studies rely on attaching multiple accelerometer sensors to different places on the human body [26, 41, 42, 43]. However, the popularity of smartphones in the past few years has shifted the research attention to use these devices for HAR [44, 45, 46, 47]. Table 2.1 summarises some of the studies related to performing HAR using either wearable sensors or smartphones, in terms of the position of the device on the user's body, the number and description of the features, and the classifier(s) used.

Table 2.1 does not provide a simple comparison between the different studies, since each research paper was applied on different datasets and considered different activities. It might be more difficult to distinguish two similar activities than distinguishing a large number of dissimilar activities. However, this table presents an overall view of the basic framework used in the related studies. We note from Table 2.1 that, although the number of the basic features used seems small (on average 6), the exact number of features to be fed to the classifier is very large (up to 75)

Table 2.1: Summary of some prior works on accelerometer-based HAR.

Device		Ref.	Position of the device	Features No.	Features	Classifiers
Wearable Sensors		[41]	Five 2-axis accelerometers (different places)	75	Mean, FFT Energy, Frequency Domain Entropy, Correlation	DTL, KNN , DT , NB
		[26]	One 3-axis accelerometer(near the pelvic region)	12	Mean, Standard Deviation, FFT Energy, Correlation	DTL, DT, KNN, SVM, NB
		[42]	One 2-axis accelerometer (waist)	10	Mean, Standard Deviation, Skewness, Kurtosis, Eccentricity	MLP
		[43]	Five 3-axis accelerometer (different places)	30	Mean, Variance, Skewness, Kurtosis, Autocorrelation, The Peaks of the DFT	BDM, RBL,LSM , KNN, DTW, ANN, SVM
Smartphone		[44]	In the pocket of the front pants leg	43	Average, Standard Deviation, Average Absolute Difference, Average Resultant Acceleration, Time Between Peaks, Binned Distribution	DT, LR, MLP
		[45]	In the user hand in front of the body	25	Velocity, Distance, Mean, Variance, Standard deviation, Interquartile Range, Root Mean Square, Correlation	SVM
		[46]	Strapped to the user's ankle	4	Mean, Variance, Skewness, Kurtosis, Eccentricity, Correlation	NB, DTW
		[47]	In the right palm of the hand with the screen faced upwards	6	Mean, Standard Deviation	NB

Note: Features No. means the exact number of features to be fed to the classifier.
Abbreviations: FFT), Discrete Fourier Transform (DFT), Decision Table (DTL), Decision Tree (DT), Naïve Bayes (NB), K-Nearest Neighbour (KNN), Multilayer Perceptron (MLP), Support Vector Machine (SVM), Logistic Regression (LR), **BDM!** (**BDM!**), Rule Based Learner (RBL), Least square method (LSM), Dynamic Time Wrapping (DTW), Artificial Neural Network (ANN).

[41] which increases the HAR overhead not only in terms of the computational time needed to calculate all of these features but also the complexity of the classifier that will use these features to classify the activities. We also note that the number of features used for classification is not the only important factor that imposes overhead for HAR, but also the types of these features. For example, features extracted from the frequency domain increase the computational burden and impose additional complexities of storage (since the signal has to pass through Fast Fourier Transform (FFT)).

References [46] and [47] use simple (time domain) and a small number of extracted features. However, in [46], the authors strapped the phone to the user's ankle to keep the y-axis of the phone aligned to the lower leg at all times. Therefore, the activities had distinguishable characteristics in the accelerometer data. This distinction in the signals made the classification process, to some extent, easy and allowed the authors to rely on only 4 features. In [47], the chosen activities were dissimilar (sitting, standing, walking, running and jumping) and hence were easy to

be distinguished using a small number of features (6 features).

2.2 Energy-efficient Accelerometer-based HAR

Our work is related to energy-efficient HAR because we reduce the power consumption of the HAR process in a self-powered device by not using the accelerometer. Reducing HAR power consumption is also important in battery-powered devices because if the sensors are out of energy, the HAR system fails to achieve its objective. As a consequence, energy efficient HAR systems have become essential. This has motivated many researchers to look for new ways to reduce HAR battery consumption. We can categorise them in three basic approaches: reducing the sampling rate of the accelerometer, reducing the classification complexity, and reducing the number of accelerometers placed on the human body.

- **Reducing the sensor sampling rate**

  Reducing the sampling rate of the accelerometer is widely used to save the system energy. However, this reduction is always achieved at the expense of recognition accuracy. Therefore, improving the trade-off between sensor energy consumption and the accuracy of HAR has been the focus of many research studies. The authors in [26, 32] used a single activity monitoring technique to adjust the sampling rate and classification set of features to a choice that is "optimal" for this activity, hence reducing system energy overheads without violating user accuracy requirements. In A3R [26], they used sets of two classification features: time domain and frequency domain. However, Ad-Sense [32] explores the feature set space by genetic programming techniques and finds the optimal feature set that effectively reduces both the classification and the sampling rates.

- **Reducing the classification complexity**

  When a large number of activities are to be classified, the model responsible for classification (the classifier) can be very complex. Higher complexity leads to higher CPU usage and battery usage. Therefore, one way to reduce HAR

battery consumption would be to reduce classifier complexity. The authors in [48] provided an adaptive HAR which, instead of using a single complex classifier based on a large set of features, employs multiple simple classifiers, each trained to classify only a subset of activities using a small number of features. Then, at runtime, according to the current context, the system switches to the right classifier as the given set of activities to recognise changes with the context.

- **Reducing the number of sensors** An alternative approach to extend the battery lifetime of HAR systems has been to reduce the number of accelerometers used [49]. This approach works when the data collected by body sensors are transmitted to a base station (PC or smartphone) to be analysed and classified. Such studies tried to exploit redundant and unreliable accelerometers in order to reduce the communication cost between the sensor nodes and the base station, and hence extend the lifetime of the monitoring system.

While it is possible to extend the battery life of HAR through the previously mentioned ways, battery-powered sensors cannot provide sustained HAR without the need for battery replacement. Recently, a research trend in energy harvesting [50] has emerged and gained the attention of the research community. Energy harvesting (EH) is a process of converting different types of energy available in the environment into electrical energy so wearable sensors can continue to function without batteries. EH devices can eliminate the need for battery replacement and significantly enhance the versatility of consumer electronics. This has motivated us to consider energy harvesting technology to provide pervasive human activity recognition (HAR), where numerous wearable tiny devices continue to sense and monitor the human on a permanent basis.

2.3 Kinetic Energy Harvesting Overview

In theory, electrical energy can be obtained from many types of energy, including kinetic (vibration) [52, 53], thermal [54, 55], Radio Frequency (RF) [56, 57]. Ta-

Table 2.2: Power Density Estimates of typical ambient energy sources.

Energy Source	Characteristics	Harvested Power Density
Vibration	Human	$4\mu W/cm^2$
	Machine	$100\mu W/cm^2$
Light	Indoor (illumnated office)	$10\mu W/cm^2$
	Outdoor (direct sun)	$10mW/cm^2$
Thermal (Heat)	Human	$25\mu W/cm^2$
	Industrial	$1 - 10mW/cm^2$
Radio Frequency	GSN	$0.1\mu W/cm^2$
	WIFI	$1\mu W/cm^2$

Source: Texas Instruments, Energy Harvesting White Paper 2009 [51].

ble 2.2 shows the power density estimates of typical ambient energy sources from Texas Instruments [51]. Of all the ambient energy options, kinetic energy harvesting (KEH) is the most relevant for wearables because it can power the wearable directly from human motion. Kinetic energy also produces 4 times as much energy as RF (WIFI) and is more abundant. A brief review of KEH is presented in this section.

Kinetic energy harvesting (KEH) is a process of converting environmental vibrations into electrical energy. Kinetic EH and vibration EH are synonyms, environment around us is full of sources of kinetic or vibration energy such as natural seismic vibration (e.g. earthquakes), wind movement, sea waves, vehicular traffic, machinery vibration and human motion. In this section, we discuss the system architecture of a KEH-based device, the transduction mechanisms, the commercially available products implementing KEH, and the possible applications of KEH.

2.3.1 System Architecture

Figure 2.4 shows a block diagram of a KEH-based device. KEH-based Hardware typically comprises three parts: a transducer to convert vibration into electrical energy, an AC/DC converter to convert the Alternating Current (AC) generated from the transducer into regulated Direct Current (DC), and a battery or capacitor to store the harvested energy and provide a constant power flow to the load. The load normally consists of sensors (e.g. accelerometer), microprocessor, and Radio Frequency Transceiver.
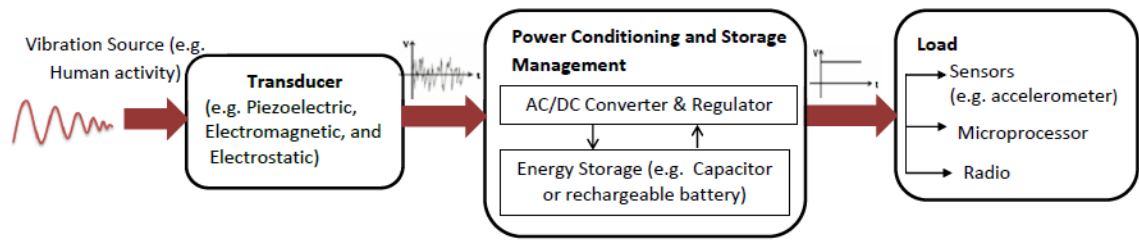
Figure 2.4: A Block Diagram of a KEH-based sensor node.

2.3.2 Transduction Mechanisms

From a hardware point of view, there are three main transduction mechanisms for converting vibration energy to electric power [58]: piezoelectric, electromagnetic (capacitive), and electrostatic (inductive). Depending on the mechanism used, the operating principle differs.

- Piezoelectric harvesters make use of certain piezoelectric materials such as Lead-zirconate-titanate (PZT) andMacroFiber Composite (MFC), which have the ability to generate an electrical potential when subjected to a mechanical strain [59, 60]. The resulting strain on the material will result in an output of alternating current which is converted into power.

- Electromagnetic harvesters make use of an oscillating mass (magnet) which traverses across a fixed coil, creating a varying amount of magnetic flux, inducing an alternating current that is converted to power [61].

- Electrostatic (capacitive) harvesters are based on separating the plates of an initially charged variable capacitor (varactor) using vibrations and converting mechanical energy into electrical energy [62]. Electrostatic harvesters are widely used though they are not as popular as piezoelectric or electromagnetic transducers since Electrostatic harvesters need a polarization source to work and to convert mechanical energy from vibrations into electricity.

Table 2.4 summarises the advantages and disadvantages of the three transduction mechanisms. Generally speaking, piezoelectric and electrostatic systems are well

Table 2.3: Transduction mechanisms of VEH.

Type	Advantage	Disadvantage
Piezoelectric	• No need for smart material • Compatible with MEMS • Compact configuration	• Depolarization • brittleness in PZT • charge leakage
Electromagnetic	• No need for smart material • No need for external voltage source	• Bulky size • Difficult to integrate with MEMS
Electrostatic	• No need for smart material • Compatible with MEMS	• External voltage source (or charger) is needed • Mechanical constraints are needed

suited to micro-scale (small scale) applications, while electromagnetic systems are preferable for macro-scale (medium scale) devices. Piezoelectric transducers are the most favorable due to their simplicity and compatibility with Micro-electro-mechanical Systems (MEMS) [63]. Electromagnetic-based energy harvesters are usually bulky in size and difficult to integrate with MEMS. Moreover, electrostatic transducers need external voltage to operate. Many kinetic or vibration EH models have been recently developed [64, 65, 58, 66, 67]. The main focus of these models is to optimise the parameters of the harvester to maximise the output harvested power. To maximise the output power, the harvester is mechanically tuned to an optimized resonant frequency present in the application environment.

2.3.3 Commercially Available KEH/VEH Devices

Several kinetic or vibration energy harvesters are commercially available. The prevalent commercial KEH devices are based on the piezoelectric and electromagnetic transduction mechanisms. Table 2.4 provides a list of the commercially available VEH devices. Perpetuum and Ferro Solutions produce electromagnetic-based VEHs, however, MIDÉ, MicroGen, PI Ceramic GmbH, and Smart Material produce piezoelectric-based VEHs. MicroStrain produces both electrodynamic gener-

Table 2.4: Commercially available KEH/VEH devices.

Manufacturer (Country)	Product	Material	Dimensions (in) $L \times W \times H$	Weight (grams)	Output (in voltage)
Perpetuum (UK)	PMG FSH	Electromagnetic	3.4×2.6	1075	DC (5 V and 8 V)
Ferro Solutions (USA)	VEH 460	Electromagnetic	–	430	DC (3.3V)
LORD MicroStrain (USA)	PVEH	Piezoelectric	1.87×1.75	185	DC (3.2 V)
	MVEH	Electromagnetic	2.25×2.56	216	DC (3.2 V)
MicroGen (USA)	BoLT PZEH	Piezoelectric	$1.18 \times 1.04 \times 0.69$	10	DC (3.3 V)
MIDÉ (USA)	Volture V25W	Piezoelectric	$2.00 \times 1.50 \times 0.03$	8	AC
PI Ceramic GmbH (Germany)	P-876.A11 DuraAct	Piezoelectric	$2.4 \times 1.38 \times 0.02$	-	AC
Smart Material (USA)	MFC M2503-P1	Piezoelectric	$1.81 \times 0.93 \times 0.01$	-	AC
OMRON and Holst Centre/imec	**Still under testing**	Electrostatic	1.96×2.36	15.4	DC

ators (MVEH Harvester) and piezoelectric materials (PVEH Harvester). Recently, OMRON and Holst Centre/imec unveiled a prototype of an extremely compact electrostatic-based VEH. Figure 2.5 shows some of the commercially available VEHs. Piezoelectric transducer are simple and compatible with MEMS [63]. The characteristic of the products show that electromagnetic-based energy harvesters are usually bulky and not compatible with MEMS as mentioned previously. Moreover, the only electrostatic transducer is still under testing and not commercially available.

Most VEH devices are available as packaged systems, including the transducer, power conditioning circuit, and local storage. They provide a constant (regulated) DC voltage which is suitable to power multi-sensor nodes, controllers, peripherals, memory, etc; however, the intermediate outputs such as the AC voltage, or the unregulated DC, cannot be accessed. Some companies (such as MIDÉ) make these intermediate outputs accessible by offering customizable energy harvesting evaluation kits, which provide modular components for power conversion and storage that afford plug-and-play compatibility with their transducers.

(a) Perpetuum **(b)** Ferro Solution **(c)** MVEH MicroStrain **(d)** PVEH MicroStrain

(e) MIDÉ Volture **(f)** MicroGen **(g)** PI Ceramic

(h) Smart Material (MFC) **(i)** OMRON and Holst Centre/imec (under testing)
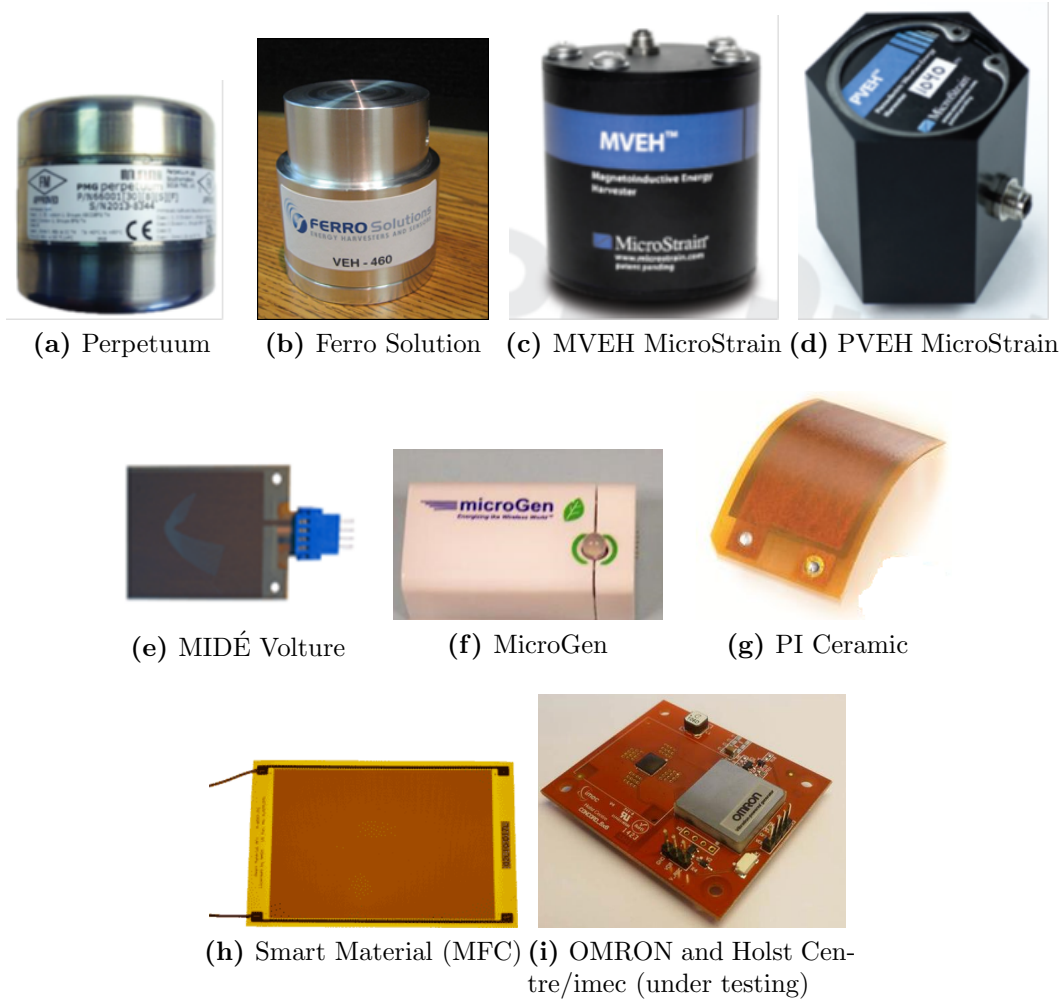
Figure 2.5: Commercial kinetic or vibration energy harvesters (a) Perpetuum, (b) Ferro Solution (VED 460), (c) MicroStrain MVEH, (d) MicroStrain PVEH, (e) Mide Volture, (f) MicroGen, (g) PI Ceramic, (h) Smart Material (MFC), and (i) OMRON and Holst Centre/imec (under testing).

2.3.4   KEH Applications

KEH has a wide area of applications, such as medical implants, consumer applications, building technologies, vehicles and aerospace. A brief summary of how KEH can be used for each of these applications is presented below.

- Medical Implants

  KEH can use a patient's own body movement and heartbeat to provide power for medical devices deployed inside the body, and which are vital to the life and well being of the patient.

- Consumer Electronics

  KEH is suitable for many low-power consumer electronics, used as a sole power source or as a means to extend battery life.

- Building Technologies

  KEH is suitable for building technology applications such as infrastructure sensing system battery and safety systems for buildings in the event of a power loss.

- Vehicles and Aerospace

  KEH provides safe, reliable, cost effective solutions to those applications in which traditional power sources are not reliable or preferred, e.g. supplying power to tyre air pressure sensors (where batteries are difficult to change and hard-wiring is impossible), supplying power to sensors mounted inside an aircraft which monitor in-flight mechanical loads on the airframe.

2.4   KEH-based HAR: Opportunities and Challenges

KEH-based HAR aims at providing a self-powered HAR which does not need batteries to operate. It allows continuous and permanent monitoring of a user's activities,

which will improve the user's experience and quality of life. KEH uses the harvested kinetic energy from human motion to supply power to the required sensors (e.g. accelerometer), microprocessor and radio communication. However, the most fundamental issue with KEH is its low power output [24]. The amount of power that can be practically harvested from human motion is too small to power all necessary functions of a wearable sensor.

2.4.1 HAR using Accelerometer

An accelerometer is used to measure human acceleration in three dimensions. Then, the acceleration samples are used to train a classifier which in turn is used to detect activities based on a window of acceleration samples. Generally, the more frequent the measurements, the more information is available to enable more accurate classification. The frequency of measurement is called the sampling rate of the accelerometer, which is measured in Hertz or the number of measurements per second. To perform a measurement, an accelerometer must be turned on for a few milliseconds. Since the accelerometer consumes power when it is active, it is turned off when it is not measuring. Therefore, an accelerometer is continuously turned on and off, at a frequency dictated by the sampling rate.

There are several types of accelerometers; however, the type that is most used in wearable and mobile devices is the capacitive accelerometer. In a capacitive accelerometer, a capacitor is formed by a "stationary" plate (the housing which moves with the base acceleration) and a moving plate attached to the seismic mass. The distance between these plates determines the capacitance which can be monitored to infer acceleration (change in capacitance related to acceleration). The authors in [25] tested the power consumption of six commonly used capacitive accelerometers. Figure 2.6 shows the results of their test when a 3.3 v power supply and a 50 HZ sampling rate were used. The results showed that accelerometers consume hundreds of microwatts at only 50 Hz.

Moreover, Figure 2.7 plots the accelerometer's power consumption as a function of the sampling rate.
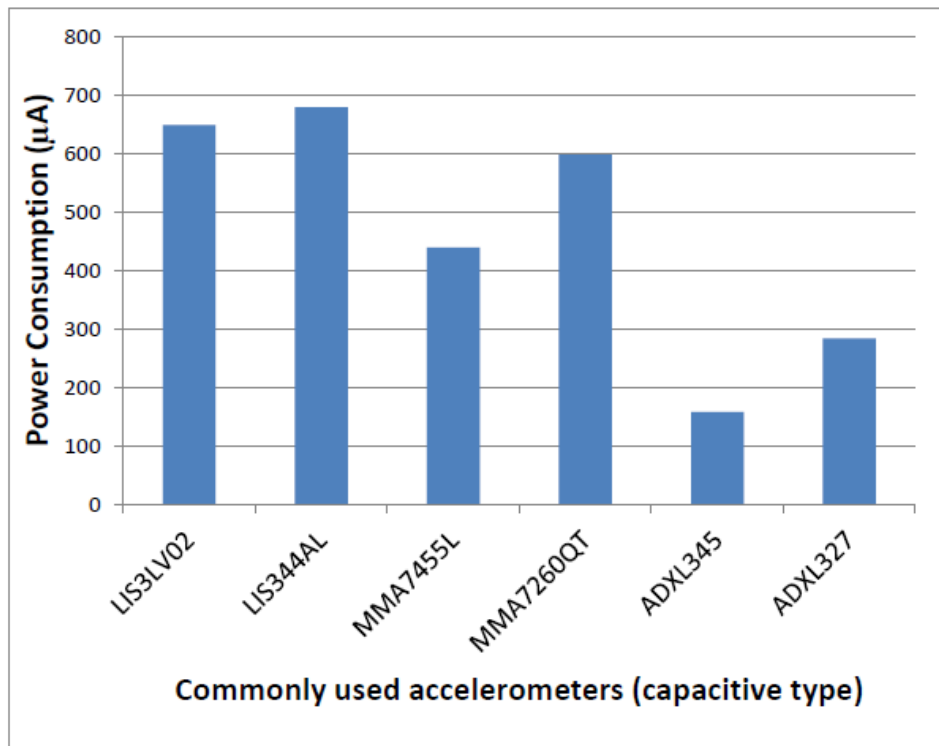
Figure 2.6: The mean power consumption of 6 commonly used accelerometers a 3.3 v power supply and a 50 HZ sampling rate were used.

Using the datasheets of three widely used capacitive accelerometers ADXL150 (used in wearable sensors), SMB380 (used in Samsung Galaxy smartphones), LIS302DL (used in IPhone smartphones), We can see that the average power consumption of the accelerometer is a linear function of the sampling rate. For example, the data sheet of an ADXL150 accelerometer [27] shows that the accelerometer consumes about 5 μW on average per Hz, which means that it would require 250 μW if a sampling rate of 50 Hz were required for a given activity set. The required sampling rate depends on the set of activities monitored and typically ranges from 1-50Hz [28, 29, 30, 31]. This means the battery must supply 5-250 μW to the accelerometer. This is simple for battery-powered wearable devices. However, it is an issue for energy harvesting wearable devices.
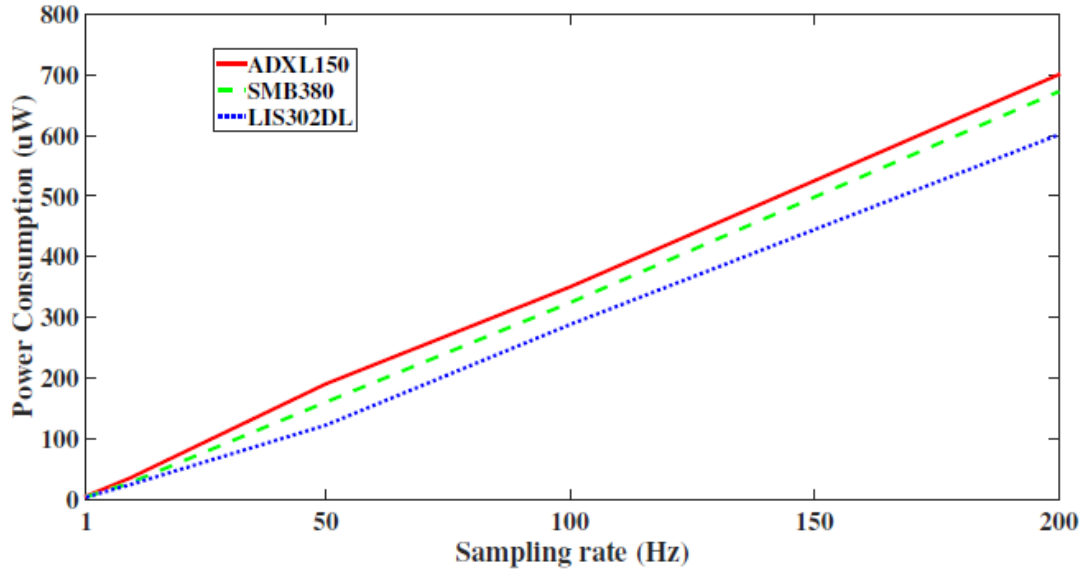
Figure 2.7: Power consumption of popular accelerometers as a function of sampling rate.

2.4.2 KEH Limitation

The most fundamental issue with KEH is that the power that can be practically harvested from human motion is too small to power all necessary functions of a wearable sensor. KEH from human activities can produce only limited power (measured in μW), which is not sufficient to simultaneously power all components in a wearable device including the accelerometer.

Table 2.5 shows the power that could be generated using a commercial kinetic energy harvester for different activities [33]. It shows that some activities generate only a few μW, much lower than what is required to sample the accelerometer at a sufficiently high rate for accurate activity classification. Clearly, this will force the sensor to reduce the power to the accelerometer, i.e., use a lower sampling rate and accept a lower activity classification accuracy, each time the user switches to one of the activities that produce small amount of power. Even if the harvested power is enough to operate the accelerometer at the required sampling rate, it reduces the amount that could be accumulated in the capacitor for future radio communications. Insufficient stored energy in the capacitor will force more aggressive duty cycling of the radio or more drastic reduction in the transmission power. In summary, when the power supply is limited by energy harvesting, powering the accelerometer trades

Table 2.5: Average Harvested Power different activities when the device is attached to the shank.

Activity	Average Harvested Power (μW)
Walking	10.30
Running	28.74
Cycling	0.36
Sitting	0.02
Lying	0.36

off the quality of radio communication.

In fact, using KEH to provide a self-powered HAR is a challenging problem that requires innovative sensing and communication solutions. We therefore explore an alternative approach to HAR that does not use an accelerometer, which can have relatively high power requirements on relatively low-power energy harvesting wearables, but instead uses the generated KEH signal for HAR.

Chapter 3

HARKE: Human Activity Recognition from Kinetic Energy

3.1 Introduction

Continuous human activity recognition (HAR) is becoming critical in many applications, including aged health care [5, 6], smart living [8], and indoor positioning [10, 68] to name a few. At the same time, there is a growing research and development momentum in realising various types of energy harvesting wireless devices [50]. These trends promise a new pervasive human activity monitoring paradigm where numerous wearable tiny devices continue to sense and monitor the human on a permanent basis.

Conventional HAR relies on accelerometers to frequently sample human motion (acceleration). Typically a triaxial accelerometer is used to measure the acceleration of a subject in three dimensions while performing different activities. Informative features are then extracted from these data and used to train a classifier, which is used later to detect activities from a given sample of acceleration values. Accelerometers are usually considered low-power electronics drawing only about a few μW per sample per second (Hz). However, the power requirements of the accelerometer for HAR, when used in kinetic-powered devices, are considered relatively higher compared to the total kinetic power available, which is also measured in μW. A linear

reduction in accelerometer power consumption is possible by reducing the sampling rates, but only at the expense of reduced accuracy for activity recognition.

In this chapter, we propose and evaluate a novel paradigm for human activity recognition using kinetic energy harvesting (KEH) patterns. The proposed use of KEH patterns for classifying human activities is based on the observation that different activities produce kinetic energy in different ways leaving their signatures in the harvested power signal. Indeed, it was recently reported that we could harvest 612-813 μW if a user was running, but walking would generate only 155-202 μW [64]. Interestingly, due to the gravitational effect, going up the stairs would generate less power than going down the stairs [64], which indicates that we could even distinguish between these two similar activities using energy harvesting data. All this could be achieved without using an accelerometer, thereby conserving the scarce power harvested from the environment.

The key contributions of this chapter are summarised as follows.

- Using experimental accelerometer data, we first model the HAR accuracy degradation in HAR under power constraints. The derived model demonstrates that down-scaling the power supply to the accelerometer reduces HAR accuracy *exponentially*. Next, we study the power consumption of the accelerometer relative to the amount of power harvested in a kinetic-powered device. We show that the power requirement of the accelerometer for HAR ranges between 71-515% of the harvestable kinetic power. These results indicate that although accelerometers are considered low-power electronics in general, they can be the bottleneck of self-powered pervasive HAR.

- We propose the use of kinetic energy harvesting (KEH) patterns as a new source of realising HAR in a kinetic-powered device. We call this approach HARKE, which stands for *Human Activity Recognition from Kinetic Energy*. By not using the acceleration for activity classification, the proposed HARKE eliminates the need for accelerometer sampling, making HAR practical for self-powered devices.

- We use a well known mathematical model to estimate the KEH power genera-

tion for different human activities. By applying information theoretic measures on estimated KEH data, we demonstrate that kinetic harvested power patterns contain rich information for discriminating many typical activities of our daily life.

- We test the performance of HARKE on 14 different sets of common activities, each containing between 2-10 different activities to be classified. We find that HAR accuracies vary from 68% to 100%, depending on the set of activities. The average accuracy over all activity sets is 83%, which is within 13% of what could be achieved with an accelerometer *not subjected to power constraints.*

The rest of this chapter is organised as follows. Related work is reviewed in Section 3.2. Section 3.3 presents the derivation of the exponential model that captures the HAR accuracy as a function of power available to the accelerometer. The power requirements of the accelerometer relative to the available KEH power is explored in Section 3.4. We present the proposed concept of using energy harvesting data for HAR in Section 3.5, followed by its performance evaluation in Section 3.6. We conclude the chapter in Section 6.6.

3.2   Related Work

Our work is related to energy-efficient HAR because we reduce the power consumption of the HAR process in a self-powered device by not using the accelerometer. Reducing HAR power consumption is also important in battery-powered devices, which motivated many researchers to look for new ways to reduce battery consumption of HAR. We can categorise them in three basic approaches, reducing the sampling rate of the accelerometer, reducing the classification complexity, and reducing the number of accelerometers placed on the human body.

Reducing the sampling rate of the accelerometer is a widely used method to save the system energy. However, this reduction is always achieved at the expense of the recognition accuracy. Therefore, improving the trade-off between sensor energy consumption and accuracy of HAR has been the focus of many research studies.

The authors in [26, 32] used a single activity monitoring technique to adjust the sampling rate and classification set of features to a choice that is optimal for this activity and hence to reduce system energy overheads without violating user accuracy requirements. In A3R [26], they used sets of two classification features: time domain and frequency domain. However, AdSense [32] explores the feature set space by genetic programming techniques and finds the optimal feature set that effectively reduces both the classification and the sampling rates.

When a large number of activities is to be classified, the model responsible for classification (the classifier) can be very complex. Higher complexity leads to higher CPU usage and battery usage. Therefore, one way to reduce HAR battery consumption would be to reduce classifier complexity. The authors in [48] provided an adaptive HAR which, instead of using a single complex classifier based on a large set of features, employs multiple simple classifiers each trained to classify only a subset of the activities using a small number of features. Then, at runtime, according to the current context, the system switches to the right classifier as the given set of activities to recognise changes with the context.

An alternative approach to extend the battery lifetime of HAR systems is to reduce the number of accelerometers used [49]. This approach works when data collected by body sensors are transmitted to a base station (PC or a smartphone) to be analysed and classified. Such studies tried to exploit redundant and unreliable accelerometers in order to reduce the communication cost between sensor nodes and the base station, and hence extend the life time of the monitoring system.

While it is possible to extend the battery lifetime of HAR through the previously mentioned ways, battery-powered sensors cannot provide sustained HAR without the need for battery replacement. Recently, a trend in energy harvesting [50] has emerged and gained the attention of the research community. Energy harvesting is commonly defined as the conversion of ambient energy such as vibrations, heat, wind, and light into electrical energy. EH devices can eliminate the need for battery replacement and significantly enhance the versatility of consumer electronics. Many energy harvesting models have been recently developed [64, 65, 58, 66, 67]. The main focus of these models is to optimise the parameters of the harvester to maximise the

output harvested power. These recent advances in energy harvesting devices have motivated us to consider the concept of self-powered pervasive HAR. The novelty of our work is the use of harvested power patterns to classify the activities that generate the power, which to our knowledge has not been addressed before.

3.3 Accuracy Degradation of HAR Under Power Constraints

Accelerometer-based HAR relies on accelerometers to frequently sample human motion. Typically, a classifier is trained with informative features extracted from a large number of acceleration samples collected during various activities, such as walking, running, standing, and so on. Later, when extracted features from new acceleration samples are presented to the classifier, it can recognise the activity using the trained model. Generally, the more frequent the measurements, the more information is available to enable more accurate classification. The frequency of measurement is called the sampling rate of the accelerometer, which is measured in Hz or the number of measurements per second. A decade of research has confirmed that accelerometers are effective in accurately detecting human activities. The purpose of this section is to model the HAR accuracy degradation under power constraints. In order to achieve this purpose, we evaluate HAR accuracy for a given set of activities by varying the sampling rate of the accelerometer. The evaluation process of HAR using accelerometer data from different activities is explained below.

3.3.1 Accelerometer Data Collection

Using a handhekd Samsung Galaxy Nexus smartphone, we collected accelerometer traces from five different subjects for ten basic activities. Since different combinations of activities pose different challenges for classifications, we created 14 different sets of activities from these 10 basic activities, as shown in Table 3.1. The original data was collected at 100Hz, but we later subsampled each of these traces at 1-50 Hz to study the effect of sampling rate on activity recognition accuracy.

Table 3.1: The considered activity sets.

Activity Set (AS)	Included Activities
AS 1	Walking (W), Running (R).
AS 2	Standing (S), Vacuuming (V).
AS 3	Going up the stairs (SU), Going down the stairs (SD).
AS 4	Standing on escalator going up (EU), Standing on escalator going down (ED).
AS 5	Standing, Walking, Going up the stairs, Going down the stairs.
AS 6	Standing, Walking, Going up the ramp (RU), Going down the ramp (RD).
AS 7	Standing, Walking, Standing on escalator going up, Standing on escalator going down.
AS 8	Going up the stairs, Going down the stairs, Standing on escalator going up, Standing on escalator going down.
AS 9	Going up the stairs, Going down the stairs, Going up the ramp, Going down the ramp.
AS 10	Standing, Walking, Running, Going up the stairs, Going down the stairs.
AS 11	Standing, Walking, Standing on escalator going up, Standing on escalator going down, Going up the ramp, Going down the ramp.
AS 12	Going up the stairs, Going down the stairs, Standing on escalator going up, Standing on escalator going down, Going up the ramp, Going down the ramp.
AS 13	Standing, Walking, Running, Going up the stairs, Going down the stairs, Vacuuming, Standing on escalator going up, Standing on escalator going down.
AS 14	Standing, Walking, Running, Going up the stairs, Going down the stairs, Vacuuming, Standing on escalator going up, Standing on escalator going down, Going up the ramp, Going down the ramp.

3.3.2 Feature Extraction and Classification

In this study, we use K-nearest neighbour (KNN) classifier, which has been widely used by other researchers [69, 70, 28] due to its simplicity and effectiveness in activity classification. The KNN classifier is trained with 12 features (see table 3.2) extracted from 5-sec windows with 50% overlapping of the accelerometer traces. Finally, for each sampling rate, we perform 10-fold cross validation test to obtain the accuracy. Next, we show the recognition accuracy as a function of the sampling rate.

3.3.3 HAR Recognition Accuracy vs Accelerometer Sampling Rate

Fig. 3.1 shows the HAR accuracy as a function of sampling frequency of the accelerometer for three different sets, 1, 3 and 7. We make several observations. We can see that the HAR accuracy increases with increasing sampling rate, but its rate of increase continues to slow down as it approaches a limit (saturates). The char-

Table 3.2: The considered feature set.

Feature Name	Description
Mean	The central value of a window of samples.
Standard deviation	A measure of the amount of variation or dispersion from the mean.
Maximum	The maximum value in a window of samples.
Inter-quartile Range	The difference between the upper quartile and the lower quartile of the window of samples.
Root Mean Square	The square root of the arithmetic mean of the squares of the values of the window of samples. It is a measure of the magnitude of a varying quantity.
Mean Absolute Deviation	The mean of the absolute deviations from a central point. It measures dispersion or variability in values of the window of samples.
Skewness	A measure of the asymmetry of the probability distribution of the window of samples.
Kurtosis	A measure of the "peakedness" of the probability distribution of the window of samples.
Auto-Correlation	The cross-correlation of a signal with itself. It measures the similarity between observations as a function of the time lag between them.
Dominant Frequency	The maximum spectral component of the Fourier transform of the signal.
Power Spectrum Mean	The mean of the power spectrum of the signal.
Frequency Domain Entropy	The normalized information entropy of the discrete FFT component magnitudes of the signal.

acteristic of this growth in HAR accuracy is captured by the exponential function $f(x) = a(1 - e^{-\lambda x})$, where a is the limiting value of HAR accuracy and λ is a constant defining the shape or slope of the curve (curve fitting results shown in the legend). Note that different sets have different limiting values and reach the limiting value at different sampling rates, which we call *critical sampling rates*. For example, activity set 1 has a critical sampling rate of 10 Hz, because the accuracy does not improve any further beyond this rate, whereas the accuracy for set 7 continues to increase until 30 Hz.

A second observation is that the accuracy falls exponentially if the accelerometer is sampled below the critical sampling rate. This means that if there is insufficient harvested power, then the accelerometer will be forced to operate at a lower sampling rate, which would cause exponential decrease in accuracy. This observation highlights the challenge facing the realisation of pervasive HAR using energy harvesting wearable devices. Next, we discuss in more details the limitations of accelerometer-based HAR in future kinetic-powered devices.
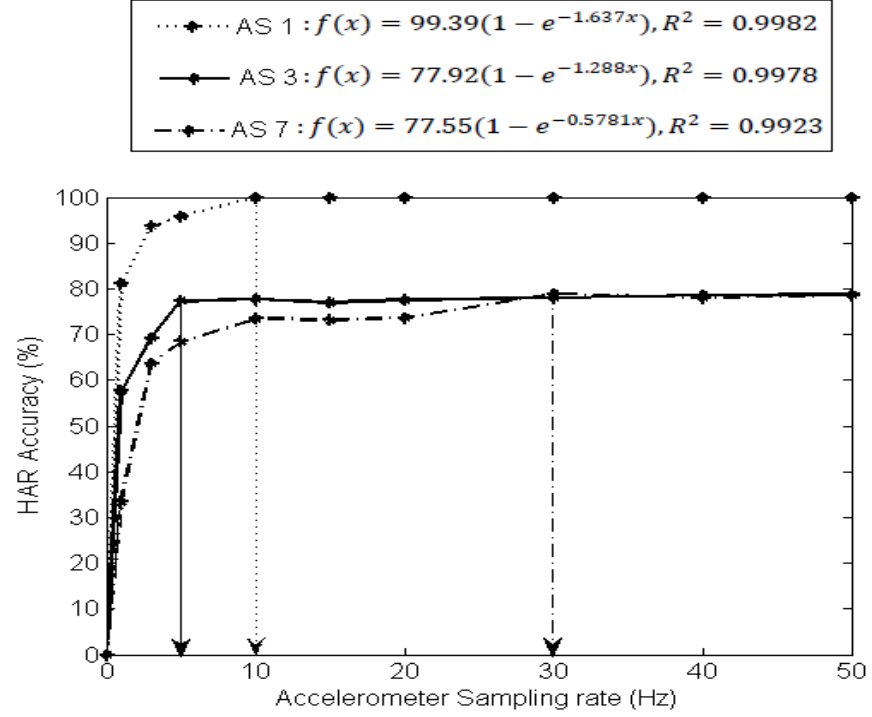
Figure 3.1: HAR accuracy as a function of accelerometer rate for three different activity sets.

3.4 Accelerometer Power Requirement in KEH-powered Devices

To study the power consumption of the accelerometer relative to the amount of power harvested in a kinetic-powered device, we first estimate the power that could be harvested for each activity set in Table 3.1. We compare it to the power requirement of the accelerometer. We use known mathematical models to estimate the harvested kinetic power generation from human motion data. Then we investigate the accelerometer power requirements relative to the available harvested power for given sets of human activities.

3.4.1 Estimating KEH Power Generation Patterns

Here, we use the recently developed mathematical model of Gorlatova et al., which has been shown to accurately estimate the amount of harvestable kinetic power from

Table 3.3: Average harvested power of different activities.

Activity	Average Harvested Power (μW)
Standing	0.063
Walking	53.50
Running	153.40
Stairs Up	44.94
Stairs Down	97.39
Vacuuming	29.94
Escalator Up	0.2198
Escalator Down	0.2522
Ramp Up	64.68
Ramp Down	56.02

accelerometer data using a standard mass-spring damping system [64]. This model has been validated using a comprehensive dataset collected from 40 participants going through unrestricted motions. Once the gravity is filtered out from the raw acceleration values, the filtered acceleration is converted to *proof mass displacement* using the Laplace domain transfer function:

$$z(t) = \mathcal{L}^{-1}\{Z(s)\} = \frac{A(s)}{s^2 + \frac{b}{m}s + \frac{k}{m}} \tag{3.1}$$

where m is the proof mass, k is the spring constant, b is the damping factor, $A(s)$ and $Z(s)$ denote, respectively, the Laplace transforms of $a(t) = \sqrt{a_x(t)^2 + a_y(t)^2 + a_z(t)^2}$, the overall magnitude of the acceleration, and $z(t)$, the proof mass displacement. Next, the resulted proof mass displacement, $z(t)$, is limited by the limit of the proof mass displacement, Z_L. Finally, the generated harvested power, $p(t)$, is determined by:

$$p(t) = b\dot{z}^2(t) \tag{3.2}$$

We used the configuration values, $m = 10^{-3}kg$, $Z_L = 10mm$, $k = 0.17$, and $b = 0.0005$, optimised in [64] for typical human activities. The entire procedure was implemented using MATLAB and SIMULINK [71]. The outcome is a trace of kinetic power samples, which we use for further analysis.

Table 3.4: Sampling rates and power consumptions of the accelerometer for different activity sets.

Activity Set	Average Harvested Power (μW)	Required Accelerometer Sampling Rate (Hz)	Required Power (μW)	Percentage of Harvesting Power consumed (%)	Achievable Accelerometer Sampling (Hz)
AS 1	103.45	10	50	48.33	20.69
AS 2	15.00	5	25	166.6	3
AS 3	71.17	5	25	35.13	14.234
AS 4	0.236	5	25	10593.2	0.047
AS 5	48.97	10	50	102.10	9.79
AS 6	43.56	30	150	344.35	8.71
AS 7	13.51	30	150	1110.3	2.70
AS 8	35.70	15	75	210.08	7.14
AS 9	65.76	15	75	114.05	13.15
AS 10	69.86	10	50	**71.57**	13.97
AS 11	29.12	30	150	**515.11**	5.82
AS 12	43.92	30	150	**341.53**	8.78
AS 13	47.46	20	100	**210.70**	9.49
AS 14	50.04	15	75	**149.88**	10.01

3.4.2 Accelerometer Power Requirement Relative to Available KEH Power

In this subsection, we study the power consumption of the accelerometer relative to the available harvested power. Table 3.3 shows the average harvested power for each activity[1]. Table 3.4 presents the average harvested power for each activity set (column 2) along with the required sampling rates of the accelerometer to achieve the maximum (limiting) accuracy (column 3). Column 4 shows the power requirement of the accelerometer to achieve the maximum accuracy assuming a 5 μW power consumption per Hz on average. This means that the accelerometer can work without power constraints only as long as the harvested power (column 2) is greater than the power in column 4. Column 5 shows the percentage of harvested power that would be required by the accelerometer to work without power constraints.

We can see that apart from a few activity sets (sets 1, 3, and 10), the accelerometer would require more power than could be harvested, forcing it to work under

---

[1]The average power generated by some of the considered activities is slightly lower compared to those reported in [64]. This is due to the different holding positions of the sensing device. In our experiment, the device was held in the hand while in [64] the sensors were placed in shirt and pant pockets.

power constraints or at reduced sampling rates, as shown in the final column. Considering only the sets for which we have five or more activities to recognise, i.e., sets 10 to 14, we find from column 5 that the power requirement of the accelerometer is between 71-515% of the harvestable kinetic power. Our findings reveal that the accelerometer becomes the bottleneck of self-powered HAR, in spite of having relatively low-power requirements.

3.5 Proposed Architecture of HARKE

Figure 3.2 contrasts the proposed HARKE and the conventional accelerometer-based HAR architectures. In the conventional HAR, the acceleration samples are used to train a classifier which in turn is used to detect activities based on a window of acceleration samples. In contrast, no acceleration data is used in the proposed architecture. Instead, training and classification are accomplished entirely using the output signal of the kinetic energy harvester. Energy saved by not using the accelerometer can be used by other on-board units, such as the radio.

Figure 3.3 compares the accelerometer signal with the estimated kinetic power signal when a subject goes through a series of five activities in 35 seconds. It provides a clear visual confirmation that, like the accelerometer signal, the power signal is affected differently by different activities. Therefore, it should be possible to use the kinetic power signal to achieve HAR. In the following section, we measure the discriminating ability of the kinetic power more formally using information theory and investigate the HAR accuracy that it can achieve for typical human activities.

3.6 HARKE Performance Evaluation

The main purpose of this section is to evaluate HAR accuracy when the kinetic power signal is used to classify different activities in a given activity set. But first, we provide an information theoretic analysis to formally assess the discriminating capacity of the kinetic power signal for typical human activities.
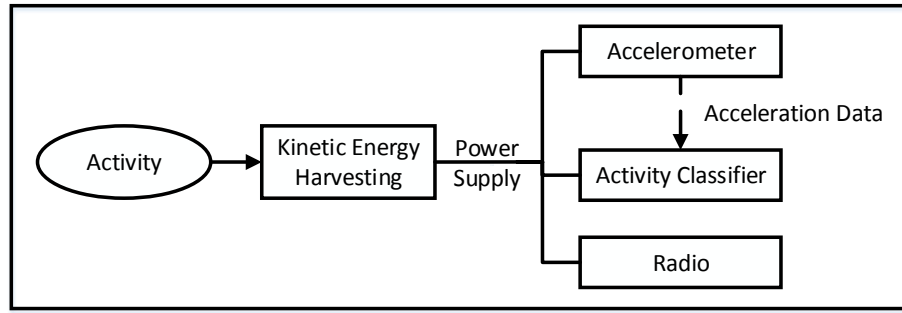
(a) Conventional acceleometer-based HAR
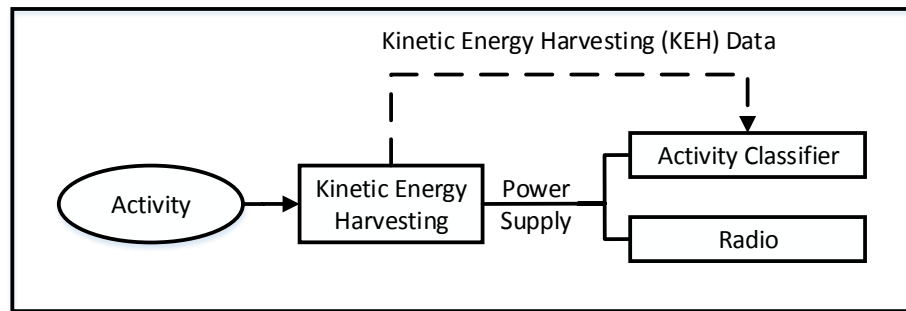
(b) Proposed HARKE

Figure 3.2: HAR Architectures: (a) Conventional accelerometer-based HAR and (b) Proposed HAR based on kinetic power signal
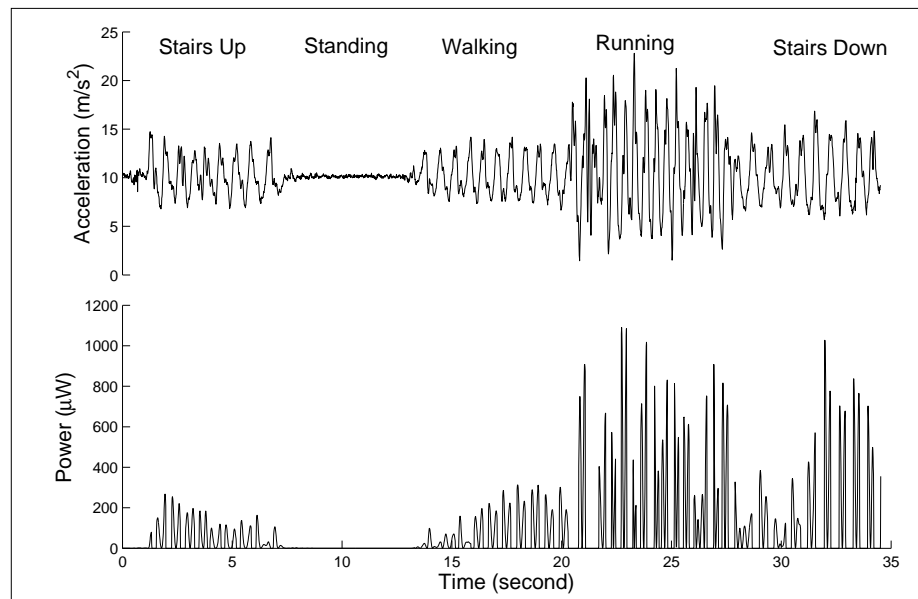
Figure 3.3: The accelerometer trace (the magnitude of the three axes) and the corresponding harvested power trace for the activity sequence: stairs up-standing-walking-running-stairs down.

3.6.1   Information Gain

Information gain (IG) is a measure that determines how useful a given feature is for discriminating between the classes (activities) to be learned [72]. The IG of feature f_i measures the expected reduction in entropy caused by partitioning the data (instances) according to this feature. The calculation of information gain is based on calculating the entropy H(S) of a set of classes S.

$$H(S) = -\sum_{i=1}^{n} p_i \log_2 p_i \tag{3.3}$$

where n is the number of different activity classes and p_i is the proportion of all instances belonging to the ith class. The information gain is then calculated using:

$$Gain(S, f_i) = H(S) - \sum_{v \in Values(f_i)} \frac{|S_v|}{|S|} H(S_v) \tag{3.4}$$

where $|S|$ denotes the cardinality of the set S and S_v is the subset of S for which feature f_i has a value v (i.e., $S_v = s \in S|Values(f_i) = v$).

A feature that cannot help with classification has zero IG. If the kinetic power signal does not contain any useful information for activity classification, then it will be difficult to find a feature with positive IG. Next, we compute IG for a range of commonly used statistical features on the kinetic power samples. The outcome for activity set 14 is shown in Figure 7.5 and the averages for all sets with 5 or more activities, i.e., sets 10-14, are shown in Table 3.5 . We see that there are many features with significant IG, confirming that the kinetic power signal contains rich information that can be used to train a classifier to detect activities (see the following subsection).

An interesting observation is that the Maximum feature, i.e., the maximum power in a window of 5-sec, provides the most information gain, beating the Mean feature. This is interesting because in the literature it is often mentioned that the average kinetic power of different activities is different [64], which may give the impression that the Mean kinetic power would be the key for activity classification. In the following subsection, we will compare the accuracies that could be obtained
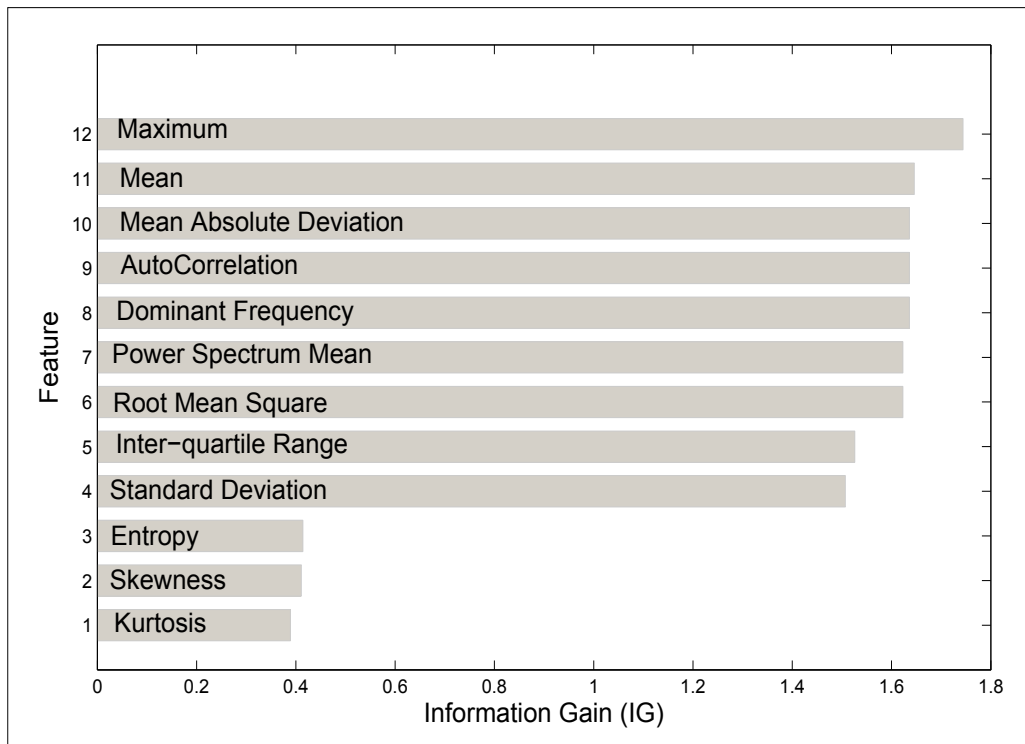
Figure 3.4: Information gain of kinetic power signal of AS 14 for 12 features commonly used for HAR.

by using different power features.

3.6.2 Classification Accuracy

In this subsection, we use the same method used in Section 3.4 to obtain HAR accuracy. There are some subtle differences in how we obtain the features from the acceleration and the kinetic power traces. For the accelerometer traces, we consider both single, i.e., the overall acceleration, and 3-axial data, which means we extract 12 features for the single but 36 features for the 3-axial traces. For the kinetic power, we only have a single trace, so only 12 features are extracted. Table 3.6 compares the accuracies of kinetic power-based HAR when different power features (Mean and Maximum) are used in isolation and also when all 12 features are used. First, we find that the Maximum feature provides better accuracy than the Mean, as is expected from the IG results presented in the previous subsection. Second, using multiple features together does not provide any accuracy gain in kinetic power-based

Table 3.5: Average Information Gain for Activity Sets 10 to 14.

Feature	Average IG
Maximum	1.5299
Mean Absolute Deviation	1.4388
Mean	1.4364
Auto-correlation	1.4364
Dominant Frequency	1.4364
Standard Deviation	1.4131
Power spectrum mean	1.4109
Root mean square	1.4109
Inter-quartile Range	1.3615
Skewness	0.4476
Frequency Domain Entropy	0.4148
Kurtosis	0.4090

HAR. This is surprising because it is well known that for accelerometer-based HAR, many features are to be used in combination to achieve high accuracy and in fact we found the same for our accelerometer dataset. It is also known that the use of the individual acceleration components in x, y, and z directions, albeit more complicated, improves accuracy significantly. We therefore evaluate two sets of accuracies for the accelerometer-based HAR, one with the overall acceleration and the other applying the 12 features on each of the three components.

Accuracies for accelerometer-based HAR are shown in Table 3.7 along with those obtained for kinetic power-based HAR with the Maximum feature used for classification. We see that kinetic power-based HAR performs better than accelerometer-based HAR only when the overall acceleration is used and remains with 13% on average when individual acceleration components are considered. These results are encouraging because Table 3.7 presents the best case results for the accelerometer, i..e, when the accelerometer is *not power constrained*. As shown in Table 3.4, the accelerometers in a self-powered device may often have to operate under power constraints due to insufficient kinetic power.

Next, we take a closer look into the classification results to identify the source of lower accuracy for kinetic power-based HAR. We examine the sets that achieved the three lowest accuracies in Table 3.7. These are sets 9 (68.40%), 12 (73.91%), and 14

Table 3.6: Accuracies for kinetic power based HAR.

Activity Set	EH-based HAR Accuracy (%)		
	Using Maximum Feature	Using Mean Feature	Using 12 Features in Table 3.2
AS 1	96.20	93.59	98.43
AS 2	100	100.00	100
AS 3	90.93	61.53	65.97
AS 4	82.67	60.00	63.21
AS 5	86.88	63.24	80.00
AS 6	81.84	60.26	67.35
AS 7	88.19	74.50	56.46
AS 8	86.21	61.36	61.07
AS 9	68.40	30.96	31.84
AS 10	84.06	55.53	79.73
AS 11	79.52	53.98	46.53
AS 12	73.91	41.80	41.39
AS 13	78.57	51.83	60.93
AS 14	72.00	41.51	49.00
Average	83.53	60.72	64.42

(72%). We find that these are the sets that contain the activities going up the ramp (RU) and going down the ramp (RD). In our experiments we collected data when subjects walked over ramps with small slopes with angles ranging between 10°-30°. For such low-angle ramps, they are very similar to the walking (on a flat surface) activity.

A triaxial accelerometer is fundamentally advantaged in separating RU, RD, walking, or any other very similar human activities due to the multi-dimensional measurement of the motion, hence achieving very high accuracy for all activity sets in our experiments including sets 9, 12, and 14. By measuring acceleration in three dimensions, new discriminating opportunities arise, which is not possible with a single-dimensional power measurement.

The advantage of a triaxial accelerometer against the single-dimensional harvested power signal is illustrated in Figure 3.5 by plotting the samples from three activities, RU, RD, and walking. We see that the signals of these three activities look very similar regardless of whether acceleration or power samples are used. Even when each axis is considered separately, they look very similar. However, when we consider the acceleration signals in y and z directions together, we find two clear

Table 3.7: Comparison of accuracies for accelerometer-based and kinetic power-based HAR.

Activity Set	HAR Accuracy (%)		
	Kinetic power	Accelerometer (Overall)	Accelerometer (3-axis)
AS 1	96.20	100	100
AS 2	100	100	100
AS 3	90.93	80	93.20
AS 4	82.67	62.14	100
AS 5	86.88	76.24	96.06
AS 6	81.84	64.47	95.86
AS 7	88.19	73.04	99.90
AS 8	86.21	63.07	96.50
AS 9	68.40	55.78	92.20
AS 10	84.06	81.21	94.64
AS 11	79.52	57.19	96.96
AS 12	73.91	51.71	94.25
AS 13	78.57	72.88	98.16
AS 14	72	64	95.45
Average	83.53	71.55	96.66

Power: using a single feature (max).
Accelerometer (Overall): using 12 Features (see Table 3.2).
Accelerometer (3-axis): using 36 features (12 features (see Table 3.2) from each axis).

discriminating patterns between the three activities.

The y and z acceleration signals closely follow the shape of a sinusoidal wave due to the periodic motion of walking and the tilting of the smartphone in the hand, but they have a phase shift relative to each other. The relative shift for walking is the maximum (close to 180°) and minimum for RU. We also see that the offsets between these two signals are different for different activities. During training, a classifier quickly learns such important differences, which allows it to accurately distinguish the activities from each other. However, when a single-dimensional power signal is used, the classifier does not have access to such information, leading to confusion. Whether we can extract multi-dimensional motion information from the harvested power signal remains an open question.

3.7 Conclusion

Although accelerometers are considered low-power electronics in general, our study has revealed that the accelerometer becomes the *power bottleneck* in realising self-
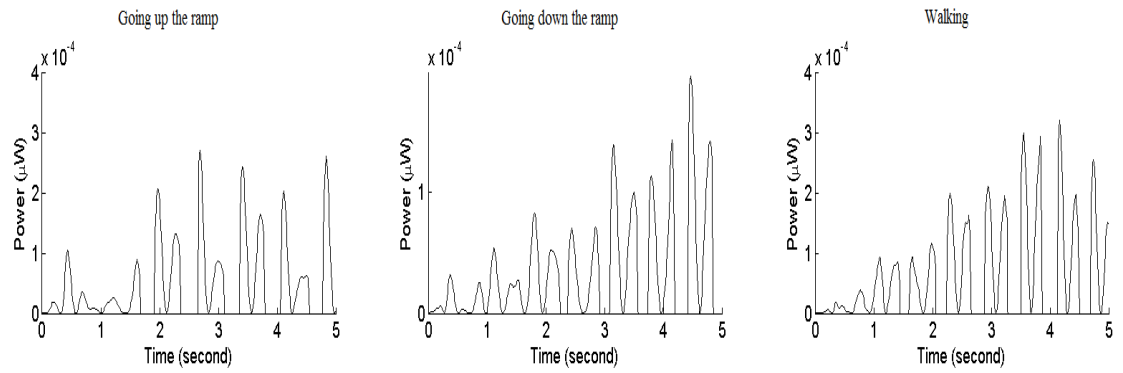
(a) Kinetic power signal for RU, RD, and W (Classification Accuracy=74.10%).
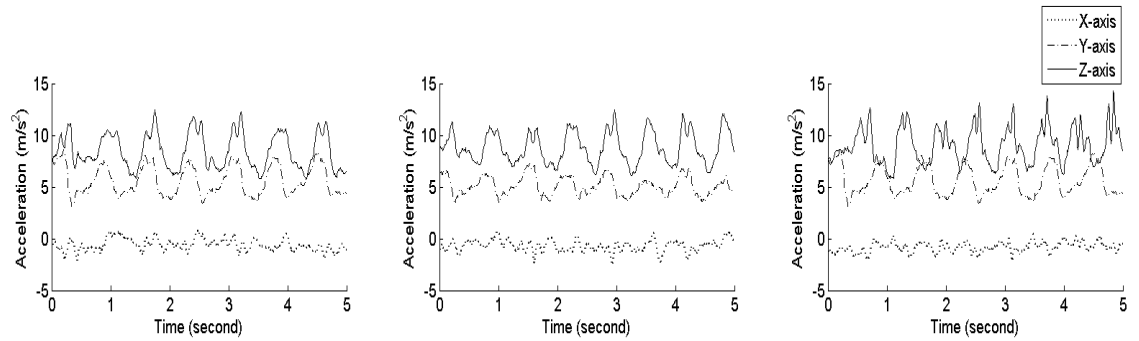
(b) 3-axis accelerometer signal for RU, RD, and W (Classification Accuracy=94.31%).

Figure 3.5: A comparison of kinetic power signal in (a) with 3-axis accelerometer signal in (b).

powered HAR. We have shown that the kinetic power signal itself contains signatures for the human activities that are to be classified and recognised. A standard KNN classifier can detect many activities with very high accuracies using only the kinetic power signal and not using an accelerometer at all. Since the kinetic power is readily available from the energy harvesting circuit, HAR based on kinetic power signals conserves a significant fraction of the scarce harvested power that would have been consumed by the accelerometer. Thus, the proposed use of energy harvesting signals for HAR can be considered a key enabler for realising the vision of pervasive self-powered human activity recognition.

The work presented in this chapter is the first study of recognising human activity directly from the energy harvesting signal. Although we have shown that good HAR accuracies are possible for many common activities, we have also found that the kinetic power signal cannot distinguish very similar activities, such as walking on a flat surface and walking on a ramp, with high accuracy. For such cases, an accelerometer has a clear advantage with its 3-axis measurement capability, which provides more detailed (multi-dimensional) motion information of these activities leading to high recognition accuracy. We have analysed HAR accuracy when the accelerometer and the energy harvester are used in a mutually exclusive manner. A logical future direction is to consider a hybrid system where a triaxial accelerometer is sampled at a low sampling rate (low power consumption), but the classifier is trained using both acceleration samples and kinetic power samples, thus enabling very accurate HAR with low power consumption. The hybrid system combines the advantages of both signals to realise a more flexible HAR with a goal to achieve a better accuracy-power trade-off than the one possible with the mutually exclusive method.

In this chapter, we used a known mathematical model to estimate the harvested kinetic power signals from human motion because portable kinetic energy harvesting dataloggers are currently not readily available. In the next chapter, the experimental validation of HARKE is provided by building a portable KEH datalogger that could be worn by a user performing different activities and collect real KEH data.

Chapter 4

Experimental Validation of HARKE

4.1 Introduction

Recent advancements in energy harvesting hardware have created an opportunity to realise self-powered wearables for continuous and pervasive human activity recognition (HAR). Unfortunately, the power consumption of accelerometers used in conventional HAR is relatively high compared to the amount of power that can be practically harvested, which limits the usefulness of energy harvesting. In the previous chapter, we showed that the power requirement of the accelerometer for detecting common human activities with high accuracy ranges between 0.71 to 5 times the harvested kinetic power. This clearly proves that power consumption of accelerometers becomes a bottleneck for realising pervasive self-powering HAR because the amount of power that can be practically harvested from the environment is small.

Instead of using an accelerometer, we propose the use of the kinetic energy harvesting (KEH) patterns as a novel source of information for HAR when motion (kinetic) energy is being harvested to power the device. The proposed use of KEH patterns is motivated by the fact that different activities produce kinetic energy in different ways, leaving their signatures in the harvested power signal. The proposed energy harvesting wearable sensor architecture is called HARKE, which stands for

Human Activity Recognition from Kinetic Energy.

In the previous chapter, we used a mathematical model to estimate KEH data from human motion data. A smartphone with incorporated accelerometer was used to collect human motion. This option allowed us to validate HARKE without the need to use special hardware. However, the generated KEH data were an approximation of the real data. For the ultimate validation of HARKE, we build a data logger to collect real KEH data. Our objective is to investigate (a) whether the generated patterns by real KEH hardware contain information about human activity as reported in the previous chapter from estimated KEH power patterns, and (b) if it does, how does the performance of HARKE compare with the conventional accelerometer-based HAR.

The contributions of this chapter can be summarized as follows:

- Using off-the-shelf products, we built a datalogger prototype which enabled us to record the generated signals of a commercially available KEH transducer. We also added an accelerometer to the prototype to compare the performance of HARKE against accelerometer-based HAR.

- We collected extensive data from ten different subjects with a diversity of gender, age, weight and height. Our data was collected for five common activities: standing (S), walking (W), running (R), going up the stairs (SU), going down the stairs (SD). We considered two placements of the device on subjects bodies (hand and waist) to study the impact of placement on recognition accuracy.

- Our analysis showed that the patterns generated from real KEH hardware switch to clearly distinguishable patterns as the user changes activities. This confirms the feasibility of using the real KEH patterns for HAR.

- We compared the performance of HARKE to accelerometer-based HAR using five different classifiers, K-Nearest Neighbour (KNN), Decision Tree (DT), Multilayer Perceptron (MLP), Support Vector Machine (SVM), and Naïve Bayes (NB). We showed that the KNN classifier gives the highest performance of HARKE when specific vibration features are used.
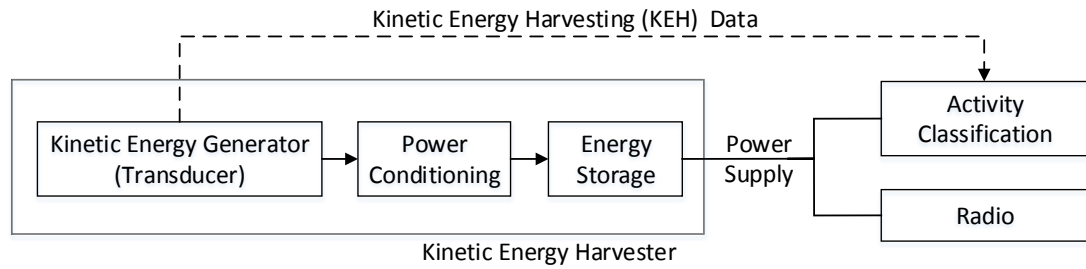
Figure 4.1: Detailed block diagram of HARKE architecture.

- We employed Correlation Feature Selection (CFS) to reduce the number of features used for HARKE to make it more energy efficient. Our results showed that the CFS algorithm is effective in reducing the number of features without affecting the recognition accuracy. This is because the CFS algorithm selects the most useful features and discards the redundant and non-informative ones.

- We showed that HARKE is as accurate as accelerometer-based HAR for distinguishing dissimilar activities such as standing, walking, and running. However, the performance of HARKE is reduced for very similar activities such as going up and down stairs, which agrees with the validation of HARKE using the mathematical modelling presented in the previous chapter. We also showed that the fundamental advantage of the accelerometer in distinguishing similar human activities is due to the multi-dimensional measurement of the motion against the single dimensional measurement of the KEH hardware.

The rest of the chapter is organized as follows. The detailed hardware architecture of HARKE is explained in Section 4.2 followed by its experimental validation in Section 4.4. The results of the experimental validation are presented and analyzed in Section 4.5. A discussion of the results is presented in Section 4.6. We conclude the chapter in Section 4.7 with a discussion of future directions.

4.2   Detailed Architecture of HARKE

The detailed hardware architecture of HARKE is depicted in Figure 6.2(a) with no accelerometer. Instead, it contains a kinetic energy harvesting (KEH) system to harvest energy from human motion. The harvested energy is then used to power the classifier and the radio when it is turned on for communication. The KEH system typically consists of three basic components:

1. A generator (transducer) to convert human motion into electrical power, typically a varying AC voltage;

2. A power conditioning circuit to provide power rectification and regulation; and

3. A storage element to store the harvested energy.

A storage element such as a battery or capacitor is needed to accumulate the harvested energy and supply regulated power, typically a constant DC voltage, which is suitable to power the classifier and the radio communication. The regulated DC voltage is not suitable for detecting human activities, because regulation would wipe out any potential pattern in the generated signal that might be used for activity recognition. Therefore, HARKE uses the AC voltage from the transducer as an input to the classifier to perform HAR.

4.3   Energy Savings by HARKE

The energy savings of HARKE is directly due to the removal of the accelerometer. A detailed measurement study in [32] indicates that the average power consumption of an accelerometer running at 20 Hz is *four* times as much as the average power consumption for extracting features and executing a classifier. Consequently, the accelerometer is responsible for 80% of the total HAR power consumption. Compared to the energy saved by removing the accelerometer, the power consumption for recording the AC voltage for activity classification is minimal. To continuously record AC voltage, HARKE needs an analog-to-digital converter (ADC) to sample the analog AC signal into digital data that can be used for feature extraction
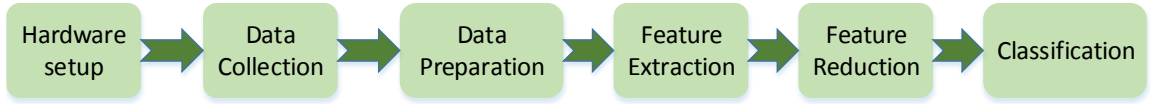
Figure 4.2: Phases of the experimental validation of HARKE.

and classification. The datasheet of ADS7042, an ultra low-power ADC from Texas Instruments, shows that the ADC consumes approximately $1\mu W$ per KHz [73]. Comparing this to 100 μW consumed by an ADXL150 accelerometer running at 20 Hz (assuming a 5 μW/Hz power consumption), we find that 99% of the power that would be consumed by the accelerometer could be saved using our architecture. Given that 80% of HAR power consumption is due to the accelerometer, HARKE saves 72% of HAR power consumption in a self-powered wearable. By adopting the HARKE architecture, a significant amount of limited harvested energy can be saved in the next generation self-powered wearables. The question is how accurately can we classify human activities using the generated patterns from a KEH hardware?

4.4   Experimental Validation of HARKE

The basic idea of HARKE is to use the patterns generated by KEH hardware to classify common human activities. In order to do so we need to go through five phases. These phases are presented in Figure 4.2. First, we build a prototype to collect the generated patterns by the KEH hardware. This hardware is then used to collect real KEH data for common human activities. The collected data is then prepared and analyzed to extract informative features. To reduce the computational complexity, we use feature reduction techniques to reduce the size of the feature vectors by removing the redundant and non-informative features. Finally, the extracted features are used to train and validate a classifier model which will be used in real time to recognize human activities from KEH patterns. The details of each phase are given in this section.

4.4.1   Hardware Setup

Our datalogger hardware includes a product called Volture from MIDÉ[1], which implements only the KEH transducer, providing AC voltage as its output. A triaxial accelerometer (MMA7361LC) was added to the design for comparison purposes. We used an Arduino Uno as a micro-controller device for sampling the data from both the KEH transducer and the accelerometer. A sampling rate of 1 KHz was used for data collection. The sampled data was saved on an 8 GB microSD card which was connected to the Arduino using microSD shield. A nine volt battery was used to power the Arduino. The data logger also includes two switches, one to switch the device on or off and the other to control the start and stop of data logging. Figures 4.3(a), 4.3(b), 4.3(c), and 4.3(d) show the block diagram, the external appearance, the circuit diagram, and the internal appearance of the datalogger hardware, respectively. In the circuit diagram, a 750 KOhm load resistor was soldered at the harvester output to obtain the AC voltage and 2×10 KOhm resistors to make the offset at 2.5 V instead of 0 to access the negative side of the AC voltage. Once the device is assembled it can be attached to different parts of the subject under test to gather the data. Below, a detailed description of each component of the datalogger is presented.

- Piezoelectric KEH transducer

  Piezoelectric KEH transducer is the most favourable type of transduction mechanisms due to its simplicity and compatibility with MEMS [63]. The piezoelectric effect was discovered in natural quartz crystals, but today's piezoelectric transducers are typically made from patented proprietary ceramics. Figure 4.4(a) shows a typical usage configuration of a piezoelectric cantilevered beam. One end of the beam is fixed to the device, while the other is set free to oscillate (vibrate). When the piezoelectric material is subjected to a mechanical stress due to any source of environmental vibration, it expands on one side and contracts on the other. Positive charges accumulate on the expanded side and negative charges on the contracted side, generating an AC voltage as the

---

[1]http://www.mide.com
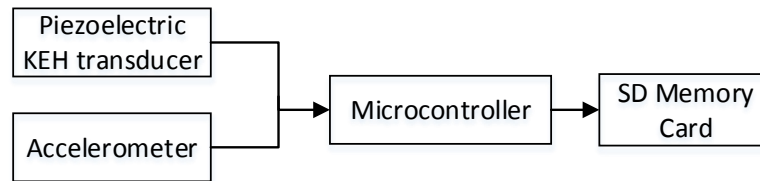
(a) A block diagram of the datalogger hardware.
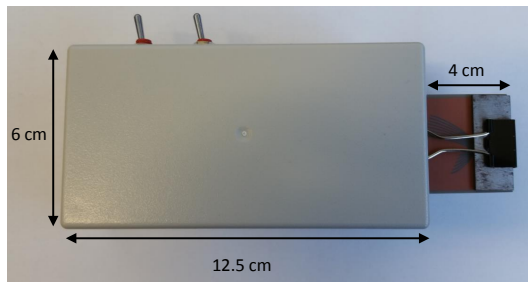
(b) The external appearance.
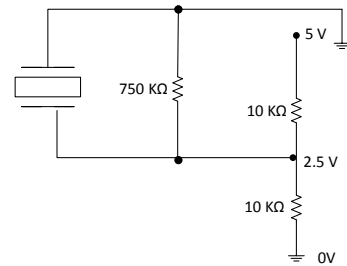
(c) The circuit Diagram.
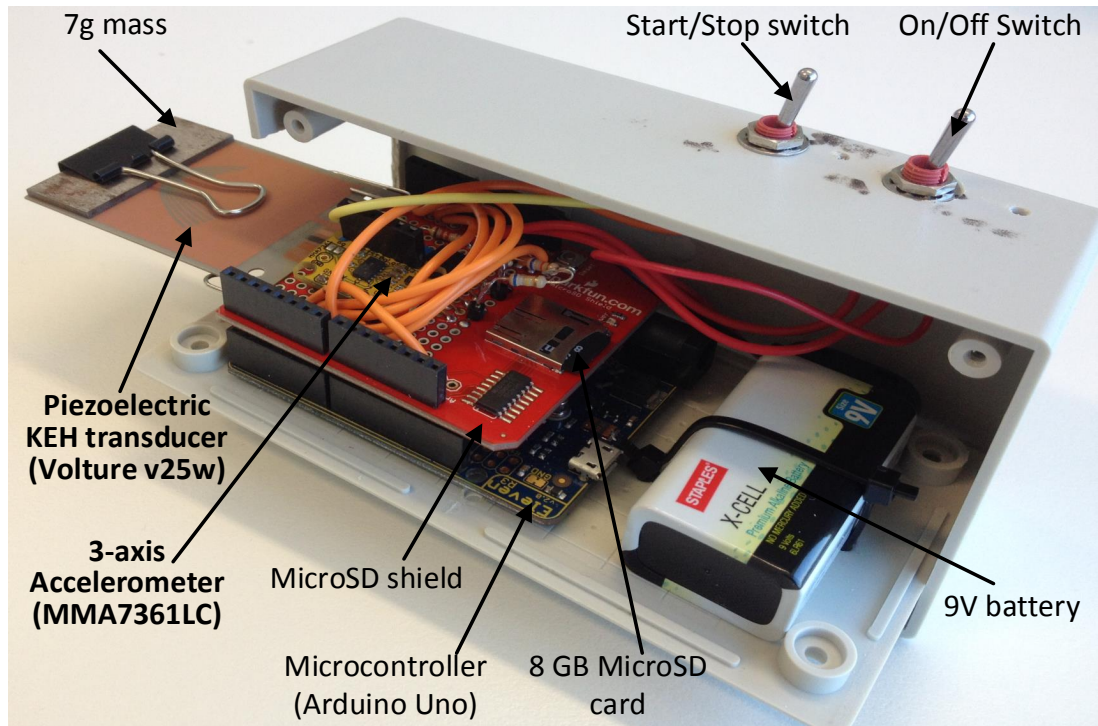
(d) The internal appearance.

Figure 4.3: The datalogger hardware setup: (a) a block diagram of the datalogger hardware, (b) the external appearance of the data logger, (c) the circuit Diagram and (d) the internal appearance of the data logger.
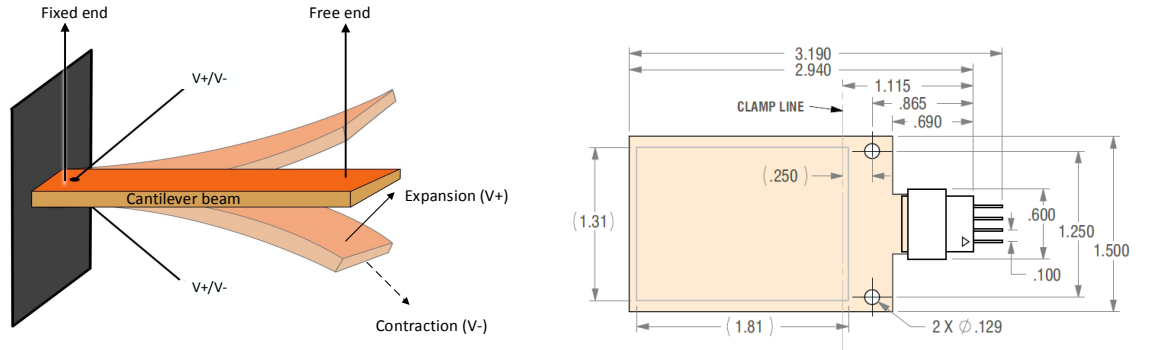
(a) A piezoelectric cantilevered beam.

(b) The dimensions of the used piezoelectric KEH product, from the datasheet of Volture[2].

Figure 4.4: Piezoelectric KEH overview: (a) a piezoelectric cantilevered beam and (b) the dimensions of the piezoelectric KEH product, from the datasheet of Volture[3].

beam oscillates around the neutral position. The amount of voltage is proportional to the applied stress, which means that different vibration patterns generate different AC voltage patterns.

We used a piezoelectric KEH transducer called Volture from MIDÉ company. It employs a cantilever that attaches to a piezoelectric crystal. When vibrations set the cantilever in motion it generates an AC voltage. Volture is available in six standard sizes. Here, we used the v25w product which has the dimensions shown in Figure 4.4(b). The typical thickness of this product is 0.024 in. Volture v25w is sensitive to the vibration frequency range 40 Hz-120 Hz and it is able to generate a maximum of 34 mW at 80 Hz. Since human motion frequency is rarely higher than 3 Hz, the output power is expected to be a few magnitudes lower. We used a 7 gm mass to make the harvester sensitive to lower frequencies. The mass was placed at the free oscillating tip of the cantilever as shown in Figure 4.3(d).

- Triaxial accelerometer

  We added a triaxial accelerometer (MMA7361LC) to the hardware prototype to collect both KEH and accelerometer patterns simultaneously, for comparison purposes. The MMA7361LC is a low power, low profile capacitive micromachined accelerometer featuring signal conditioning, a 1-pole low pass filter,

---

[3]`http://www.mide.com/pdfs/Volture_Datasheet_001.pdf`

Table 4.1: The specifications of the Arduino Uno microcontroller.

Microcontroller	ATmega328
Operating Voltage	5V
Input Voltage (recommended)	7-12V
Input Voltage (limits)	6-20V
Digital I/O Pins	14 (6 provide PWM output)
Analog Input Pins	6
DC Current per I/O Pin	40 mA
DC Current for 3.3V Pin	50 mA
Flash Memory	32 KB (0.5 KB used by bootloader)
SRAM	2 KB
EEPROM	1 KB
Clock Speed	16 MHz
Length	68.6 mm
Width	53.4 mm
Weight	25 g

temperature compensation, self-test, 0g-Detect which detects linear freefall, and g-Select which allows for the selection between 2 sensitivities ($\pm 1.5g$, $\pm 6g$). The 0-g offset and sensitivity are factory set to $800mV/g@1.5g$. The MMA7361LC operates on $2.2 - 3.6$ V. It has a current consumption of $400\mu A$ and only $3\mu A$ at sleep mode which makes it ideal for handheld battery powered electronics..

- Processor (Micro-controller)

We used an Arduino Uno as a microcontroller. Table 4.1 shows the specifications of the Arduino Uno. Arduino Uno uses the ATmega328 microcontroller board. The ATmega328 has 32 KB (with 0.5 KB used for the bootloader). It also has 2 KB of SRAM and 1 KB of EEPROM (which can be read and written with the EEPROM library). The Arduino Uno can be powered via USB connection or with an external power supply (either an AC-to-DC adapter or battery). The power source is selected automatically. The board can operate on an external supply of 6 to 20 V. However, the recommended range is 7 to 12 V since the use of less than 7 V may make the board unstable and more than 12 V may overheat the voltage regulator and damage the board. In our design, we used a 9 V battery to power the Arduino.

- Storage memory

Since the internal storage of the Arduino is very limited, we equipped it with an 8 GB microSD card through microSD shield so it can be used for data-logging. This provides the ability to save information to a file system and retrieve megabytes of data.

- Other features

  We added two switches to the dataolgger hardware, one to switch the device on and off and the other to control the starting and stopping of the data logging process.

4.4.2 Output Transformation

The Arduino is programmed to sample data from the Volture and accelerometer and store them on an 8 GB microSD card. It has 10 bits of output resolution (i.e. 1024 different values). Therefore, the range of the output measurements is from 0 to 1023. To map the range of the measurements to the actual voltage range $(0 - 5V)$, we used Eq. (4.1).

$$Voltage = \frac{5 \times m}{1023},\tag{4.1}$$

where m is the measurement sampled by the Arduino.

For the accelerometer output, we then used Eq 4.2 to calculate the corresponding acceleration of the three axes.

$$Acceleration = \frac{Voltage - 1.65}{0.8},\tag{4.2}$$

where 1.65 is the 0g acceleration, which is usually defined as half the supply voltage (in this case 3.3 V) and 0.8 is the scaling factor between the measured voltage and acceleration in g. Then we divide Eq (4.2) by 9.81 to get the acceleration in m/s^2. Finally, we subtract 2.5 from the Volture output to compensate changing the Volture offset to $2.5V$ instead of $0V$ in the hardware setup. The Volture's offset has been changed in the design to allow accessing the negative samples of the AC voltage.
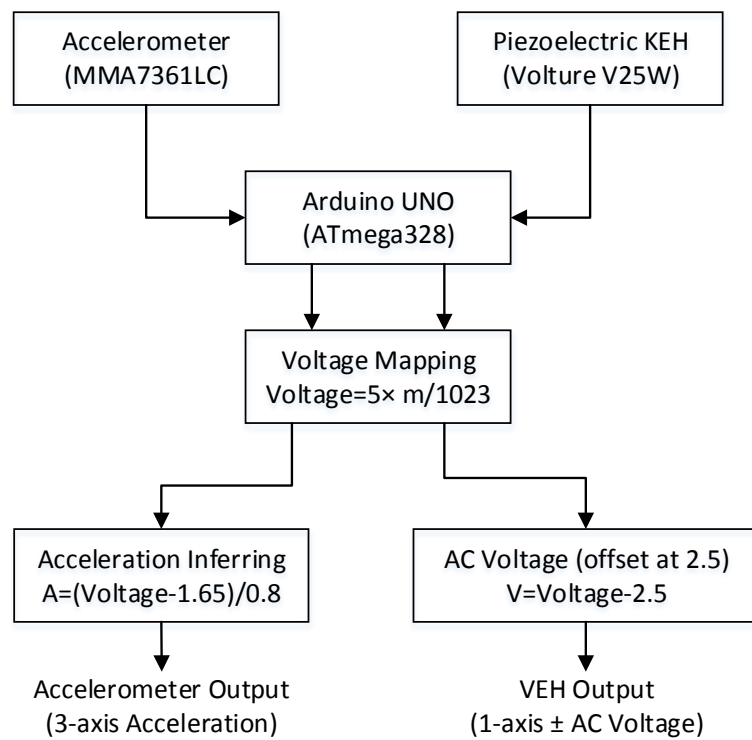
Figure 4.5: Data Preparation Procedure

Table 4.2: The physical characteristics and the statistics of the volunteers for data collection.

Subject ID	Gender	Age	Weight (kg)	Height (cm)
1	Female	27	75	171
2	Female	28	61	160
3	Female	26	65	164
4	Female	34	73	164
5	Female	29	58	158
6	Female	29	58	154
7	Male	27	70	175
8	Male	35	91	184
9	Male	28	65	175
10	Male	27	77	180
range		26-35	58-91	154-185
mean		29	69.3	168.5
standard deviation		3.06	10.21	9.98

Figure 4.5 shows the output transformation procedure.

4.4.3 Data Collection

Our data was collected using the previously explained datalogger and ten different subjects volunteered to participate in this study. The data includes diversity in gender (4 male and 6 female), age, weight, and height. Table 4.2 shows the physical characteristics of each subject. We considered five different activities from the most basic and common activities in daily life: standing (S), walking (W), running (R), going up stairs (SU), and going down stairs (SD). All subjects performed the last four activities at their natural speed, i.e., there was no special speed requirement. We considered two different placements of the datalogger on the subject's body to study the impact of the device placement on both the accelerometer and the KEH data. The subjects were asked to first hold the data logger in either their left or right hand and perform the five mentioned activities and then repeat the data collection process using the waist placement. Figures 4.6 and 4.7 show the data collection process of the five activities and the two placements of the device on the subject's body, respectively.

At the beginning of the data collection process, each user had to make sure that
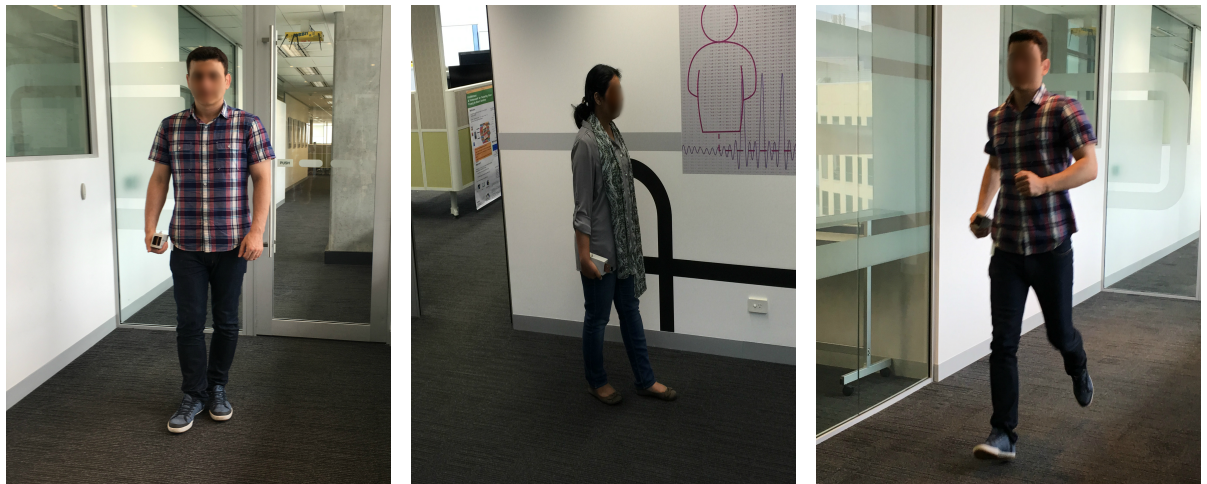
(a) Standing   **(b)** Walking   **(c)** Running
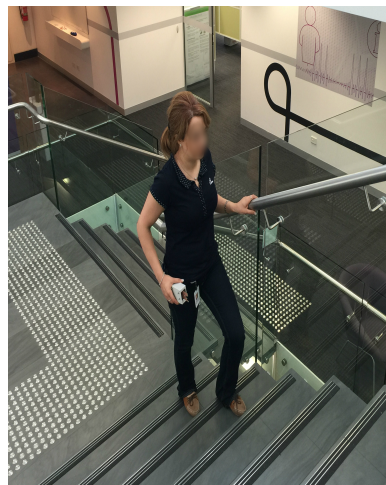
(d) Going up the stairs   **(e)** Going down the stairs

Figure 4.6: Data Collection Process (a) Standing, (b) Walking, (c) Running, (d) Going up stairs, and (e) Going down stairs.

(a) Hand   **(b)** Waist

Figure 4.7: Device placements on the person's body: (a) hand and (b) waist.
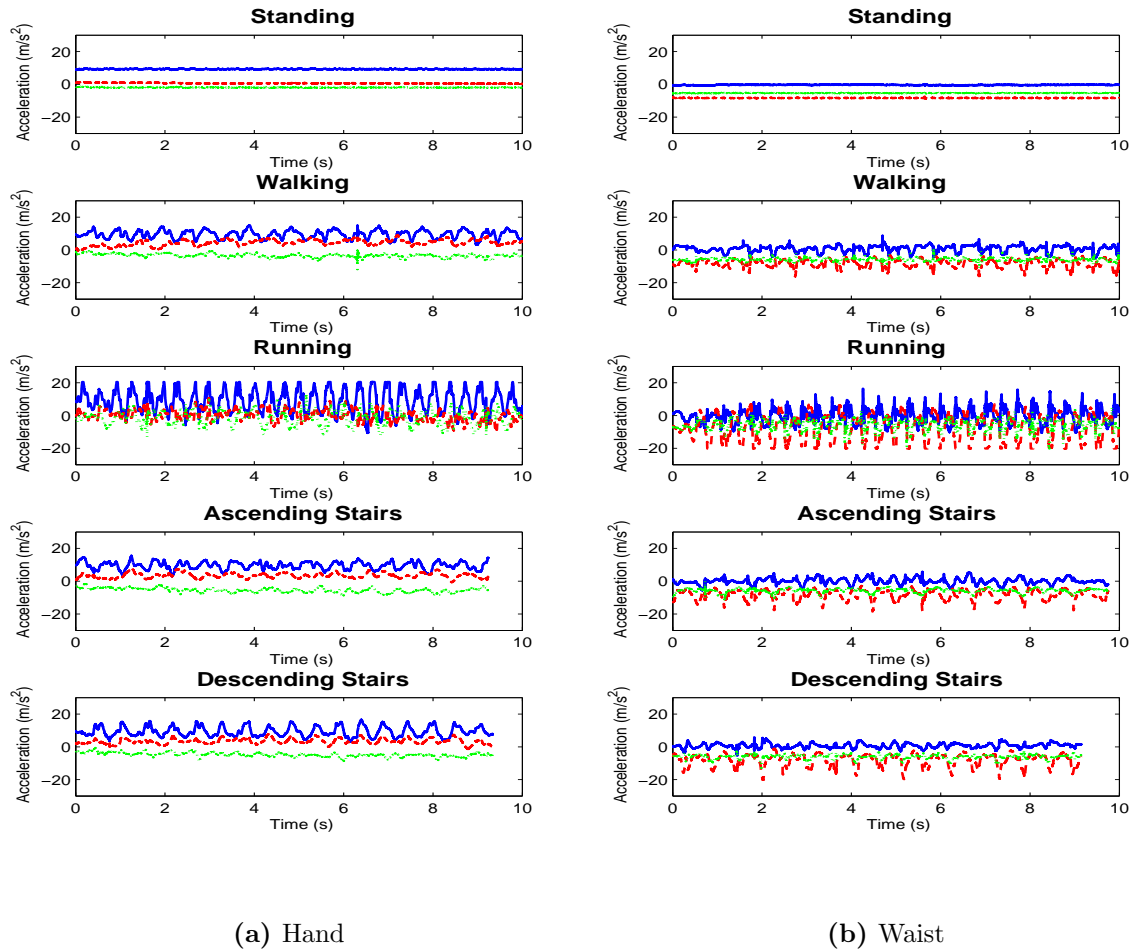
(a) Hand

(b) Waist

Figure 4.8: The accelerometer patterns of the five activities for two placements of the device: (a) hand (left) and (b) waist (right).

the device is switched on, then uses the start/stop switch to start and stop data collection at the beginning and end of each activity. Subjects were asked to stop and wait a few seconds after one activity and before starting the next. The data collected between the start and stop times of an activity was recorded in a separate file on the microSD card which was labeled with the name of that activity. Each file on the microSD card contains a trace of single-axis KEH signal (first column) and a triaxial accelerometer signal (the next three columns). With 1000 Hz data collection frequency, we have 1000 1D samples of KEH data and 1000 3D samples of accelerometer data for each second of the trace.

Our traces were of variable length, each subject provided between 20 to 30 sec-
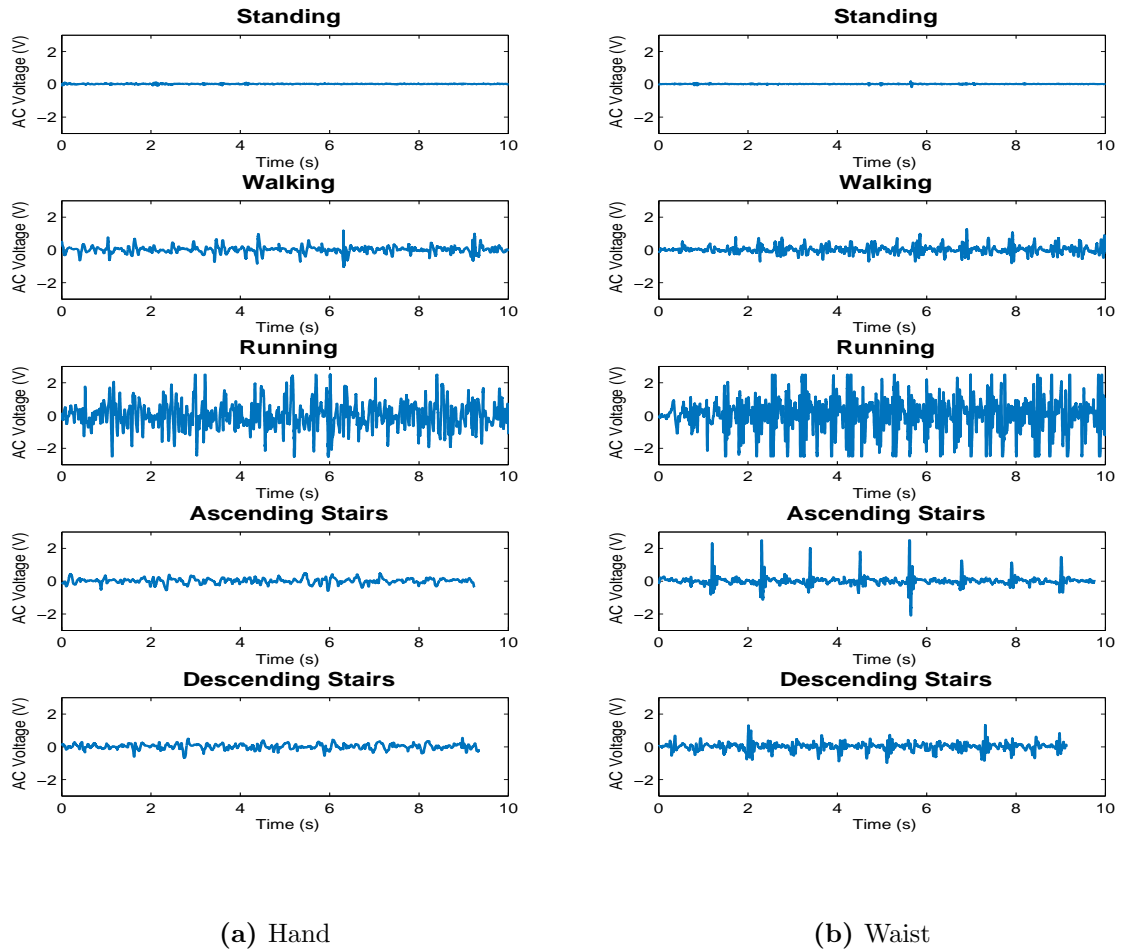
(a) Hand   **(b)** Waist

Figure 4.9: The KEH patterns of the five activities for two placements of the device: (a) hand (left) and (b) waist (right).

onds of data per trace for standing (S) and walking (W), 10 to 12 seconds of data per trace for running (R), and 8 to 10 seconds of data per trace for going up (SU) and down (SD) stairs. For each placement of the device on the person's body, we collected a total of 80 traces, including 10 Ws, 10 Ss, 20 Rs, 20 SUs, and 20 SDs. Figures 4.8 and 4.9 show the accelerometer and the KEH signals, respectively, for the two placements of the datalogger and the five activities.

4.4.4 Features Extraction

Feature extraction is a critical initial step in any classification process. This step is responsible for extracting the hidden information from the raw input data in

order to perform the desired task. A technique of *window overlapping* is usually considered for feature extraction. In this technique, the data traces are subdivided into smaller windows, then the features are extracted from consecutive windows. Using overlapping windows is a common practice to reduce the information loss at the edges of a window.

We used the raw collected data without applying noise filtering techniques. For each of the 80 traces collected in the previous section, we divided each trace into 5-second windows with 50% overlap between consecutive windows. Each window represents an instance for feature extraction and classification. For the hand placement case, we have a total of 262 windows (instances), including 64 Ws, 73 Ss, 54 Rs, 39 SUs, and 32 SDs. For the waist placement case, we have a total of 285 windows (instances), including 66 Ws, 72 Ss, 66 Rs, 42 SUs, and 39 SDs. For each window, we extracted the features presented in Table 4.3.

As the accelerometer generates three time series along the X-, Y-, and Z-axes, some features are extracted from each axis separately (single-axis features) and some are extracted as a combination between the three axes (multiaxial features). Table 4.3 includes nineteen single-axis features and five multiaxial features that are commonly used for accelerometer-based HAR. Table 4.3 shows both time and frequency domain features. For the accelerometer signal, the single-axis features are extracted from each axis separately giving a total of 57 features, in addition to the 5 multiaxial features extracted as a combination between the three axes, giving a total of 62 features. On the other hand, the KEH transducer generates one series of AC voltage, giving a total of 19 single-axis features. Overall, we extracted a total of 62 features from the accelerometer signal and 19 features from the KEH signal. We call this the Original Feature Set (OFS) of both accelerometer and KEH data.

Since the accelerometer is generally a vibration sensor and KEH is a vibration generator (the conversion of ambient vibrations generated from human motion into electrical energy), we proposed to use the seven features presented in Table 4.4. These features are used to quantify the vibration level which is a characteristic describing the severity of the vibration. Therefore, we call it the Vibration Feature Set (VFS). All the features in the VFS are single-axis features which are extracted

Table 4.3: The original feature set (OFS) of both accelerometer and KEH data.

		Feature	Abbreviation	Description
Single axis features	Time-domain features	mean	mean	the central value of a window of samples.
		variance	var	a measure the amount of variation or dispersion from the mean.
		standard deviation	std	the square root of the variance.
		minimum	min	the minimum value in a window of samples
		maximum	max	the maximum value in a window of samples
		range	range	the difference between the maximum and the minimum values in a window of samples
		Absolute Mean	absMean	average of absolute values,
		Coefficient of Variation	CV	ratio of standard deviation and mean times 100; measure of signal dispersion,
		Skewness	skew	measure of asymmetry of the probability distribution of the window of samples,
		Kurtosis	kurt	measure of peakedness of the probability distribution of the window of samples,
		Quartiles: 1st Quartile: 2nd Quartile 3rd Quartile	Q1 Q2 Q3	measures the overall distribution of the signal samples over the window,
		Inter Quartile Range	IQR	the difference between the upper (third) quartile and the lower (first) quartile of the window of samples; also measures the dispersion of the signal samples over the window,
		Mean Crossing Rate	MCR	measures the number of times the signal crosses the mean value; captures how often the signal varies during the time window,
		Absolute Area	absArea	the area under the absolute values of the signal samples. It is the sum of absolute values of the signal samples over the window,
	Frequency-domain features	Dominant Frequency Ratio	DFreqR	it is calculated as the ratio of highest magnitude FFT coefficient to sum of magnitude of all FFT coefficients.
		Energy	FDEnergy	it is a measure of total energy in all frequencies. It is calculated as the sum of the squared discrete FFT component magnitudes. $$Energy = \sum_{i=1}^{L/2} F_i^2 \qquad (4.3)$$ where F_i is the magnitude of FFT coefficients.
		Entropy	FDEntropy	captures the inpurity in the measured data. It is calculated as the information entropy of the normalized values of FFT coefficient magnitude. $$Entropy = -\sum_{i=1}^{L} Fn_i log_2(Fn_i) \qquad (4.4)$$ where Fn_i is the normalized value of FFT coefficient magnitude.
multiaxes features	Time-domain features	Total absolute area	TAA	sum of the absolute area of all three axis. $$totalAA = \sum_{i=1}^{L} |Acc_x| + |Acc_y| + |Acc_z| \qquad (4.5)$$ where $|Acc_x|$, $|Acc_x|$, and $|Acc_x|$ are the absolute values of the three axes of the accelerometer x, y, and z respectively. L is the length of the window.
		total magnitude area	MMA	the signal magnitude of all accelerometer signal of three axis averaged over the time window. $$totalMA = \frac{\sum_{i=1}^{L} \sqrt{Acc_x^2 + Acc_y^2 + Acc_z^2}}{L} \qquad (4.6)$$
		Correlation Corr(X,Y) Corr(X,Z) Corr(Y,Z)	CorrXY CorrXZ CorrYZ	it measures the dependence relationship between two axes of the accelerometer signal

Table 4.4: The vibration feature set (VFS) which is added to quantify the vibration level in both accelerometer and KEH data.

Feature	Abbreviation	Description
root mean square	RMS	it is the square root of the arithmetic mean of the squares of the values. The RMS is a measurement of the effective energy content in a the signal.
peak-to-peak	PktPk	it is the difference between the maximum peak value and the minimum peak value. It indicates the maximum excursion of the signal.
peak-to-peak difference	PktPkDiff	The difference between the maximum difference between peak values and the minimum difference between peak values of the sinusoidal wave. It indicates the maximum excursion of the time periods.
mean Peak	meanPk	The mean value of the differences between all the peak values. It quantifies the average variation level of the values of the signal.
mean Peak Distance	meanDisPk	The mean value of the differences between the all the distances (time periods) between peak values. It quantifies the average variation level of the time periods of the signal.
maximum Peak	maxPk	The maximum value of the differences between all the peak values. It quantifies the maximum variation level of the time periods of the signal.
maximum Peak Distance	maxDisPk	The maximum value of the differences between all the distances (time periods) between peak values. It quantifies the maximum variation level of the time periods of the signal.

separately from each axis of the accelerometer signal and from the single axis KEH signal. Adding the VFS to the OFS gives a total of 83 features extracted from the accelerometer signal and a total of 26 features extracted from the KEH signal.

4.4.5 Feature Selection

The purpose of this subsection is to first assess the discriminating capacity of the KEH signal for HAR, and second to select the most useful features which can be used for HAR, discarding the redundant and non-informative ones. We employ two classical techniques for feature selection [74], Information Gain (IG) and Correlation Feature Selection (CFS).

- Information Gain: IG is usually used to determine how well a given feature can accurately classify the considered activities. It is usually used in decision tree analysis to select the candidate feature for branching at each step, while growing the tree [75]. The IG of feature f_i measures the expected reduction in entropy caused by partitioning the instances according to this feature. The calculation of information gain is based on calculating the entropy of a set of features S, from:

$$H(S) = -\sum_{i=1}^{n} p_i \log_2 p_i \qquad (4.7)$$
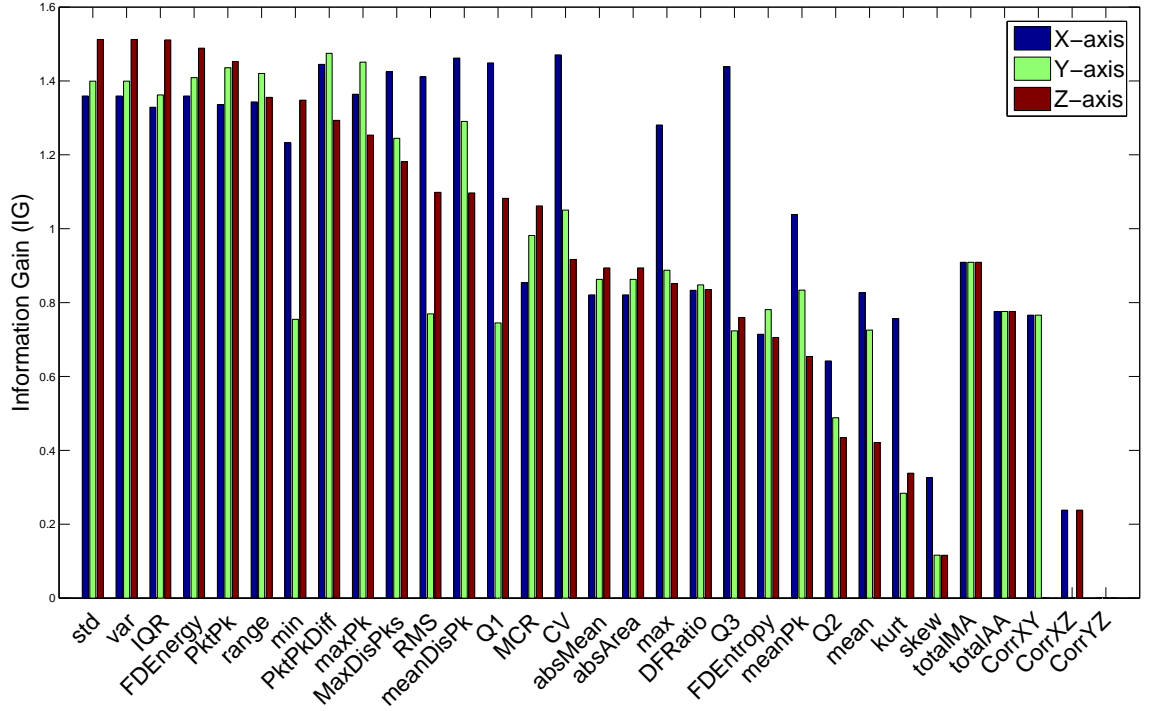
Figure 4.10: Information Gain Accelerometer Hand.

where n is the number of activity classes (in our case, 5 activity classes) and p_i is the proportion of all traces belonging to the ith class. The information gain is then calculated using:

$$Gain(S, f_i) = H(S) - \sum_{v \in Values(f_i)} \frac{|S_v|}{|S|} H(S_v) \qquad (4.8)$$

where S_v is the subset of S for which feature f_i has a value v (i.e., $S_v = s \in S | Values(f_i) = v$) and $|S|$ denotes the cardinality of the set S.

Figures 4.10 and 4.11 show the IG of the combined feature set (OFS+VFS) for the accelerometer data for hand and waist placements, respectively. The IG of the single-axis features is shown separately for X-, Y-, and Z-axes, while the multiaxial features have the same IG value for each axis. Figure 4.12 shows the IG of the combined feature set (OFS+VFS) for the KEH data for both hand and waist cases.

It is interesting that the ranking of features based on IG is different for KEH
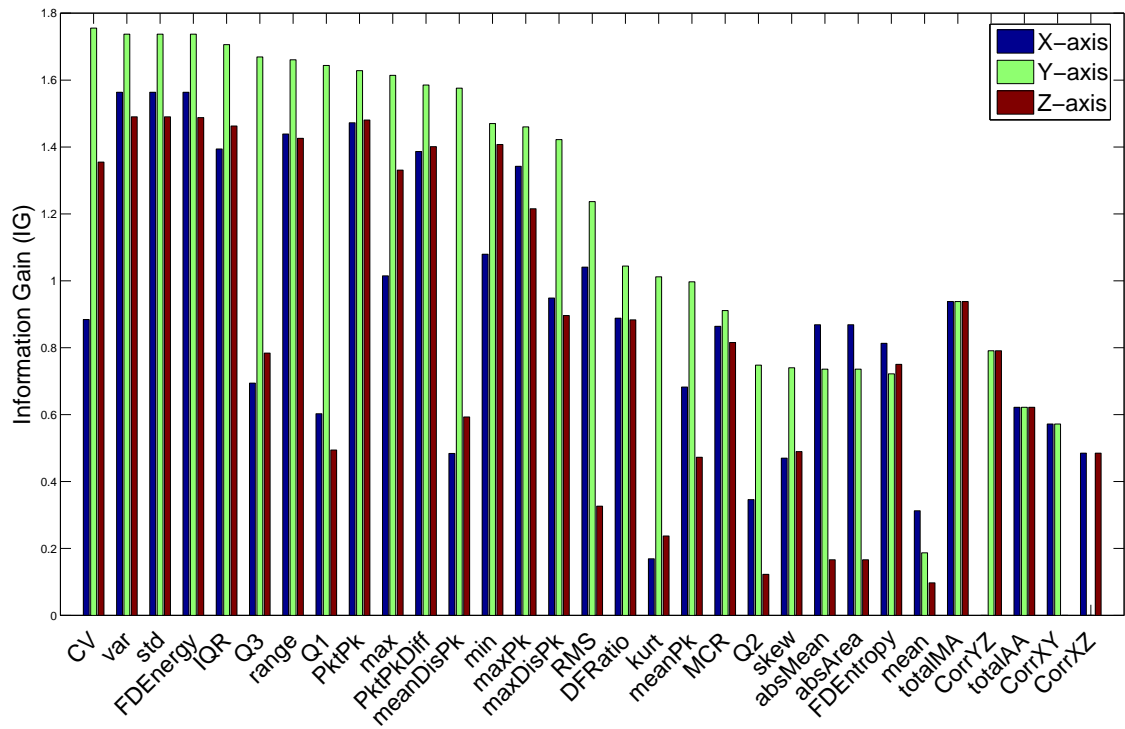
Figure 4.11: Information Gain Accelerometer Waist.
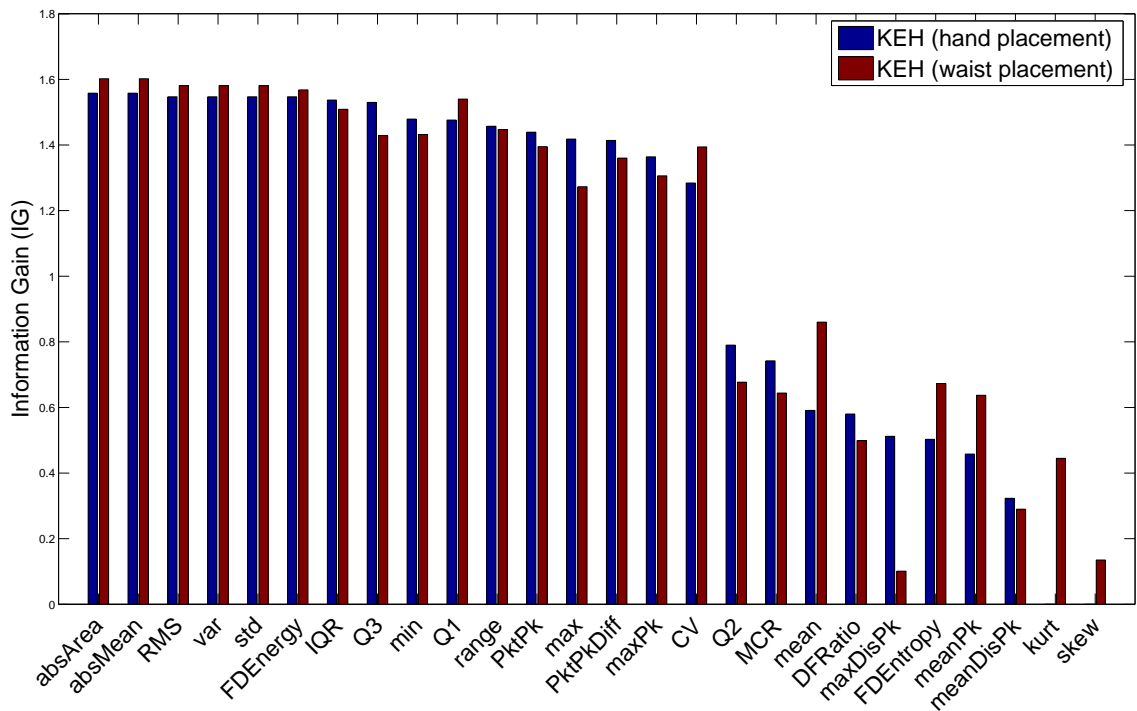
Figure 4.12: Information Gain HARKE, Hand and Waist.

and the accelerometer; it is even different for different placements. In the waist placement case, for both accelerometer and KEH results, no features with zero information gain were identified. In the hand placement case, the accelerometer results identified the CorrYZ feature with zero information gain, however, the KEH results found the Skewness and Kurtosis features to have zero information gain. A reduced feature set is usually obtained by discarding features with zero information gain. It is clear that the IG analysis had no effect in reducing the number of features but it confirms that, like the accelerometer signal, the KEH signal contains rich information that can be used for HAR.

- Correlation Feature Selection: The set of n features is partitioned to subsets of size k, $1 \leq k \leq n$, CFS then evaluates the worth (or merit) of each subset of features, M_S, using:

$$M_S = \frac{k\bar{r_{cf}}}{\sqrt{k + k(k - 1)\bar{r_{ff}}}} \tag{4.9}$$

where, $\bar{r_{cf}}$ is the mean feature-class correlation ($f \in S$), and $\bar{r_{ff}}$ is the average feature-feature inter-correlation. The merit score takes into account the usefulness of individual features for predicting the class label. Broadly speaking, feature subsets with high average correlation to the class and low inter-correlation receive higher merit scores. CFS, then acts as a simple filter algorithm that ranks feature subsets having a reasonably high merit, according to a search strategy based on a correlation evaluation function, and the optimal subset is the one that satisfies the CFS criterion in:

$$CFS = \max_{S_k} \left[\frac{r_{cf_1} + r_{cf_2} + \cdots + r_{cf_k}}{\sqrt{k + 2(r_{f_1 f_2} + \cdots + r_{f_i f_j} + \cdots + r_{f_k f_1})}} \right] \tag{4.10}$$

where Pearson's correlation coefficient is used to calculate the correlation between pairs of features ($r_{f_i f_j}$) and Spearman's correlation coefficient for each feature with the target (r_{cf_i}). More details about CFS are given in [76].

The reduced subsets of features, based on the CFS algorithm, for both accelerometer and KEH signals in both placement cases are presented in Table 4.5. For the accelerometer data, the number of features is reduced from 83

Table 4.5: The resulted feature sets of the Correlation Feature Selection (CFS) algorithm.

Accelerometer-based HAR		HARKE	
Hand Placement	Waist Placement	Hand Placement	Waist Placement
Hand	Waist	Hand	Waist
varZ	CVY	absArea	absMean
stdZ	VarY	var	absArea
IQRZ	FDEnergyY	IQR	RMS
PktPkDiffY	IQRY	Q3	Q1
CVX	Q3Y	min	range
meanDismPkX	Q1Y	Q1	min
PktPkZ	MaxY	range	Q3
MaxPeaksY	PktPkDiffY	PktPk	PktPk
PktPkDiffX	meanDisPksY	max	maxPk
RMSX	stdX	PktPkDiff	
MaxPeaksX	FDEnergyX		
IQRY	RMSX		
MinZ	DFRatioX		
meanDisPkY	skewY		
meanDisPkZ	skewZ		
Q1Z	CorrXZ		
CVY			
totalMA			
absArea			
CorrXY			
MinY			
SkewX			

to 22 in the hand placement case and 16 in the waist placement case. For the KEH data, the number of features is reduced from 26 to 10 in the hand placement case and 9 in the waist placement case. These results show that the CFS algorithm is more effective than the IG algorithm in reducing the number of features. But whether this reduction affects the recognition accuracy or not will be investigated in the coming subsections.

4.4.6 Classification

Based on the success of other researchers in classifying a range of human activities using accelerometer data, we chose the following five classifiers to evaluate the recognition accuracy of HARKE and compare it with accelerometer-based HAR.

- Decision Tree (DT)

  DT is a powerful and popular tree-based tool for classification and prediction [77]. The classification process starts at the root of the tree and grows sequentially until reaching a leaf node. The central focus of the tree growing algorithm is testing and selecting the attribute with the most inhomogeneous

class distribution, based on its information gain, explained in the feature selection subsection in this section. A well-known algorithm, which has been widely used for building decision trees over the years, is C4.5 [78]. In this algorithm, pruning is used to reduce the tree to its optimal size, without reducing predictive accuracy. A tree that is too large risks overfitting the training data and poorly generalizing to new samples. A small tree might not capture important structural information about the sample space [79].

- K-Nearest Neighbour (KNN)

  KNN is one of the simplest machine learning algorithms. It is a type of instance-based learning, or lazy learning where the function is only approximated locally and all computation is deferred until classification [80]. The KNN algorithm classifies new examples based on identifying the k-nearest example(s) in the training set of features according to some distance metric (in WEKA, the Euclidean distance is used) and then taking the majority vote. The parameter k is a positive integer, typically small. If k=1, then the object is simply assigned the class of its nearest neighbour. The best choice of k depends upon the data.

- Multilayer Perceptron (MLP)

  MLP represents the most prominent and well researched class of Artificial Neural Network techniques in classification, implementing a feedforward and supervised paradigm [81]. Although many types of neural network techniques can be used for classification purposes, MLP remains one of the fastest tools for neural network studies [82] [83]. MLP consists of several layers of nodes, interconnected through weighted acyclic arcs from each preceding layer to the following, without lateral or feedback connections. Each node calculates a transformed weighted linear combination of its inputs.

- Support Vector Machine (SVM)

  SVM is a classifier method that relies on the concept of decision planes that

define decision boundaries. It works by constructing hyperplanes in a multidimensional space that separate instances having different class labels. A subset of training points called support vectors is used in the decision function. Different decision (kernel) functions can be specified. SVM is known to be effective in high dimensional spaces. However, if the number of features is much greater than the number of instances, the method is likely to give poor performance.

- Naïve Bayes (NB)

  NB classifier employs a simplified version of Bayes formula [84], with strong (naïve) independence assumptions, to decide to which class a new instance belongs. The posterior probability of each class is calculated, given the feature values present in the instance; the instance is assigned to the class with the highest probability. Equation (4.11) shows the NB classifier, which makes the assumption that feature values are statistically independent within each class.

$$c_{NI} = \arg\max_{c_i \in C} P(c_i) \prod_j P(f_j|c_i) \qquad (4.11)$$

  Where c_{NI} is the class of the new instance, $C = (c_1, c_2, \ldots, c_n)$ is the classes, and f_j is the feature value.

The following section presents the results of applying the previously discussed classifiers to evaluate the performance of HARKE and compare it to accelerometer-based HAR.

4.5   Results

In this section, we evaluate the performance of HARKE using the previously mentioned classifiers against conventional accelerometer-based HAR for the two placement cases, hand and waist. First, we show the performance of both HARKE and accelerometer-based HAR when the OFS, shown in Table 4.3, is used. Next, we

explore if adding the VFS, shown in Table 4.4, to the OFS yields an improvement in the performance. Then, we investigate whether the use of the CFS reduced feature set, shown in Table 4.5, affects the recognition performance of both HARKE and accelerometer-based HAR. To train and test the classifiers with different datasets, we apply a k-fold cross validation scheme [85]. The entire dataset is divided into k sets, where $k - 1$ of them are used for training and one set for testing. This is repeated k times and then the average of the results is reported. We used $k = 10$.

Table 4.6 compares the accuracies of accelerometer-based HAR and HARKE when the OFS is used for both hand and waist placement cases. Table 4.7 compares the accuracies of accelerometer-based HAR and HARKE when the combined feature set of OFS and VFS is used for both hand and waist placement cases. Table 4.8 compares the accuracies (%) of accelerometer-based HAR and HARKE when the reduced feature set of the CFS algorithm is used for both hand and waist placement cases. For each case, the highest accuracy obtained is shown in bold.

We make the following observations.

- Although MLP and DT classifiers give slightly better accuracies in a few cases, in most cases the KNN classifier achieves the highest accuracies for both accelerometer-based HAR and HARKE.

- Table 4.6 shows that, using the KNN classifier and the OFS, the recognition accuracies of accelerometer-based HAR are 95.44 % and 99.64% for hand and waist placement cases, respectively. The corresponding recognition accuracies of HARKE are 70.21 % and 83.51 %.

- Table 4.7 shows that adding the VFS to the OFS has negligible impact on the performance of accelerometer-based HAR. However, it improves HARKE accuracies noticeably from 70.21 to 80.11% for the hand placement case and 83.51 % to 87.36 % in the waist placement case, when the KNN classifier is used.

- Table 4.8 shows that using the reduced feature set of the CFS algorithm does not reduce the recognition accuracies of accelerometer-based HAR and

Table 4.6: Comparing the accuracies (%) of accelerometer-based HAR and HARKE when the original feature set (OFS) is used for both hand and waist placement cases.

Classifier	Accelerometer-based HAR		HARKE	
	Hand placement	Waist placement	Hand placement	Waist placement
KNN	**95.44**	**99.64**	**70.21**	**83.51**
MLP	**95.78**	98.95	74.39	82.78
DT	87.02	90.59	**76.34**	79.27
SVM	90.43	96.86	72.89	75.74
NB	84.69	88.44	70.58	69.15

Table 4.7: Comparing the accuracies (%) of accelerometer-based HAR and HARKE when the combined feature set of OFS and VFS is used for both hand and waist placement cases.

Classifier	Accelerometer-based HAR		HARKE	
	Hand placement	Waist placement	Hand placement	Waist placement
KNN	**95.81**	**99.64**	**80.11**	**87.36**
MLP	95.78	98.60	73.26	87.71
DT	88.19	91.27	79.76	80.34
SVM	88.89	98.24	72.89	79.66
NB	85.44	88.09	70.58	70.90

HARKE in either placement cases. This is because the CFS algorithm tries to reduce the number of features by removing the redundant features which have high correlation with other features. This result shows that the CFS algorithm is effective in reducing the number of features significantly with a noticeable effect on recognition accuracy.

- In all cases, we found that waist placement gives higher classification accuracies than hand placement for both accelerometer-based HAR and KARKE. This is quite meaningful because in waist placement case, the device is more attached to the body and hence it captures the activity more accurately.

- Our results show that, in all cases, accelerometer-based HAR achieves better performance than HARKE. There is about 18% gap in classification performance between accelerometer-based and HARKE for hand placement when the KNN classifier is used. The gap is 15% for waist placement.

To better assess the performance of HARKE against accelerometer-based HAR

Table 4.8: Comparing the accuracies (%) of accelerometer-based HAR and HARKE when the reduced feature set of the CFS algorithm is used for both hand and waist placement cases.

Classifier	Accelerometer-based HAR		HARKE	
	Hand placement	Waist placement	Hand placement	Waist placement
KNN	**95.01**	*99.15*	**80.19**	**86.08**
MLP	93.00	98.09	71.98	80.27
DT	86.33	93.26	74.93	77.89
SVM	88.38	87.51	71.72	72.41
NB	88.54	91.51	70.80	73.63

and identify the source of the performance gap between them, we use the confusion matrix tool. The confusion matrices of accelerometer-based HAR for hand and waist placements are presented in Tables 4.9 and 4.10, respectively. The confusion matrices of HARKE for hand and waist placements are presented in Tables 4.11 and 4.12, respectively. The true positive (TP) rate is shown in the last column in all tables. We make the following observations from the confusion matrices.

- Standing (S) and running (R) activites are identified with very high (100%) accuracy in both placement cases for both the accelerometer-based HAR and HARKE.

- There is confusion of the three activities, W, SU and SD, due to their high similarity which imposes challenges in distinguishing one from another.

- The performance of HARKE is reduced due to the confusion of those three activities and hence the TP rate is reduced.

- Accelerometer-based HAR performs better with the three activities, W, SU and SD, and hence the TP rate is better.

- The confusion of the three activities, W, SU and SD, is reduced for both accelerometer-based HAR and HARKE when waist placement is considered. As mentioned previously, this is because the waist placement means the device is attached to the lower part of the body and hence it recognises the activities more accurately.

Table 4.9: Confusion Matrix of accelerometer-based HAR for hand placement using the CFS reduced feature set when the KNN classifier is used.

		Classified as					TP Rate
		W	R	S	SU	SD	
	W	64	0	0	0	0	1
	R	0	54	0	0	0	1
Actual Activity	S	0	0	73	0	0	1
	SU	1	0	0	34	4	0.75
	SD	1	0	0	7	24	0.95

Table 4.10: The confusion matrix of accelerometer-based HAR for waist placement using the CFS reduced feature set when the KNN classifier is used.

		Classified as					TP Rate
		W	R	S	SU	SD	
	W	66	0	0	0	0	1
	R	0	66	0	0	0	1
Actual Activity	S	0	0	72	0	0	1
	SU	0	0	0	42	0	1
	SD	2	0	0	0	37	0.95

In the next section, we discuss the main differences between accelerometers and KEH transducers which may provide a better understanding of the performance of both accelerometer-based HAR and HARKE.

4.6 Discussion

Both accelerometers and KEH transducers rely on the same principle, however, they serve different purposes. Accelerometers are used to sense vibration, but KEH

Table 4.11: The confusion matrix of HARKE for hand placement using the CFS reduced feature set when the KNN classifier is used.

		Classified as					TP Rate
		W	R	S	SU	SD	
	W	48	0	0	12	4	0.75
	R	0	54	0	0	0	1
Actual Activity	S	0	0	73	0	0	1
	SU	17	0	1	18	3	0.46
	SD	10	0	0	6	16	0.5

Table 4.12: The confusion matrix of HARKE for waist placement using the CFS reduced feature set when the KNN classifier is used.

		Classified as					TP Rate
		W	R	S	SU	SD	
	W	61	0	0	2	3	0.92
	R	0	66	0	0	0	1
Actual Activity	S	0	0	72	0	0	1
	SU	5	0	1	29	7	0.69
	SD	9	3	0	9	18	0.46

is used to generate electrical energy from the wasted vibration energy. Generally speaking, accelerometers require some means for inferring acceleration from sensed vibration.

4.6.1 Capacitive Accelerometers Vs. KEH Transducers

In this work, we used an analog accelerometer made by Freescale. This accelerometer relies on a capacitive sensing mechanism using silicon micromachined beams. In a capacitive accelerometer, a capacitor is formed by a stationary plate (the housing which moves with the base acceleration) and a moving plate attached to the seismic mass. The distance between these plates determines the capacitance, which can be monitored to infer acceleration (change in capacitance related to acceleration). Capacitive accelerometers are capable of measuring constant acceleration such as gravity as well as slow transient and periodic acceleration.

On the other hand, the KEH transducer used in this work, which is made by Mide Technology, uses a piezoelectric transducer to convert kinetic energy into electricity. It employs a cantilever that attaches to a piezoelectric crystal. When vibrations set the cantilever in motion it generates alternating electrical current. One feature of the piezoelectric material is that it cannot measure constant force such as gravity which explain the performance gap between accelerometer-based HAR and HARKE.

4.6.2 Accelerometer (3-axis) versus KEH Volture (1-axis)

A triaxial accelerometer provides X, Y, and Z components of acceleration, whereas the KEH transducer gives a 1-axial AC voltage output. A triaxial accelerometer is fundamentally advantaged in separating similar human activities such as going up and down stairs due to the multi-dimensional measurement of the motion, hence achieving high accuracy for our considered activity set. By measuring acceleration in three dimensions, new discriminating opportunities arise, which are not possible with a single-dimensional AC-voltage measurement.

The advantage of a triaxial accelerometer over a single-dimensional harvested power signal has been illustrated in the previous chapter, showing clear discriminating patterns when the three axes of the accelerometer are considered. To show the effect of using only single-axis data on the performance of accelerometer-based HAR, we run the K-nearest neighbour classifier on the features extracted separately from each axis and show the results in Table 4.13. We found that the accuracy of accelerometer-based HAR in the hand placement case is reduced from 95% when triaxial accelerometer data is used to 83% on average when single-axis accelerometer data is used.

Table 4.13: Accelerometer-based HAR accuracies (%) for single-axis accelerometer data in the hand placement case when the K-nearest neighbour classifier and the OFS are used.

Data	Accuracy (%)
Accelerometer X-axis	86.64
Accelerometer Y-axis	79.39
Accelerometer Z-axis	83.97
Average over three axis	83.33

4.7 Conclusion

Our analysis shows that accelerometer power consumption is a major obstacle for realising HAR in self-powered energy-harvesting wearables. In this chapter, we experimentally validated HARKE, which infers human activity directly from energy harvesting patterns without using an accelerometer. We show that HARKE con-

sumes only a small fraction of energy compared to the conventional accelerometer-based HAR. Using off-the-shelf products, we built a datalogger prototype which enabled us to record the generated signals of a commercially available KEH transducer. We also added an accelerometer to the prototype to compare the performance of HARKE against accelerometer-based HAR. We collected extensive data from ten different subjects, five different activities, and two different placements of the device on the body.

Our experimental results demonstrated that HARKE is as accurate as accelerometer based HAR for dissimilar activities such as standing, walking, running. However, the performance of HARKE is reduced for similar activities such as ascending and descending stairs. This confirms the validation of HARKE using mathematical modelling presented in the previous chapter. The accelerometer is fundamentally advantaged in distinguishing similar human activities due to its multi-dimensional measurements (triaxial). An interesting future direction would be to investigate the possibility of extracting multi-dimensional (multi-axial) information from the kinetic power signal. One possibility is to consider energy harvesting methods capable of harvesting kinetic power separately from each components of human motion. This would yield three separate power signals, one for each axis, enabling more advanced training of the classifier, similar to a HAR based on a triaxial accelerometer.

Chapter 5

Energy Neutral Self-powered Wireless HARKE

5.1 Introduction

Human activity recognition (HAR) using wearable sensors has become a topic of intense research due to its immense economic benefits in health and medical domains [86, 87, 88]. Deployments of such systems have already begun, such as Fitbit, Apple Watch, and Google Glass. It is predicted that the wearable market for health and fitness monitoring will grow and reach 70 billion dollars by 2025 [40]. Almost all existing wearable products are powered by batteries. While battery technology has improved over the years, users are still required to recharge them frequently, which is inconvenient and impractical for many elderly users, who may have to critically depend on such systems. Due to this, researchers are now investigating kinetic energy harvesting solutions [17, 18, 19], which will allow continuous and permanent operation of wearable sensors with no need for battery recharge or replacement.

The most fundamental issue with kinetic energy harvesting is that the amount of power that can be practically harvested from human motion is insufficient to power all necessary functions of a wearable device. A typical wearable device will need power for accelerometer measurements at a high sampling rate, which would consume most of the limited power that can be possibly harvested in a small form factor

[89], leaving insufficient power for processing and communication. Self-powering an activity-monitoring wearable sensor is therefore a challenging problem that requires innovative sensing and communication solutions.

In the previous two chapters, we showed that HAR is possible using only the piezoelectric energy harvesting (PEH) generated patterns. Although this is an important step forward for realising self-powered activity monitoring, it still cannot guarantee *system energy neutrality*. Activity classification using PEH signals would still consume most of the power in the device, and if classification is done in a server then energy consumption due to communication of massive amounts of PEH voltage data would challenge energy neutrality. How to guarantee energy neutral operation for continuous activity monitoring using energy-harvesting wearable sensors therefore remains an unsolved problem.

In this chapter, we build on our previous work, but propose a new framework based on Bayesian Decision Theory [90] that guarantees energy neutrality for activity recognition with wearable sensors. The proposed Bayesian framework utilizes a capacitor to store incoming energy harvested from a PEH for a fixed-length time window and then uses all the stored energy to transmit an unmodulated signal, called an *activity pulse*. Since different activities generate power at different rates, the transmission and receiving signal strengths also differ, so those signal strengths can be used to classify the activities. Energy neutrality is guaranteed because the transmission power of the activity pulse uses only the energy harnessed in the last time window; no additional energy is required to power any sensing or classification components in the wearable device.

The contributions of this chapter can be summarised as follows:

- We propose an energy-neutral HAR framework which uses the accumulated energy within a fixed interval to transmit an activity pulse. The receiver uses Bayesian decision theory to classify activities based on the detected signal strength of the received pulse. Neither accelerometer nor classifier is required on the wearable devices, which therefore guarantees the system energy-neutrality.

- We show that the accumulated energy within a fixed time window is a random variable that follows a Gaussian distribution where different activities have different values of the statistical parameters.

- We validate our proposed energy-neutral HAR framework theoretically and experimentally.

- Using long-length traces (up to 700 seconds) collected from a healthy subject by a PEH wearable device coupled with a Bluetooth prototype, we were able to achieve an overall accuracy of 91% when a distance of 30 cm between the transmitter and the receiver is considered. We also point out that the overall accuracy falls to 85% and 65% when the distance is increased to 60 cm and 100 cm, respectively.

The rest of the chapter is structured as follows. Related work is reviewed in Section 6.2. Section 5.3 explains our proposed energy-neutral HAR framework. Section 5.4 presents the data collection campaign. Section 5.5 introduces the Bayesian decision theory for human activity recognition, and defines the mathematical model. We validate our proposed framework theoretically in Section 5.6. The experimental validation is presented in Section 5.7. We conclude the chapter in section 5.8.

5.2 Related Work

Almost all existing wearable devices are battery-operated, therefore, reducing power consumption is considered the most challenging task for continuous activity recognition using wearable sensors. Existing studies in power-efficient human activity recognition achieve energy savings by optimizing the trade-off between classification accuracy and energy efficiency. Krause et al. [91] studied the trade-off between power consumption and classification accuracy for the eWatch wearable device. They proved that the deployment lifetime of the device can be extended by selecting the optimal sampling strategy without losing accuracy. Their results indicate the existence of a sampling threshold, below which accuracy falls dramatically. They also suggest using a sampling rate equal to the sampling threshold to save energy.

Similar results are given in [89], in which the authors use commercial smartphone to find the accuracy for different sampling frequencies. In [92], the authors pointed out that the trade-off is activity-specific, and introduced the A3R algorithm, which adapts the sampling frequency and classification features in real time, based on the activity type.

Instead of managing the sampling rate, many projects achieve energy efficiency by reducing feature set complexity, because an imprudent selection of features can also result in high energy consumption. In the work of Palmerini et al. [93], a feature selection algorithm was implemented for Parkinson's disease (PD) detection. The algorithm maximises the robustness of feature selection in the identification of a subset of measures that classifies the behavior of PD and control subjects [93]. More recently, in [94] the authors introduced the notion of power-aware feature selection, and proposed a graph-based model to characterise the computing complexity of individual features.

Although it is possible to achieve a longer lifetime of continuous activity recognition by applying the previously mentioned methods, battery recharge or replacement is still needed. Thus, researchers are now investigating the kinetic energy harvesting solutions to self-power wearable devices [17, 18, 19]. Unfortunately, the power that can be practically harvested from human activities is insufficient to power all necessary functions of wearable devices [95]. In a more recent work [89, 95], we proposed the idea of using the power generation features of the PEH to classify human activity. Although it is the first attempt to achieve self-powered activity monitoring, it still cannot guarantee system energy neutrality because classification onboard the device still consumes much power. In contrast, our approach ensures the system energy-neutrality by removing the classification component from the wearable device, and monitoring the activity using only the power of the energy harvester.

5.3   Proposed Energy-neutral HARKE Framework

Fig. 5.1 shows our proposed architecture, which achieves the system energy neutrality. The idea behind our proposed architecture is that different activities produce
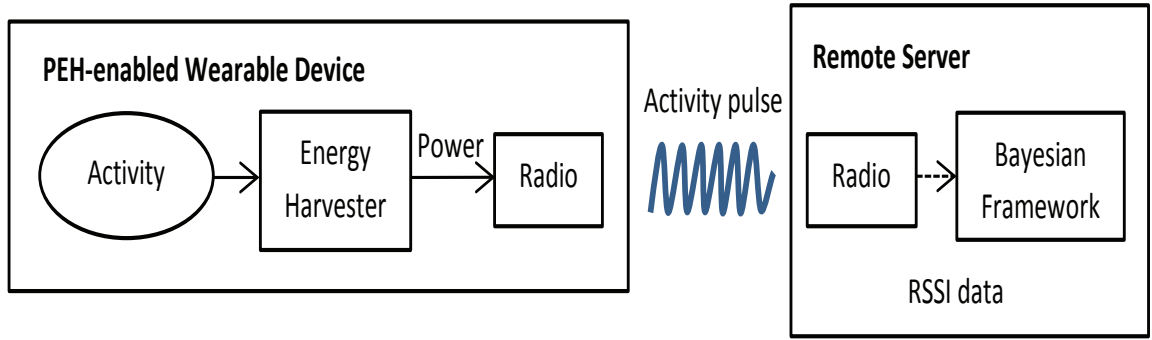
Figure 5.1: Our proposed energy-neutral HARKE framework.

different amounts of harvested power. We assume that the harvested power is usually accumulated in a capacitor for a certain time. By using all the stored harvested energy to power the radio component, to transmit an unmodulated signal called an *activity pulse*, the transmission power of this activity pulse will be affected by the power harvested from the activity. Thus, the transmitted and received signal strengths of the activity pulse differ for different activities.

As a consequence, the signal strength can be used as a feature to recognize the activity. Assuming that the distributions of the signal strength of the activities are known, then the Bayesian decision theory can be used for HAR, based on the observed signal strength of the activity pulse. Bayesian decision theory is a widely used statistical approach which is usually used for decision making and pattern recognition [90]. Our proposed architecture guarantees energy neutrality because the transmission power of the activity pulse uses only the amount of accumulated energy in the last time window, and no additional energy is required to power any sensing or classification components in the wearable device.

5.4 Energy Harvesting Data Collection

We used the datalogger presented in Chapter 4 to collect PEH power signals. The data logger includes a piezoelectric energy harvesting product from MIDÈ Technology called Volture, which provides AC voltage as its output. An Arduino Uno was used as a micro-controller device for sampling the data from the Volture. A

sampling rate of 1 KHz was used for data collection. The sampled data was saved on an 8GB microSD card.

We collected our data from a healthy subject. The subject was asked to hold the datalogger in the hand and perform five different activities with the natural speed: standing (S), walking (W), running (R), stairs-up (SU), and stairs-down (SD). The subject was asked to stop and wait a few seconds after an activity and before starting the next activity. To avoid mislabeling during the data collection, we used a switch to control the start and stop of data collection at the beginning and end of each activity. Since we need to infer the probability distributions that the different activities follow, long activity traces were required to raise the accuracy of the fitted distributions for the Bayesian analysis. Therefor, we collected over 700 seconds of data for each of the five activities at a sampling frequency of 1000 Hz.

The output of the datalogger is AC voltage signal. To calculate the corresponding PEH power signals, we used Eq. 5.1.

$$Power = \frac{V^2}{R}, \tag{5.1}$$

where V is the output PEH voltage signal, R is the load resistance which is $750K\Omega$. The power signals are then presented in dBm.

Figure 5.2 shows the output PEH power signals for the five activities. The amounts of the harvested power on average are -33, -45, -43, -39, and -55 dBm for running, walking, stairs-up, stairs-down, and standing, respectively. Obviously, the amount of PEH power from human activities is very low, thus the energy neutrality of the system is not guaranteed. The next section presents a version of Bayesian decision theory accommodated to HAR to achieve energy neutrality.

5.5 Proposed Bayesian Framework for HAR

To apply the Bayesian decision theory for HAR, we need to analyse the distributions of the harvested power signals of the activities. Therefore, we first discuss the distributional analysis of our PEH data for the five activities. Next, we describe

(a) Running.

(b) Walking.

(c) Stairs-up.

(d) Stairs-down.

(e) Standing.
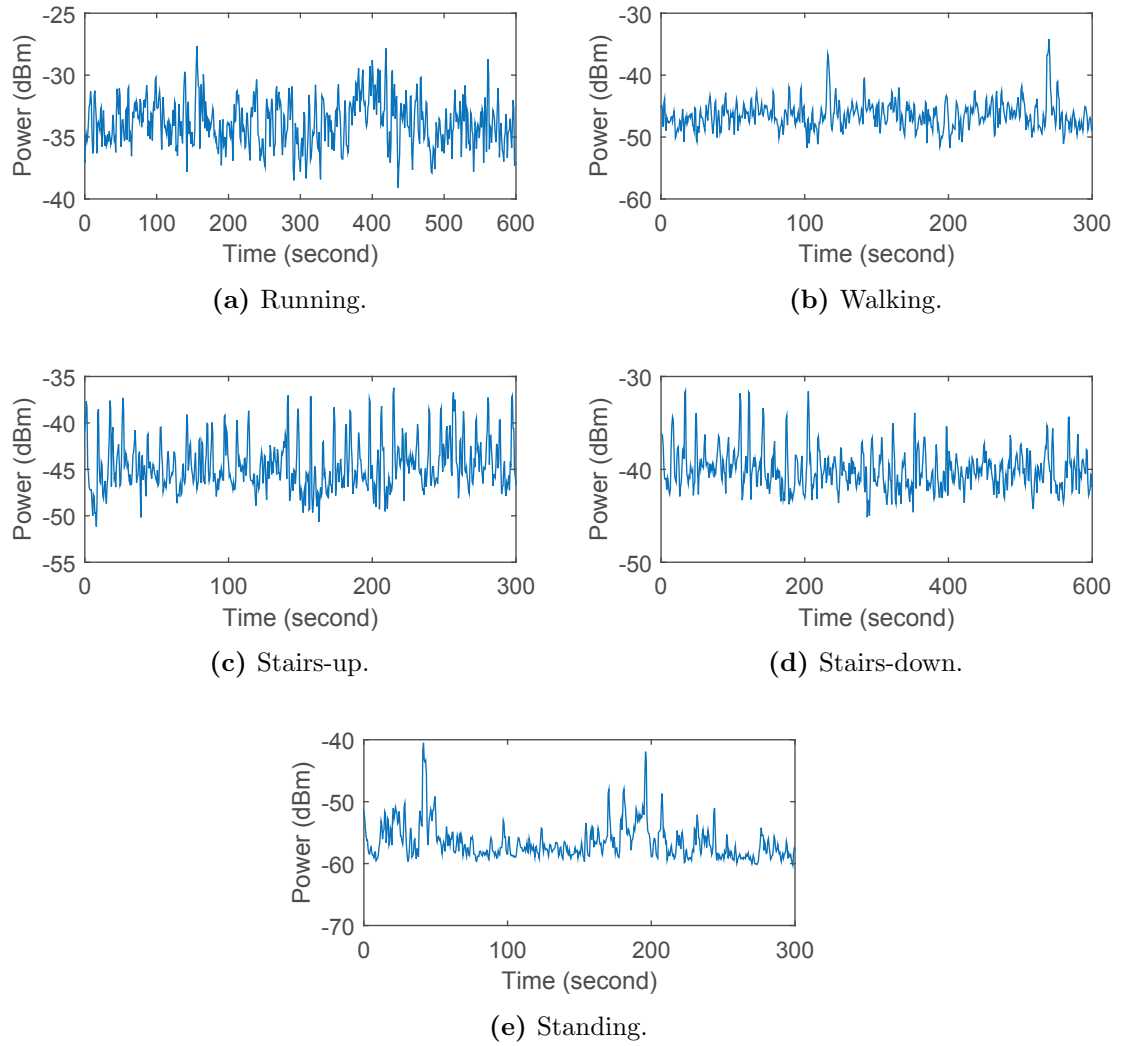
Figure 5.2: The output harvested power signals of our PEH device for the five considered activities. Note that different scales are used in the y axis.

Table 5.1: The estimated means (μ) and standard deviations (σ) of the Gaussian distributions of $Power_H(i)$ using different time windows w.

Activity	window size (second)					
	w = 4		**w = 8**		**w = 10**	
	μ	σ	μ	σ	μ	σ
S	-56.65	2.60	-56.46	2.42	-56.41	2.38
W	-45.71	1.82	-45.58	1.56	-45.53	1.47
R	-33.35	1.63	-33.29	1.42	-33.30	1.38
SU	-43.84	2.03	-43.51	1.14	-43.51	1.10
SD	-39.37	1.51	-39.23	1.08	-39.22	1.02

HAR using Bayesian decision theory, followed by the mathematical modelling of our PEH-based HAR.

5.5.1 Distribution Analysis

For an activity $i \in \mathcal{I}, (i = 1, \ldots, 5)$, we define the amount of harvested power (in dBm) from activity i, $Power_H(i)$, as a random variable. We assume that the $Power_H(i)$ follows a Gaussian distribution with mean μ_i and standard deviation σ_i:

$$Power_H(i) \sim \mathcal{N}(\mu_i, \sigma_i^2) \tag{5.2}$$

This assumption is experimentally validated in this section. Using the power calculations of the collected PEH dataset, we obtained estimates of the statistical parameters, μ_i and σ_i, using different window sizes w. When the sampling frequency used in collecting the data is 1 KHz with a window size of w seconds, $1000 \times w$ observations are used to estimate the average harvested power. The estimates of the statistical parameters for $Power_H(i)$ with different w are shown in Table 5.1. The results indicate that, for all five activities, the estimates of the means μ_i remain stable with the increase of w, while the estimates of σ_i decrease with the increase of w.

Figure 5.3 shows the cumulative distribution functions (CDF) of the experimental data obtained from a ten-second window for all activities. The results indicate that the harvested power, $Power_H(i)$, follows Gaussian distributions with different
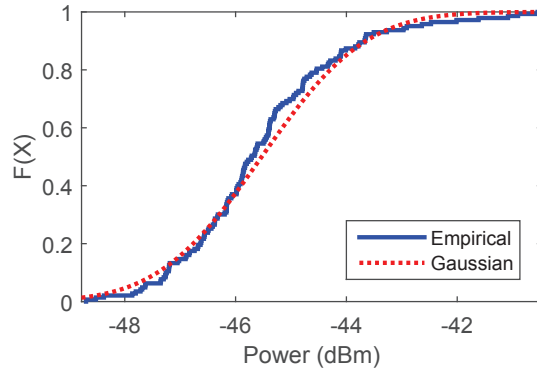
(a) Walking.
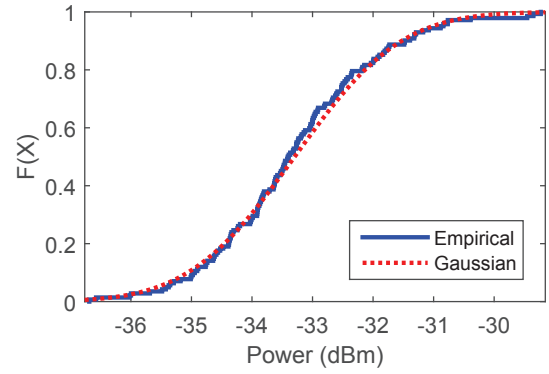
(b) Running.
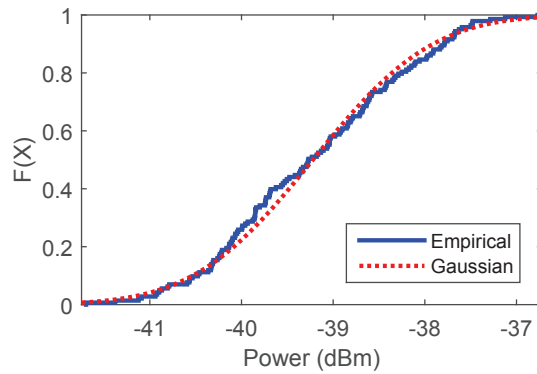
(c) Stairs-Down.
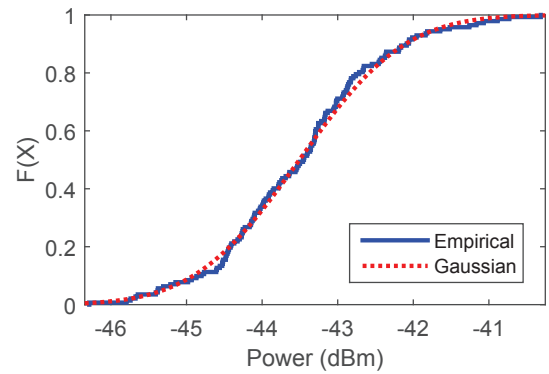
(d) Stairs-Up.
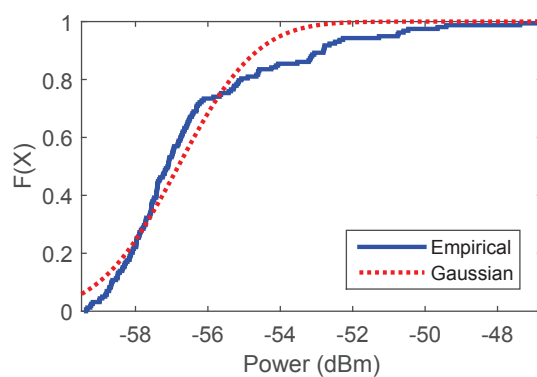
(e) Standing.
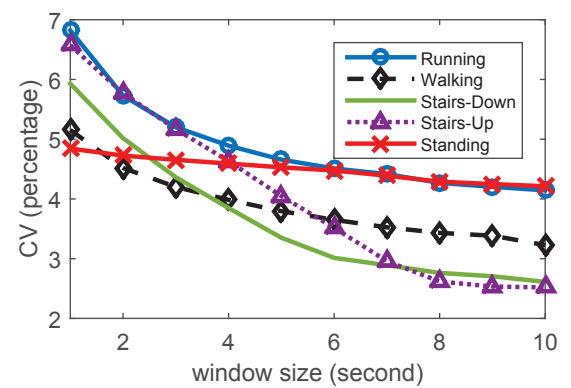
(f) Plots of the CV with different window sizes

Figure 5.3: (a)-(e) The CDFs of the empirical distributions and the Gaussian distributions for the five activities using a window size of 10 seconds. (f) The coefficient of variation (CV) for different window sizes.

parameters. Fig. 5.3(f) plots the coefficient of variation (CV) for all five activities. The CV tends to be stable as the window size increases. This suggests that a window of ten seconds will keep the dispersions in the harvested power stable at an acceptable level.

5.5.2 Bayesian Decision Theory

For each activity $i \in \mathcal{I}, (i = 1, \ldots, 5)$, we assume the signal strength, P, is a random variable. Our objective is to classify a given observation p of P to belong to the activity i. According to Bayesian decision theory, p will be assigned to the activity i if $\mathcal{P}(p \mid i)$ is the largest as shown in Eq. 5.3.

$$\mathcal{P}(p, i) \geq \mathcal{P}(p, j), \quad \forall p \in Ri, \forall j \in \mathcal{I}, \tag{5.3}$$

where $\mathcal{P}(p \mid i)$ denotes the conditional pdf of p given the activity i and R_i is the decision region. Thus, the overall recognition accuracy of each activity using the Bayesian decision rule is obtained using Eq. 5.4 and Eq. 5.5, respectively.

$$\mathcal{A}(overall) = \sum_{i}^{i \in I} \int_{R_i} \mathcal{P}(p, i) dp, \quad p \in R_i \tag{5.4}$$

$$\mathcal{A}(i) = \int_{R_i} \mathcal{P}(p, i) dp, \quad \forall i \in \mathcal{I} \tag{5.5}$$

where,

$$\mathcal{P}(p, i) = \mathcal{P}(p \mid i) \mathcal{P}(i), \quad \forall i \in \mathcal{I} \tag{5.6}$$

Assuming uniform prior probabilities for all activities (i.e., $\mathcal{P}(i) = 0.2, \quad \forall i \in \mathcal{I}$), Eq 5.6 can be rewritten as:

$$\mathcal{P}(p, i) = 0.2 \times \mathcal{P}(p \mid i), \quad \forall i \in \mathcal{I} \tag{5.7}$$

5.5.3   Mathematical Modeling

We define the transmission signal strength of the activity pulse as $Power_{T_X}(i)$:

$$Power_{T_X}(i) = Power_H(i) + 10 \log_{10} K, \tag{5.8}$$

where, K is defined as the transmission power amplification factor, and is affected by the transmission duration of the activity pulse, t_{T_X}, and the accumulation time of the harvested energy in the capacitor, t_{ACC}. Thus, K is obtained by:

$$K = t_{T_X} \times t_{ACC} = \frac{r}{8p} \times t_{ACC}, \tag{5.9}$$

where, r is the data rate used to transmit the activity pulse (in bps), and p is the packet size (in Bytes, where one Byte equals 8 bits). we note when K equals 1, the transmission time of the activity pulse is one second and the transmission power is the accumulated harvested power over a one-second window. Based on the additive property of the Gaussian distribution, $Power_{T_X}(i)$ is given by:

$$Power_{T_X}(i) \sim \mathcal{N}(10 \log_{10} K + \mu_i, \sigma_i^2), \tag{5.10}$$

Further, given $Power_{T_X}(i)$, the receiving signal strength at the remote receiver with distance d can be defined as follows:

$$Power_{R_X}(i, d) = Power_{T_X}(i) - PL(d) + Noise, \tag{5.11}$$

where, d is the distance between the transmitter and receiver. $PL(d)$ indicates the reduction in the signal strength due to path loss and shadowing. This loss is, in general, a logarithmic function of the distance d, and is given by:

$$PL(d) = \overline{PL}(d_0) + 10n \log_{10}(\frac{d}{d_0}) + X_\sigma, \tag{5.12}$$

where n is the path loss exponent which depends on the propagation medium and decides the speed of the signal power reduction with distance; $\overline{PL}(d_0)$ is the reference

free space path loss at a short distance d_0 [96]; X_σ is a random variable (in dB) and follows a Gaussian distribution with zero mean and a standard deviation of σ_X. X_σ is introduced to represent the uncertainty of the power loss during transmission in different environments.

The values of σ_X range from 2 to 12 dB depending on the specific environment [97], and vary cubically with the distance d [98]. The variable *Noise* used in Eq. 5.11 is the Gaussian noise with mean μ_N, and standard deviation σ_N. We further assume that the random variables X_σ, *Noise*, and $Power_{T_X}$ are independent. Thus, with Eqs. 5.8 to 5.12, one observes that the receiving signal strength, $Power_{R_X}(i,d)$, follows a Gaussian distribution:

$$Power_{R_X}(i,d) \sim \mathcal{N}(\mu_{R_X}, \sigma_{R_X}^2), \tag{5.13}$$

where,

$$\mu_{R_X} = 10\log_{10} K + \mu_i + \mu_N - PL(d), \tag{5.14}$$

$$\sigma_{R_X}^2 = \sigma_i^2 + \sigma_X^2 + \sigma_N^2, \tag{5.15}$$

By using the distribution analysis of $Power_H(i)$ and applying the previously explained mathematical model, we obtain the distributions of the transmission power strength, $Power_{T_X}(i)$, and the receiving signal strength, $Power_{R_X}(i)$, for all five activities.

5.6   Theoretical Validation

This section provides the theoretical validation of our proposed HAR framework. We apply Bayesian decision theory for HAR based on the observed signal strength of the activity pulse, which can be either the transmitted signal strength or the received signal strength. This is followed by the use of the transmission power amplification
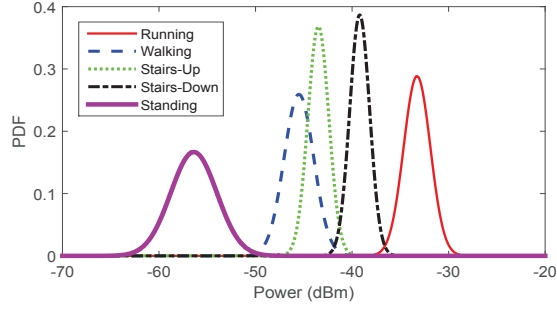
Figure 5.4: The Gaussian distributions of $Power_{T_X}$ for the five activities.

Table 5.2: The estimated statistical parameters and the HAR classification accuracies using Bayesian decision theory based on transmitted signal strength.

Activity I_i	Decision Region R_i	μ_{T_X}	σ_{T_X}	Accuracy
S	$(-\infty, -49.94)$	-56.39	2.37	99.72%
W	$(-49.99, -44.60)$	-45.53	1.47	73.55%
SU	$(-44.60, -41.31)$	-43.51	1.10	81.76%
SD	$(-41.31, -36.60)$	-39.22	1.02	97.36%
R	$(-36.60, +\infty)$	-33.30	1.38	99.21%

factor (K) to improve the accuracy of HAR.

5.6.1   HAR based on the transmitted signal strength

We assume that the PEH-enabled wearable device is embedded in a smartphone, so the smartphone can easily capture the transmitted signal strength of the activity pulse. We first consider the case in which the transmission signal strength is used for activity recognition. According to Eq. 5.10, we estimate the statistical parameters of $Power_{T_X}(i)$ from our PEH dataset using a ten-second time window. The transmission power amplification factor K is configured to be 1. The values of

Table 5.3: The estimates of the parameters in the theoretical model.

Parameter	Value
n	4
d_0	0.02 meter
μ_N	-90 dBm
σ_X	1 dB

(a) distance = 2 cm.

(b) distance = 100 cm.

(c) distance = 200 cm.
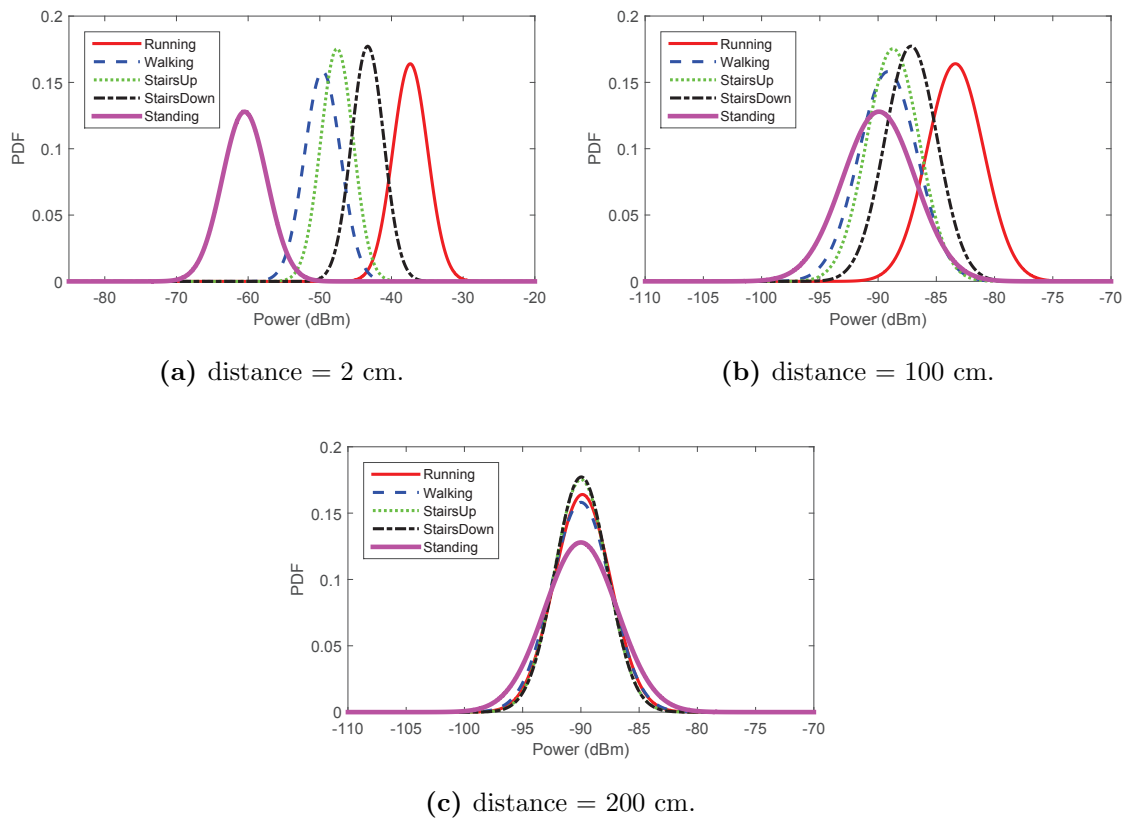
Figure 5.5: The empirical distributions of the received signal strength at three different distances between transmitter and receiver.

the statistical parameters, together with the corresponding decision region and the classification accuracies for all five activities are given in Table 5.2. We note that the overall accuracy of HAR is 90.32%. The empirical distributions of $Power_{T_X}$ for the five activities are shown in Figure 5.6. From the figure, it can be seen that a high overlap between walking, stairs-up, and stairs-down distributions exists, while the distributions for standing and running are well separated. This overlap (or separation) has resulted in high accuracies for standing and running activities (99.72% and 99.21%, respectively), and lower accuracies for stairs-up, walking, and stairs-down (81.76%, 73.55%, and 97.36% , respectively).

5.6.2   HAR based on the received signal strength

The activity pulse is transmitted over uncertain wireless medium and its signal strength is detected by the remote smartphone. Apart from the transmitted signal strength, the received signal is usually affected by the harvested power, environmental noise, and path loss. We obtain the distributions of $Power_{R_X}$ from our PEH dataset using Eq. 5.13. The estimates of the parameters in the theoretical model are given in Table. 5.3. The path loss exponent, n, is set to 4, in order to simulate the obstructed environment [96]. The reference distance d_0 for the free space path loss model is set to 2 cm. The standard deviation of the random variable in the log-normal path loss model σ_X is set to 1 dB. The strength of the noise signal is configured to -90 dBm.

Our primary interest at this point is to figure out the effect on the HAR accuracy of any increase in the distance between the transmitter and receiver. With the value of K fixed at 1, we set the initial distance between the transmitter and the receiver to 2 cm with successive increments of 10 cm until it reaches 200 cm. This is done to simulate the wearable device scenario, in which the receiver would be a smartphone held in the user's hand, and the transmitter is a PEH-enabled wearable sensor attached to the human body.

We notice that the path loss of the signal strength increases logarithmically with the distance between transmitter and receiver. Consequently, the mean of
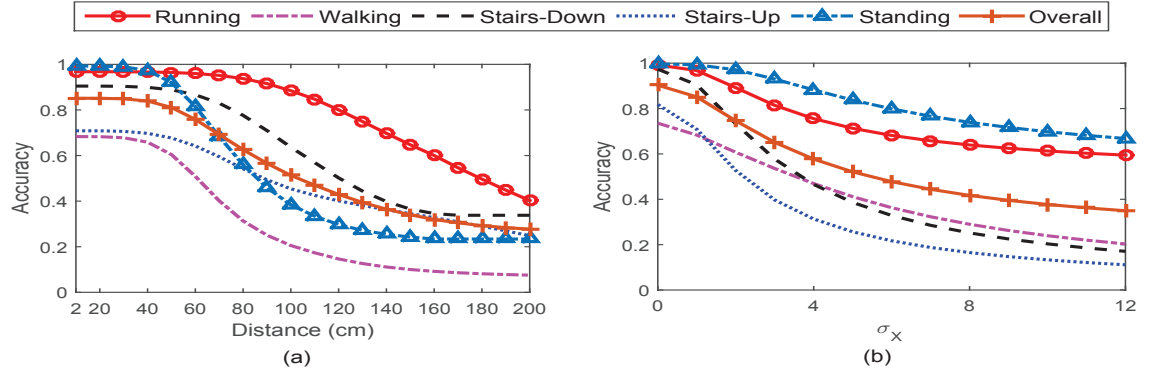
Figure 5.6: (a) The accuracies of HAR based on the received signal strength at different distances and using σ_X equals to 1; (b) The accuracies of HAR as a function of σ_X when the distance between transmitter and receiver d_0 is set to 2 cm.

the received signal strength decreases and eventually becomes equal to the signal strength of the background noise (-90 dBm), leading to a high overlap among the distributions of activities. Figure 5.5 plots the variation in the distributions of the received signal strength at three different distances. The distributions are well separated when the distance is 2 cm. However, when the distance is increased to 200 cm, the distributions become highly overlapped.

Figure 5.6(a) plots the achieved HAR accuracy versus the increase in the distance. As expected, the HAR accuracy drops dramatically when the distance increases. As shown in Figure 5.6(a), the achieved HAR accuracy using the received signal strength is much worse than that of using the transmitted signal strength. This phenomena has occurred due to the high variance of the received signal strength at the receiver side caused by noise and interference from the surrounding environment.

From Eq. 5.15, the standard deviation σ_{R_X} of the received signal strength is affected by the standard deviation of the random variable X_σ. In practice, the value of σ_{R_X} is usually estimated using the recorded data, and ranges between 2 to 12 dB. Fig. 5.6(b) plots the HAR accuracy at 2 cm distance when σ_X is allowed to vary from 0 and 12. It shows that HAR accuracy drops with the gradual increase in σ_X, due to the uncertainty introduced by the environment.

5.6.3 Improving HAR Accuracy by increasing the transmission power amplification factor (K)

Increasing the distance between the transmitter and the receiver leads to a drop in the received signal strength, due to the path loss during the transmission. As a result, the signal-to-noise ratio (SNR) also drops and makes it difficult to distinguish the received signal strength from the background noise. Figure 5.5(c) indicates that, as distance rises to 200 cm, the received signal strength becomes almost equal to that of background noise (-90 dBm), resulting in low HAR accuracy. To resolve this problem, we propose the use of the transmission power amplification factor K to control the SNR. As defined in Eq. 5.9, K can be adjusted by allowing the accumulation time of the harvested energy in the capacitor to vary. As a result the average received signal strength will increase resulting, in a higher SNR at a given distance. This will consequently reduce the overlap among the distributions of the received signal strengths and hence achieving better HAR accuracy.

Keeping the same configuration presented in the previous subsection (as shown in Table 5.3), we allowed K to take the values, 1, 100, 1000, 3205, 10000, and 20000. In order to simulate the case of using Bluetooth low energy (BLE), K is assigned the value 3205. This is because the transmission data rate of BLE is typically 1 Mbps and the packet size is 39 Bytes. This value of K is obtained by adjusting the accumulating window t_{ACC} to one second. Moreover, enlarging the accumulation window of the capacitor, one can harvest more power to transmit the pulse with a higher transmission power and accordingly a higher value of K.

Figure 5.7 shows the achieved HAR accuracies at different distances and different values of K. It is noted that an increase in the distance between the transmitter and the receiver leads to a reduction in the accuracies of all five activities. However, the concavities of all the curves shows that this reduction in accuracy decreases at a decreasing rate with the increase in K. For instance, in Figure 5.7(f) with K being larger than 10,000, an overall accuracy over 70% can be achieved, even when the distance is increased to 200 cm.

Eq. 5.9 asserts that K is determined by both the transmission duration of the

(a) Running.

(b) Standing.

(c) Walking.

(d) Stairs-Down.

(e) Stairs-Up.

(f) Overall accuracies.
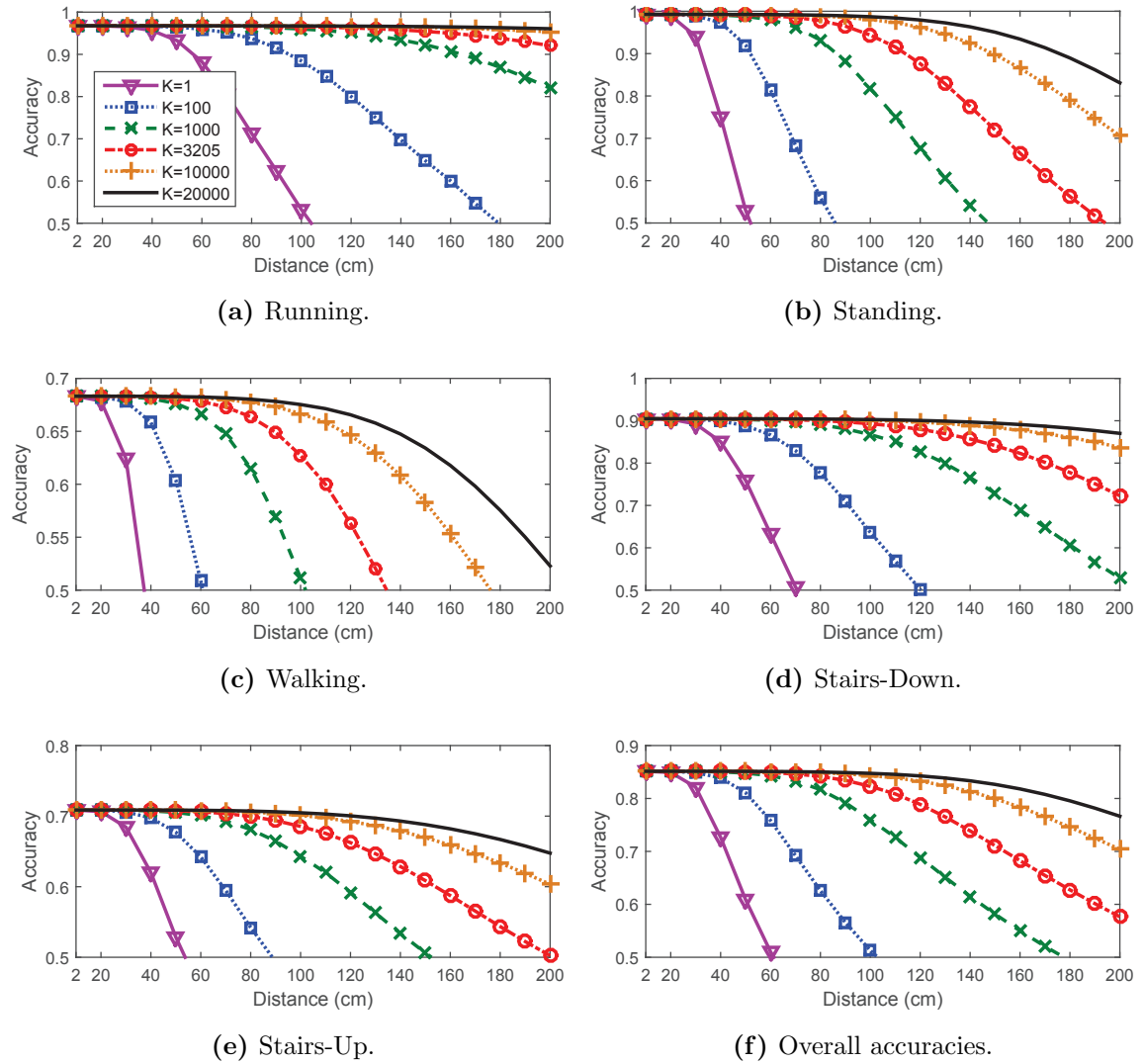
Figure 5.7: The classification accuracies of applying the Bayesian decision theory based on the received signal strength for each of the five activities using different vales of K (note that different scales are used in y axis).

activity pulse, t_{T_X}, and the accumulation window of the harvested power in the capacitor, t_{ACC}. As an example, if t_{ACC} is equal to one second, the transmission frequency of the activity pulse will be 1 Hz. Similarly, if t_{ACC} is extended to ten seconds, the transmission frequency will be 0.1 Hz. Thus, there is a trade-off between HAR accuracy and latency. By extending t_{ACC}, we can get a larger K and higher HAR accuracy at the expense of higher latency. This is because we must wait longer to accumulate more energy in the capacitor. This leaves an open question about the trade-off between HAR accuracy and latency, which can be considered as future work.

5.7 Experimental Validation

In this section, we validate the practicality of the proposed method by using a Bluetooth testbed. We used the iBeacon product from the *Kontakt.io* as the signal transmitter. The details of the bluetooth device are shown in Fig. 5.8(a). It implements the nRF51822 Bluetooth chip from Nordic Semiconductor to support 2.4 GHz Bluetooth Low Energy wireless communication. It offers eight levels of transmission power, from -30 dBm to 4 dBm, with sensitivity of -93 dBm. The data transmission rate is 1 Mbps. The device is powered by a 3 V cell battery. We used a Samsung Galaxy Note 4 smartphone as the receiver and applied the Android application (nRF master control panel) implemented by Nordic Semiconductor to monitor the received signal strength indication (RSSI).

5.7.1 Experiment Setup

We configured the transmission power of the Bluetooth device at five different power levels, each of them corresponding to one of the five activities. Based on our PEH dataset, shown in Table 5.1, the average harvested power over one-second windows for each of the five activities are -56.39 dBm (for standing), -45.53 dBm (for walking), -43.51 dBm (for stairs-up), -39.22 dBm (for stairs-down) and -33.30 dBm (for running). We assume that the capacitor stores enough power to provide an am-

(a) The details of the (b) The experimental setup.
bluetooth device.
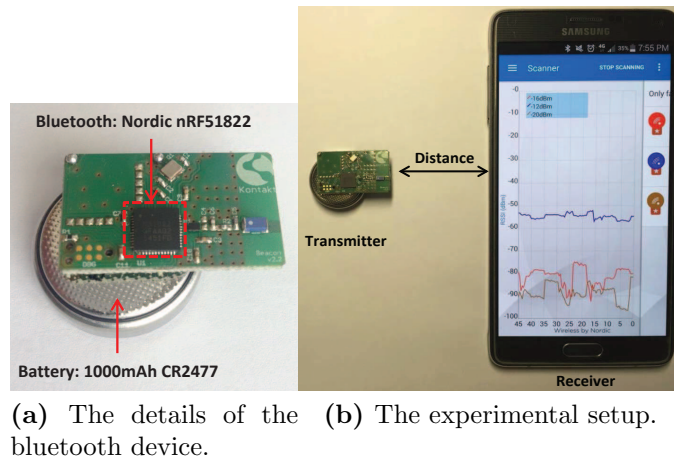
Figure 5.8: The Bluetooth hardware and the experimental setup.

(a) distance = 30 cm.

(b) distance = 60 cm.

(c) distance = 100 cm.
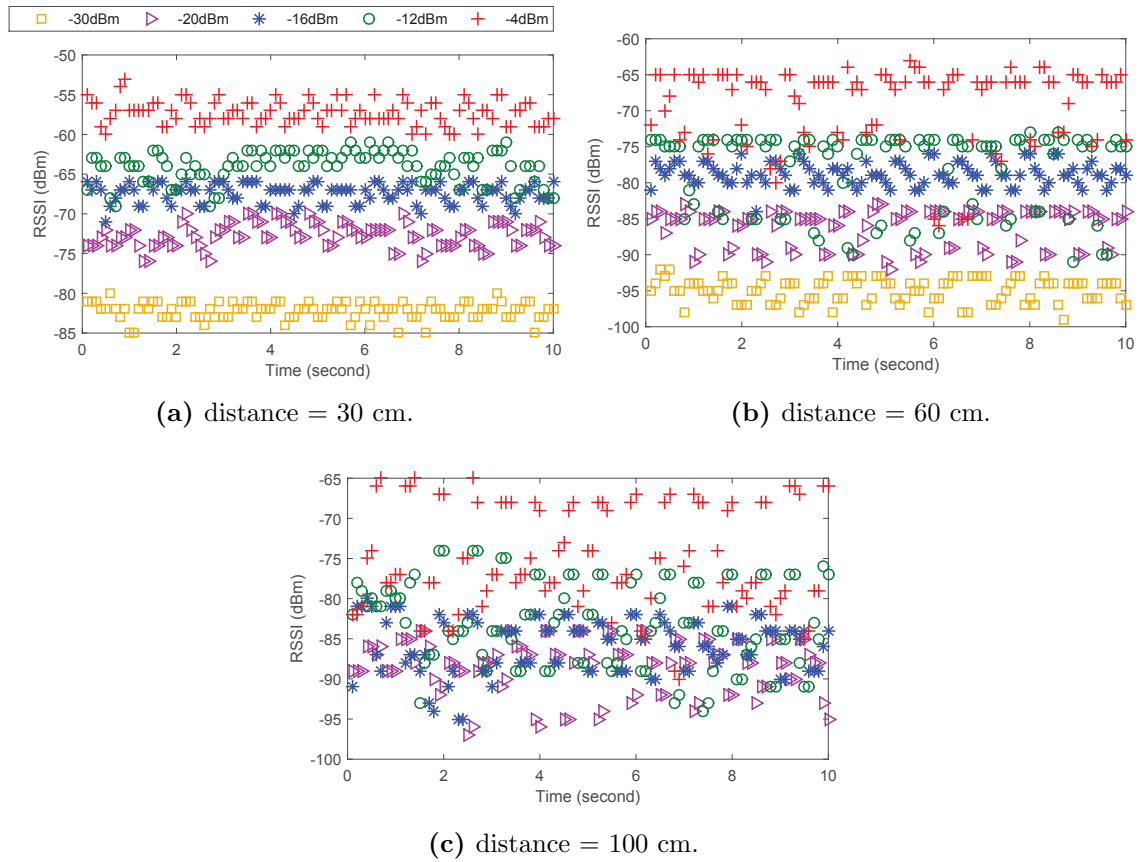
Figure 5.9: The plots of the RSSI at three distances between transmitter and receiver.

Table 5.4: The estimated statistical parameters of the RSSI (mean μ and standard deviation σ) for three distances between transmitter and receiver.

Activity (power)	Distance					
	30 cm		60 cm		100 cm	
	μ	σ	μ	σ	μ	σ
R (-4dBm)	-57.21	1.46	-69.02	4.99	-75.32	6.29
W (-20dBm)	-72.57	1.39	-86.29	2.76	-88.06	3.73
SD (-12dBm)	-64.53	2.06	-78.53	5.94	-82.57	3.30
SU (-16dBm)	-67.20	1.47	-78.91	1.60	-85.64	3.30
S (-30dBm)	-82.02	1.14	-95.11	1.99	null	null

Table 5.5: The accuracies of HAR using RSSI for different distances between transmitter and receiver.

Activity (power)	Distance		
	30 cm	60 cm	100 cm
R (-4dBm)	99.89%	77.09%	69.24%
W (-20dBm)	99.89%	98.47%	43.49%
SD (-12dBm)	72.96%	61.24%	13.60%
SU (-16dBm)	85.36%	91.82%	57.82%
S (-30dBm)	100%	99.74%	100%
Overall	91.62%	85.67%	65.83%

plification of 26 dB in the transmission power. To simulate the five activities, we configure the transmission power of the Bluetooth devices as -30 dBm (for standing), -20 dBm (for walking), -16 dBm (for stairs-up), -12 dBm (for stairs-down) and -8 dBm (for running). The advertising intervals of the Bluetooth devices are set to 20 ms, and the smartphone continuously records the RSSI of the advertising packets. To show the impact on HAR accuracy of the distance between the Bluetooth device and the smartphone, we studied three different distances: 30 cm, 60 cm, and 100 cm.

5.7.2   Simulation Results

Table 5.4 presents the estimated values of the statistical parameters of the measured RSSI at three distances for five activities. The results indicate that the means of RSSI drop as the distance increases, while the standard deviations rise. This is due to the drop in signal strength caused by path loss and standard deviations rise due

Table 5.6: The confusion matrix of HAR using RSSI at 30 cm distance between transmitter and receiver.

Activity	R	W	SD	SU	S
R	894	0	1	0	0
W	0	894	0	1	0
SD	0	48	653	194	0
SU	0	48	83	764	0
S	0	0	0	0	895

to the uncertainty introduced by the surrounding environment. Figure 5.9 plots the recorded RSSIs at the three distances. As indicated in Figure 5.9(a), when the distance is 30 cm, the RSSIs for all five transmission powers are well separated. This results in good HAR accuracy using the proposed Bayesian framework and achieves an overall accuracy of 91.62%. However, Figures 5.9(b) and 5.9(c) show that when the distance increases, the RSSIs for the five transmission powers overlap and as a result the HAR accuracy falls, which conforms with our theoretical analysis given in Figure 5.5. Note that, in Figure 5.9(c), no RSSI of standing activity is recorded by the smartphone because the RSSI of standing (-30dBm) is lower than the sensitivity threshold (-93dBm) of our device. Figure 5.10 plots the CDFs of the empirical RSSI with the corresponding Gaussian distribution with a 100 cm distance. The plots indicate that the measured RSSI follows the Gaussian distribution, which proves the feasibility of the proposed Bayesian framework for HAR.

The detailed results of the achieved HAR accuracies using the Bluetooth prototype are presented in Table 5.5. The overall accuracies of our proposed HAR are 91%, 85%, and 65% for 30 cm, 60 cm, and 100 cm, respectively. To analyse the results reported in this chapter, we show the confusion matrix for HAR accuracy using RSSI at 30 cm. While the classification results of running and standing activities are high (up to 100% accuracy), there is high confusion between walking, stairs-down, and stairs-up activities. This is due to the high similarity between these activities. The RSSI distributions are highly overlapped, which conforms with our theoretical analysis results given in Figure 5.5(a).

By increasing the distance between the Blutooth device and the smartphone, the confusion of these three activities increases and results in reduced accuracy.
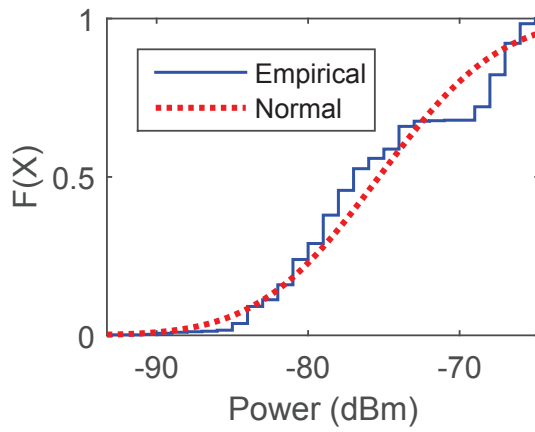
(a) Running (-4dBm).
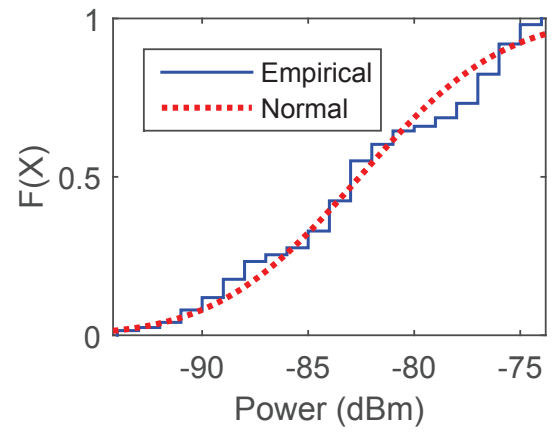
(b) Stairs-Down (-12dBm).
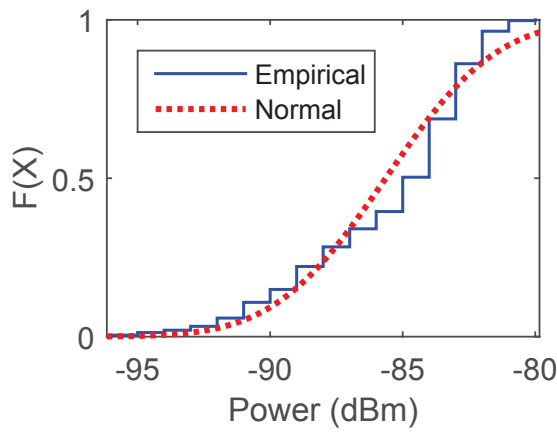
(c) Stairs-Up (-16dBm).
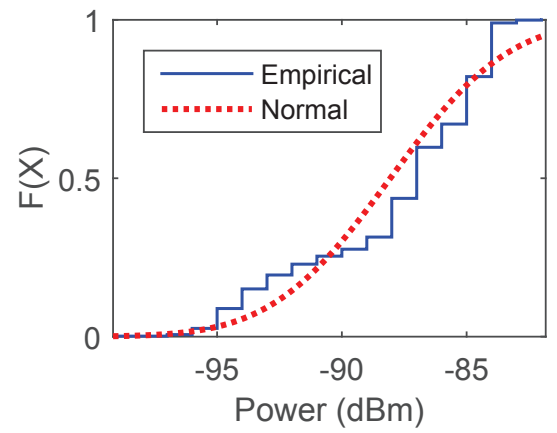
(d) Walking (-20dBm).

Figure 5.10: The CDFs of the empirical RSSI and the corresponding Gaussian distributions using 100 cm distance between transmitter and receiver.

However, as indicated in Table 5.5, the proposed method can achieve an overall HAR accuracy above 85% using 60 cm, which is generally the average distance between the wearable sensors and smartphone.

5.8 Conclusion

Achieving energy efficiency is a challenging task in human activity recognition. Continuous activity sensing using an accelerometer and burdensome on-node classification rapidly deplete the limited battery resources of wearable nodes. To reduce the energy overhead and achieve the system energy neutrality, we propose a novel Bayesian framework for energy-neutral human activity recognition with PEH-enable wearable devices. The proposed framework ensures system energy neutrality by removing both the accelerometer and the activity classifier from the wearable device, and using only the signal strengths of the activity pulse to fulfill continuous human activity recognition. Using a collected PEH power generation dataset from an energy-harvesting wearable device, we demonstrate the feasibility of the proposed framework through theoretical analysis, and validate the results using a Bluetooth prototype. The experimental results show that an overall accuracy of 91% is achieved when the distance between the transmitter and the receiver is 30 cm. We also show that the overall accuracy drops to 85% and 65% when the distance increases to 60 cm and 100 cm, respectively.

It is worth noting that the recognition accuracy for both 30 cm and 60 cm is higher than the accuracy reported in the previous chapter (80%) where the classification was assumed to be done on board with no communication. This is due to the personalized model used in this chapter which was built with data from one subject and then applied to new data from the same subject. In fact, it has been demonstrated in many research studies that the personalized models perform dramatically better than impersonal models built using training data from a panel of subjects and then applied to new users [99]. Therefore, these studies strongly argue for the construction of personal models whenever possible.

Chapter 6

Step Detection from Piezoelectric Energy Harvesting Patterns

6.1 Introduction

Step detecting wearable devices are increasingly being used for monitoring health and fitness [100, 101]. These devices use accelerometers to detect steps as human acceleration exhibits distinctive peaks when steps are taken. Step detection accuracies close to 100% can be achieved by using simple peak-detection algorithms that continuously monitor the accelerometer signal. Figure 6.1 shows a real accelerometer trace from a wearable device carried by a subject walking along a straight indoor walkway. The peaks, which correspond to steps, are unmistakable.

While high step detection accuracy is considered a remarkable feature of wearables, their power supply remains heavily dependent on batteries, which must be recharged or replaced. It is only recently that technological advancements in piezoelectric energy harvesting (PEH) materials have created some real opportunities for wearables to generate power of their own by converting natural phenomena such as human motion into usable electricity [50, 58]. This is a very important development, which may ultimately help realise self-powered wearable devices in the future.

The focus of this chapter is to propose and validate the concept of step detection directly from the patterns of power generation in wearable devices when human
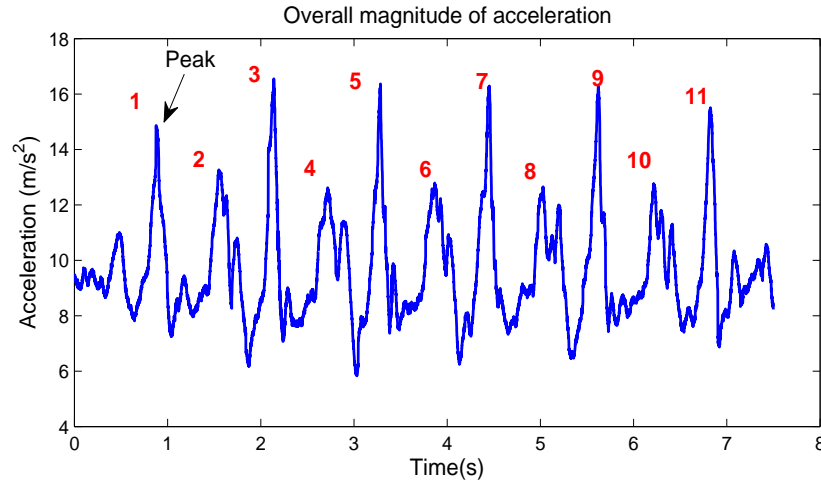
Figure 6.1: The raw output patterns of an accelerometer from a wearable device attached to the waist of a subject walking along straight walkway for 11 steps.

motion is used as the basis of energy harvesting. The concept is intuitive because if steps are known to show distinctive *acceleration peaks*, they are also expected to produce *power peaks* if power generation is based on motion (acceleration). The concept is also immensely beneficial from energy conservation points of view, because if steps can be detected directly from power generation patterns, then no power needs to be allocated to an accelerometer to measure acceleration. Finally, the proposed concept can help simplify the circuit board of the device by removing the accelerometer, which can further reduce the overall device power consumption as well as the form factor.

The contributions and outcomes of this chapter can be summarized as follows:

- We conducted the first experimental study to validate the concept of step detection from the generated patterns of PEH wearable devices.

- We collected the generated patterns of a PEH wearable device from four subjects under different walking scenarios, including walk along straight and turning paths as well as descending and ascending stairs, covering a total of 570 steps.

- We found that, like acceleration, power traces also exhibit distinctive peaks for steps, which can be detected accurately using widely used peak detection algorithms.

- We demonstrated that widely used peak detection algorithms can detect steps from PEH power generation patterns with an accuracy of 96%.

The rest of the chapter is structured as follows. Related work is reviewed in Section 6.2. Section 6.3 provides a review of peak-detection algorithms widely used for detecting steps from accelerometer signals. PEH-based step detection, including data collection experiments and threshold determination, is explained in section 6.4. Results are presented in Section 6.5. We conclude the chapter in Section 6.6.

6.2   Related Work

Step detection algorithms have been widely used in health monitoring and indoor positioning applications [102, 103, 104, 105, 106]. In these applications, steps are usually detected by using the output of an accelerometer. Three different algorithms have been discussed in the literature for step detection: peak detection, zero-crossing detection, and moving variance detection.

1. The peak detection algorithm is one of the most widely used methods for step detection [102, 103, 104, 105, 106]. It searches for the peaks and valleys of the waveform by selecting thresholds in order to identify a distinct step. The step is detected when a valid maximum peak and a valid minimum peak (valley) are detected in sequence in a certain interval.

2. The zero crossing detection algorithm determines the number of steps by counting the number of times the signal crosses the zero level and dividing it by two [107, 103]. The division by two is due to the observation that the signal crosses the zero level twice in each step during walking.

3. The moving variance detection algorithm implements the moving variance filter while keeping in view that acceleration variance has a tendency to increase with respect to step length [107]. Then the local mean acceleration is calculated for each sample of the overall acceleration. Finally, a step is detected when the acceleration variance is above a certain threshold level.

Ayub et al., [107] have shown that the zero crossing detection algorithm is more robust than the moving variance detection algorithm for step detection. On the other hand, Kang et al., [103] have shown that the zero crossing and the peak detection algorithms are precise enough to detect user steps.

In our work, we have used the peak detection algorithm to demonstrate the feasibility of detecting steps from the output voltage of a PEH wearable. However, it would be interesting to study the performance of the two other algorithms when the PEH signal is used for step detection. To the best of our knowledge, this is the first study to demonstrate that step detection is viable using PEH wearables.

6.3 Accelerometer-based step detection using peak identification

Step detection is usually defined as the automatic identification of the moments in time at which footsteps occur. In the literature, steps are usually detected by using the output of the accelerometer. The accelerometer records acceleration in three axes $a_x(t)$, $a_y(t)$, and $a_z(t)$. The overall magnitude of the axes, $a(t) = \sqrt{a_x(t)^2 + a_y(t)^2 + a_z(t)^2}$, is usually used to represent the accelerometer signal for step detection. Figure 6.1 shows the raw output patterns of an accelerometer in a wearable device attached to the waist of a subject walking along a straight walkway for 11 steps. The peaks, which correspond to steps, are unmistakable.

One of the most widely used methods for step detection is peak detection. Several studies [108, 109] showed that the peak detection method is precise enough to detect user steps. In this method, a step is detected when a local maxima (local peak) is detected. A local maxima is a data point that is larger than its two neighbours as shown in Figure 6.1. However, because of irregular movements and hardware noise, not all detected peaks are valid steps. Some peaks can be very low in amplitude or very close to each other. Two thresholds are used to filter out these peaks and recognize the steps:

1. The minimum peak height, T_1.

(a) Device placement on the subject's body.

(b) Experimentation while turning walkways scenario.

Figure 6.2: Experiments Design: (a) Device placement on the subject's body, and (b) Experimentation while turning walkways scenario.

2. The minimum distance between every two consecutive peaks, T_2.

T_1 is determined from the amplitude of the signal and T_2 is determined from the time between two consecutive peaks. Using these thresholds, the only valid peaks that represent steps are those that are higher than T_1 and separated by at least T_2.

6.4 Proposed PEH-based step detection

In this section, we validate the concept of using the generated patterns of PEH devices for step detection. First, we collect experimental data using a PEH device with real subjects taking steps in different scenarios. Then, the widely used peak detection algorithm is used to identify a user's steps from the PEH patterns.

6.4.1 Data Collection

To validate the concept of PEH-based step detection, we used the datalogger prototype presented in Chapter 4 to collect the generated patterns of a PEH transducer when steps are taken by the subject. Simultaneously, accelerometer data were recorded for comparison purposes. Four subjects, two male and two female, between 26 and 35 years of age, volunteered to participate in this study. The subjects were asked to place the prototype at their waist as shown in Figure 6.2. We considered four different walking scenarios:
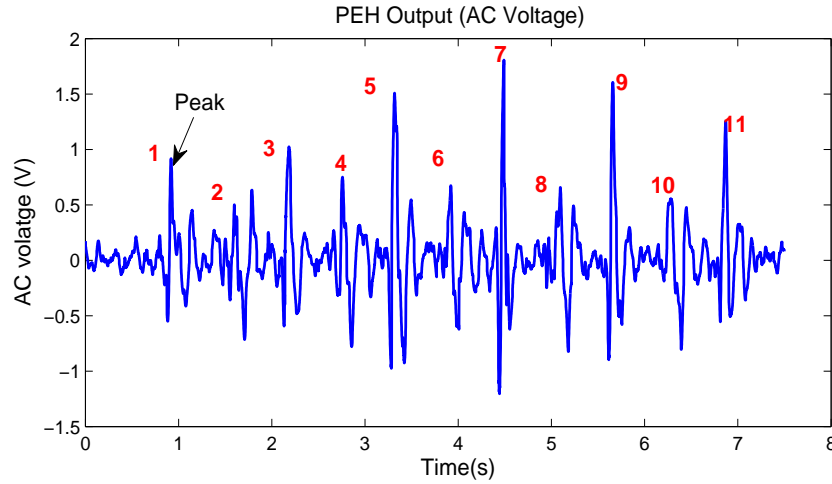
Figure 6.3: The raw output patterns of a piezoelectric vibration energy harvester from a wearable device attached to the waist of a subject walking along straight walkway for 11 steps.

- Straight walkways (7.5 meters long).

- Turning walkways (a square path of 4×4 meters, 16 meters in total).

- Ascending stairs.

- Descending stairs.

Each of these walking scenarios was performed twice by each subject. All subjects performed all the walking scenarios at normal walking speed. A switch was used to start and stop data collection at the beginning and end of each scenario. Subjects were asked to stop and wait a few seconds after and before each scenario. To allow a natural walking style, subjects were not asked to count their steps. Instead, one more volunteer was responsible to monitor the walking of each subject and count the actual number of steps taken in each scenario. In this way, we had the ground truth values which are used in the performance evaluation stage. In total, we had 570 steps from all subjects, experiments and scenarios.

6.4.2   Thresholds Determination

Figure 6.3 shows the raw output pattern of the PEH when the device was attached to the waist of a subject walking along the straight walkway for 11 steps. We

Table 6.1: Experimentally determined thresholds for a step detection algorithm for both accelerometer and PEH patterns.

Accelerometer Thresholds	T1 = 11 m/s^2
	T2 = 0.4 ms
PEH Thresholds	T1 = 0.2 $volt$
	T2 = 0.4 ms

clearly see the step occurrences in the PEH output pattern. This confirms that, like acceleration, power traces also exhibit distinctive peaks for steps, which can be detected accurately using widely used peak detection algorithms. Note that some steps are observed to be higher than other steps in both accelerometer and PEH outputs when the patterns are collected from a waist placement. The steps taken by the leg that is closer to the device have more effect on the output patterns.

As explained in Section 6.3, in order to detect a valid step, two thresholds are required. The minimum peak height, T_1, and the minimum distance between every two consecutive peaks, T_2. T_1 is determined from the amplitude of the signal and T_2 is determined from the time between every two consecutive peaks. These thresholds are usually determined experimentally.

The PEH transducer and the accelerometer have different output patterns. In our prototype, the accelerometer gives acceleration in m/s^2 but the PEH transducer gives AC voltage in *volts*. As shown in Figures 6.1 and 6.3, the amplitudes (the range of the output) of the accelerometer and the PEH patterns are different. T_1 was found experimentally in our data to be 11 m/s^2 for accelerometer and 0.2 *volt* for PEH. T_2 was found to be 0.4 *milliseconds* for both accelerometer and PEH patterns. This is due to the fact that at normal walking speed, humans take approximately two steps per second.

6.5   Results

In this section, we investigate the performance of PEH-based step detection and compare it to accelerometer-based step detection. Table 6.1 shows the experimentally determined threshold for both accelerometer and PEH based on our data.
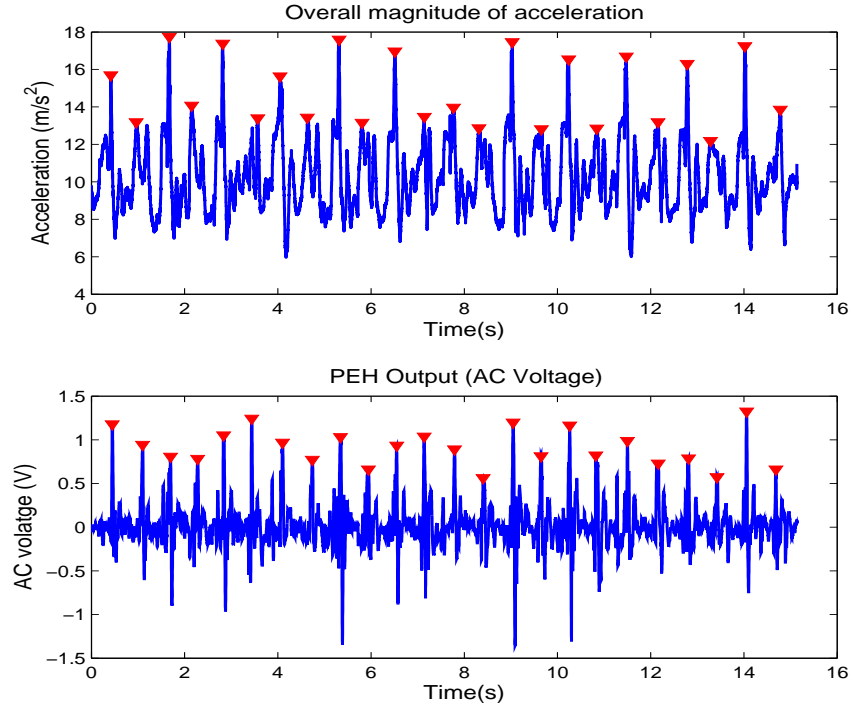
Figure 6.4: The output patterns of the accelerometer (top) and the PEH (bottom), with the detected steps marked on both (turning walkways scenario).

Figure 6.4 shows the identified steps using the previously determined thresholds for both accelerometer (overall magnitude) and PEH signals when square walking scenario and waist placement of the device are considered. The accuracies of the step detection algorithm in both the accelerometer and PEH cases are calculated using Equation 6.1.

$$Accuracy = (1 - \frac{|Actual - Estimated|}{Actual}) \times 100\%, \tag{6.1}$$

where *Actual* is the actual step count and *Estimated* is the estimated step count.

Tables 6.2, 6.3, 6.4, and 6.5 show the accuracy (%) of PEH-based step detection for the four considered scenarios: straight line, turning walkway, ascending, and descending stairs, respectively. These tables also show the actual number of steps (ground truth), the estimated number of steps for each individual subject per each experiment.

Table 6.2: PEH-based step detection accuracy for the straight walkway scenario for each subject and over all the subjects.

Subject No.	Experiment No.	Actual # of steps (Ground Truth)	Estimated # of steps	Accuracy (%)
S1	E 1	12	12	
	E 2	12	12	100
S2	E 1	12	12	
	E 2	12	12	100
S3	E 1	11	12	
	E 2	12	12	100
S4	E 1	12	12	
	E 2	13	14	96.15
Accuracy (%) overall subjects			99.04	

Table 6.3: PEH-based step detection accuracy for the turning walkway scenario for each subject and over all the subjects.

Subject No.	Experiment No.	Actual # of steps (Ground Truth)	Estimated # of steps	Accuracy (%)
S1	E 1	24	24	
	E 2	24	24	100
S2	E 1	25	25	
	E 2	25	25	100
S3	E 1	21	21	
	E 2	21	21	100
S4	E 1	27	27	
	E 2	27	27	100
Accuracy (%) overall subjects			100	

Table 6.4: PEH-based step detection accuracy for the ascending stairs scenario for each subject and over all the subjects.

Subject No.	Experiment No.	Actual # of steps (Ground Truth)	Estimated # of steps	Accuracy (%)
S1	E 1	17	15	
	E 2	17	17	94.12
S2	E 1	17	17	
	E 2	17	17	100
S3	E 1	18	16	
	E 2	18	13	80.56
S4	E 1	18	17	
	E 2	18	18	97.22
Accuracy (%) overall subjects			92.97	

Table 6.5: PEH-based step detection accuracy for the descending stairs scenario for each subject and over all the subjects.

Subject No.	Experiment No.	Actual # of steps (Ground Truth)	Estimated # of steps	Accuracy (%)
S1	E 1	17	17	
	E 2	17	15	94.12
S2	E 1	17	15	
	E 2	17	13	82.35
S3	E 1	18	18	
	E 2	18	18	100
S4	E 1	18	18	
	E 2	18	17	97.22
Accuracy (%) overall subjects			93.42	

Our analysis shows that PEH-based step detection can be achieved with 99.08% and 100% accuracy for straight and turning walkways, respectively. However, the accuracies for ascending and descending stairs scenarios are 92.97% and 93.42%, respectively.

By looking at the step counts for each scenario, we found that only one placement in the straight walkway scenario shows overcount. On the other hand, in ascending and descending stairs, the results were more inclined to undercount than overcount. Figures 6.5 and 6.6 show the accelerometer-based and PEH-based step detection for ascending stairs of subject 3, experiment 2 and for descending stairs of subject 2, experiment 2, respectively. Some steps have been missed by the PEH-based step
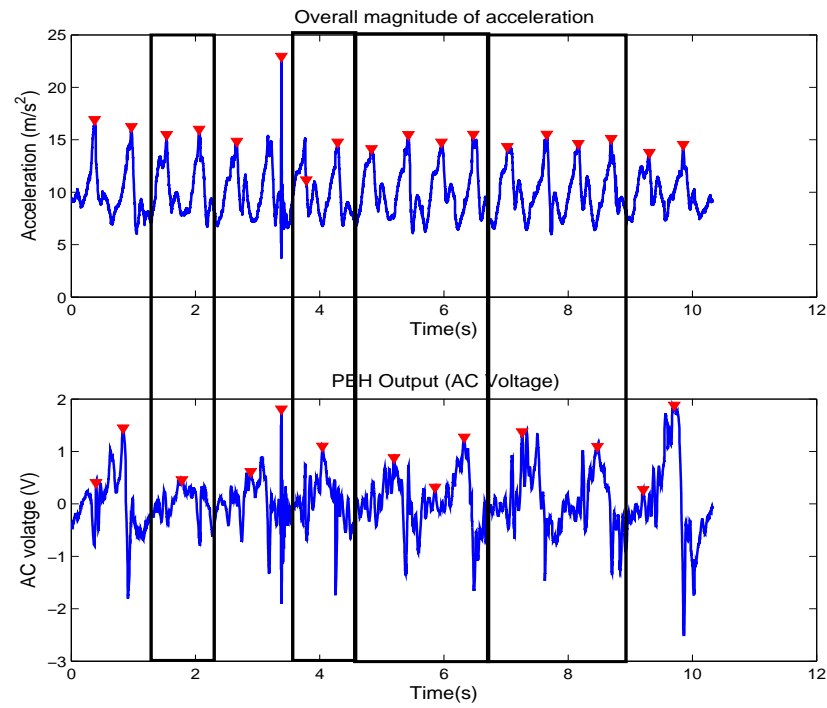
Figure 6.5: Showing the false negative errors of PEH-based step detection when the ascending stairs scenario of subject 3, experiment 2 is considered.
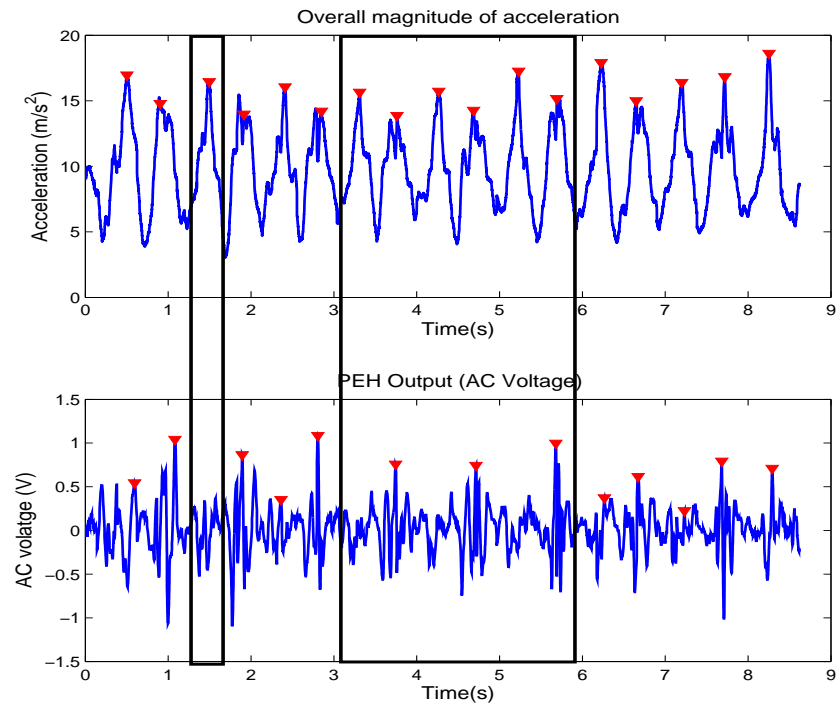
Figure 6.6: Showing the false negative errors of PEH-based step detection when the descending stairs scenario of subject 2, experiment 2 is considered.
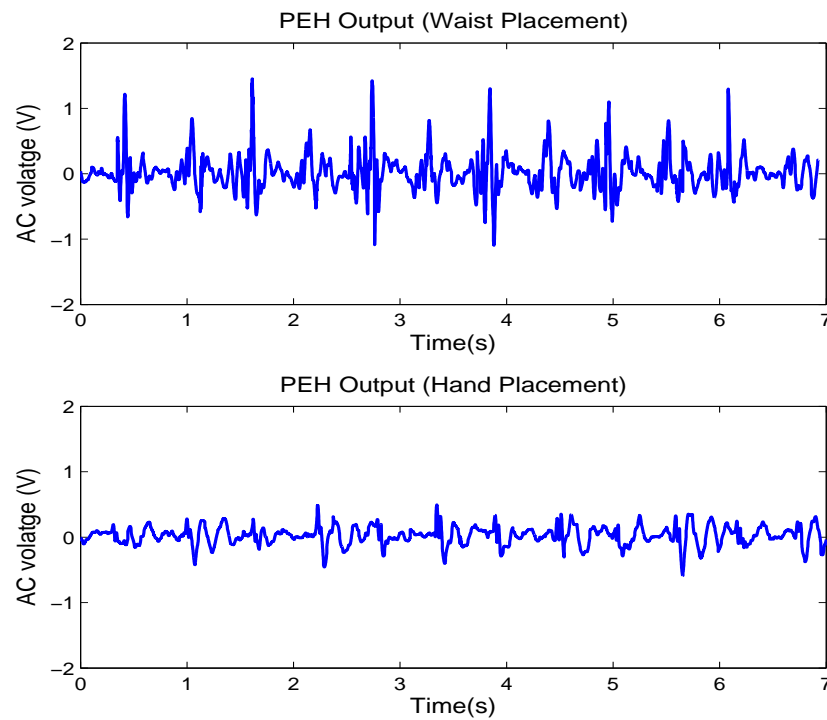
Figure 6.7: Comparing PEH's output patterns for two placements of the prototype on the subjects's body: waist placement (up) and hand placement (down).

detection due to the irregular shape of the signal in these scenarios, leading to some false negative errors. These false negative errors could be due to the use of a universal threshold which might not be correct, because of the different styles of motion for normal walking and ascending or descending stairs.

In total, over all subjects and all walking scenarios, 550 steps out of 570 were successfully detected achieving a 96% step detection accuracy when PEH patterns are used, compared to 100% accuracy when the accelerometer is used.

All of our results were based on waist placement. Previous studies [110, 111, 112] have shown that different placement of the accelerometer affects step detection accuracy. To investigate this for PEH signals, we conducted a simple experiment to compare waist placement to hand placement. One volunteer was asked to hold our prototype in her hand and walk along straight walkway for 11 steps.

Figure 6.7 shows the PEH's output signals for waist and hand placement of the device. One observation is that the steps have less contribution to the peaks of

the signal. This is because, in the hand holding position, leg movement is not contributing to the signal's output, making step occurrences unclear. This means that, for hand placement, PEH-based step detection will be more challenging. Further experimentation is still needed in this direction.

6.6 Conclusion

Energy-harvesting wearable devices generate power by converting natural phenomena such as human motion into usable electricity. In this chapter, we proposed the concept of step detection directly from the patterns of power generation in wearable devices when human motion is used as the basis of energy harvesting. This proposal is particularly beneficial in energy conservation, because if steps can be detected directly from the power generation patterns, then no power needs to be allocated to an accelerometer to measure acceleration. Thus, the accelerometer can be removed from the design, leading to further savings of overall device power consumption as well as reduced size.

Using experimental data, we have shown that steps can be accurately detected from PEH power generation patterns with an average accuracy of 96%. We believe that the proposed idea will contribute toward the realisation of more pervasive and permanent step detection. To our knowledge, this is the first study investigating the viability of step detection using piezoelectric energy harvesting signals. More experimentation is still needed to study how different device placements affect the results.

Although this is specific research focused only on step detection, the positive outcomes imply that PEH signals may have a wide range of applications for sensing and tracking human health. For example, it may be possible to identify a "walking signature" of a person that could help realise various applications including user authentication or detecting abnormal walking behaviour. Investigations of these applications remain the focus of our ongoing efforts [113, 114, 115].

Chapter 7

Hotword Detection from Vibration Energy Harvesting Patterns

7.1 Introduction

With increasing user demand for more power and functionality, manufacturers of mobile devices are forced to find new energy solutions beyond batteries. For this, there is a recent focus on vibration energy harvesting (VEH) as a viable option for mobile devices to generate electrical energy from ambient sources [116, 117]. VEH is considered one of the most effective energy harvesting options for the future internet of things, due to the ubiquitous presence of vibration sources in the environment. Recent research confirms that VEH can harvest usable electric power for personal mobile devices by harnessing vibrations caused by human motion [118, 64, 119]. These developments point to future mobile devices that will be equipped with some sort of VEH hardware to ease the dependence on batteries.

Although the primary purpose of VEH is to convert vibrations to electric power, in principle it could also be used as a potential sensor to detect or identify the source of the vibration. The ability to detect the vibration source can lead to many potential applications for VEH hardware beyond its primary use of energy harvesting. Indeed, we have convincingly demonstrated in the previous chapters that VEH can be used as an effective sensor for human activity recognition due to

the fact that different activities create characteristic patterns of ambient vibration, which produce different energy generation patterns in the VEH circuit.

In this chapter, we investigate VEH as a potential new source of information for detecting hotwords, such as "OK Google", which are used by voice control applications to distinguish user commands from background conversations. Pervasive hotword detection requires continuous sensing of audio signals, which results in significant energy consumption when a microphone is used as an audio sensor. How to reduce audio sensing energy costs using alternative low-power sensors that can also register voice signals is a recent research trend in the literature. For example, researchers have shown that, instead of microphones, gyroscopes [34] or even accelerometers [35] can be used to detect hotwords at a fraction of the energy consumption. Unlike gyroscopes and accelerometers, our proposal enables pervasive voice control at a minimum energy cost.

The contribution of this chapter can be summarized as follows:

- We conduct the first study to assess the viability of using the generated VEH signal for hotword detection.

- Using off-the-shelf piezoelectric energy harvesting circuits, we conduct a comprehensive experimental study involving 8 subjects. Our experiments involve the analysis of two possible usage scenarios, indirect and direct. In the first, the VEH is only expected to pick up the *ambient* vibrations caused by user speech in the vicinity of the device. In the second, the user talks directly to the surface of the piezoelectric beam. For both usage scenarios, we evaluate two types of hotword detection, speaker-independent, which does not require speaker-specific training, and speaker-dependent, which relies on speaker-specific training.

- We show that, in the direct scenario, VEH can detect hotwords with accuracies of 73% and 85%, respectively, for speaker-independent and speaker-dependent detections. We further demonstrate that these accuracies are comparable to what could be achieved with an accelerometer sampled at 200 Hz.

- Finally, for the direct scenario, we provide evidence that orientation of the piezoelectric beam relative to the speaker has an impact on hotword detection accuracy. This finding may serve as an important input to the design of next generation energy-harvesting mobile devices.

7.2 Related Work

Voice control applications such as Siri [120] and Google Now [121] have emerged recently to improve device interactivity. These voice control applications use hotwords such as "Okay Google" or "Hi Galaxy" to distinguish user's voice command from other conversations. One major challenge of voice control applications is the intensive sensing of audio signals which requires the microphone to be continuously ON to monitor user's voice commands [122]. One way to reduce the energy cost of audio sensing is the use of less power sensors such as Microelectromechanical Systems (MEMS) sensors, (e.g., accelerometers and gyroscopes) instead of microphones.

MEMS sensors have been widely used for human activity recognition [123, 124, 125, 20] and indoor positioning applications. Matic et al, [126] have shown that accelerometers can also be used for recognizing speech activity based on detecting phonation caused vibrations at the chest. This can help in activating voice control applications automatically, which usually require user interaction by a simple gesture on a button, or using a Near Field Communication (NFC) tag.

In an attempt to reduce audio sensing energy cost, Michalevsky et al., [34] used a gyroscope sensor for digit recognition instead of a microphone. Gyroscope sensors consume less power than microphones, however, the authors in [34] had to upsample the received gyroscope samples at 4000 Hz to achieve acceptable accuracy, which is also power consuming. On the other hand, Zhang et al., [35] exploited an accelerometer sensor for energy-efficient hotword detection. They showed that an accelerometer sampled at only 200 Hz can detect hotwords with accuracy comparable to microphones. They also showed experimentally that the accelerometer is more energy efficient than both microphone and gyroscope sensors.
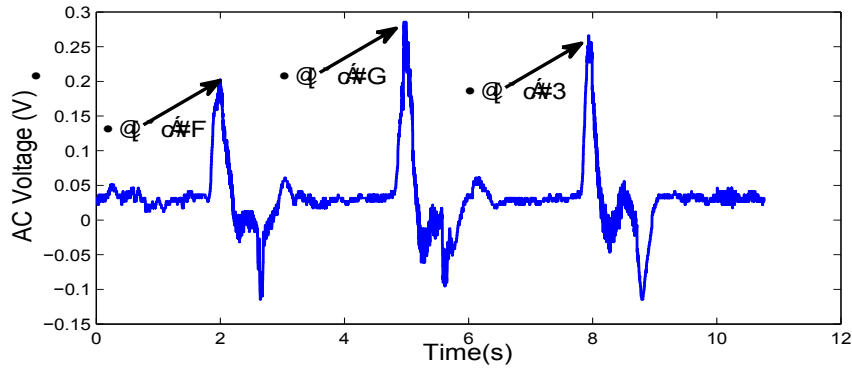
Figure 7.1: Effect of shouting on the VEH piezoelectric beam.

To our knowledge, this is the first work to demonstrate that hotword detection is viable with VEH signals. Since VEH does not require power supply, the proposed method provides hotword detection at minimum energy cost, which will contribute to more pervasive deployments of voice control applications.

7.3   Impact of speech on VEH

As mentioned in Chapter 2, VEH is the process of capturing environmental vibrations and converting it into electrical energy. Human speech creates vibrations (sound waves) which move through the air in the form of pressure. Therefore, a P-VEH transducer should be able to detect changes in air pressure caused by human voice. To experimentally demonstrate this effect, we asked a user to shout three times on top of a piezoelectric cantilever, while the generated voltage signal was being recorded. Figure 7.1 shows the impact of the air pressure on the piezoelectric material. The device responds by giving a voltage peak each time the air pressure hits the beam. This small experiment provides evidence that VEH may be used as a potential sensor to detect the presence of speech. As the patterns of air pressures would be different when the human pronounces different phrases, we should be able to detect hotwords using VEH.
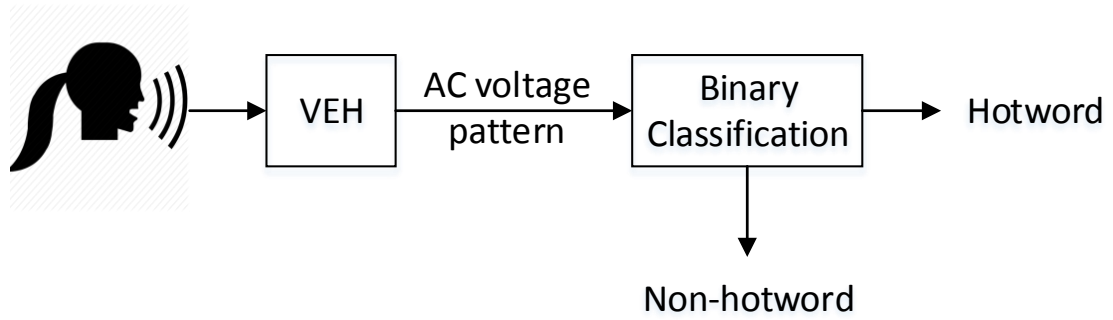
Figure 7.2: Proposed architecture for VEH-based hotword detection.

7.4 Proposed use of VEH for hotword detection

Figure 7.2 shows the proposed architecture for hotword detection using VEH. AC voltage data is continuously fed to a trained binary classifier, which classifies the input signal into either hotword or non-hotword. No actions will be taken during the normal conversation (speech contains no hotword), but if hotword is detected, the system will switch to command mode. To realise the proposed binary classifier, we first need to collect AC data from both hotword and non-hotword speeches, and then train a suitable classifier to detect hotwords. These steps are explained in the following sections.

7.5 VEH Data Collection

In this section, we explain the process of hotword data collection from a piezoelectric VEH (P-VEH) transducer.

7.5.1 VEH Data Logger

We refer to the hardware presented in Chapter 4 as the VEH datalogger to be used in this chapter. However, the piezoelectric VEH transducer is used here to pick up vibrations generated from human speech. The triaxis accelerometer added in the middle of the data logger is used to record any ambient vibrations in the form of

Table 7.1: Experimental Setup.

Participants	8 volunteers: 4 male and 4 female.

Classes	2 classes: 'hotword' and 'non-hotword':
	
	 • 'hotword' class includes one phrase
	
	    – 'Okay Google'
	
	 • 'non-hotword' class includes three phrases
	
	    – 'Fine, thank you'
	    – 'Good morning'
	    – 'How are you?'

Dataset	60 instances/participant: 30 'hotwords' and 30 'non-hotwords'. In total, 480 instances.
Device orientation	2 orientations: horizontal and vertical (as shown in Figure 7.3).
Device position	on a table with 3 cm distance between subject's mouth and the device.

acceleration. We also used a sampling rate of 1000 Hz for both the VEH and the accelerometer. The start/stop switch in the data logger was used to save the data from different phrases into different files.

7.5.2 Experimental setup

We collected data from different experimental setups as summarised in Table 7.1. We collected data from eight participants, four males and four females. Since our aim is to detect hotwords from phrases commonly used in typical conversations, we collected data in two different phases. In phase one, the user was asked to repeat the hotword 'OK Google' 30 times. In the second phase, the user was asked to repeat each of three choices of a non-hotword phrases, 'fine, thank you', 'good morning', and 'how are you' 10 times, giving a total of 30 non-hotword cases per user. The subjects were asked to utter all the phrases at normal speaking levels and took a break of a few seconds between phrases. All experiments were carried out in a quiet room to eliminate background noise as much as possible.

7.5.3   VEH Usage Scenarios

During data collection, we considered two possible usage scenarios of the VEH hardware, *direct vibrations* and *indirect vibrations*. The former scenario represents the case when the user is expected to bring the device close to his mouth when giving a command and talk directly on the surface on the piezoelectric beam. In our design, the piezoelectric energy harvester is left visible outside the VEH hardware case to implement the direct scenario. The latter scenario is designed for cases when it is not practical or desirable to have a visible piezoelectric surface, but hotwords are expected to be detected from ambient vibrations captured by a VEH embedded somewhere in the mobile device. Data collection for these two scenarios are explained below.

- Direct vibration scenario:

  In this scenario, the subject is asked to direct his voice towards the piezoelectric beam from 3 cm away. To study the effect of the piezoelectric beam orientation on hotword detection, we considered two orientations. The data is first collected while the piezoelectric beam has a horizontal orientation. Then, the data is collected with the beam in a vertical orientation. Figure 7.3 shows the two orientations and how the direction of the airflow from subject's speech affects the cantilever beam.

- Indirect vibration scenario:

  In this scenario, the VEH is only expected to pick up *ambient* vibrations caused by speech in the vicinity of the device. The triaxis accelerometer in the data logger is used to capture the ambient vibration in terms of acceleration using the 2nd order mass spring damping model explained in Chapter 3. This model was used in Chapter 3 to estimate the amount of power harvested from human motion vibrations. The configuration values, $m = 10^{-3}kg$, $Z_L = 10mm$, $k = 0.17$, and $b = 0.0005$, were optimised for typical human activities. In this study, we use the same model parameters to capture the vibrations generated by speech in the vicinity of the device, as our main interest is hotword detection rather than power maximization and the VEH in mobile devices is

(a) Horizontal orientation.

(b) Vertical orientation.
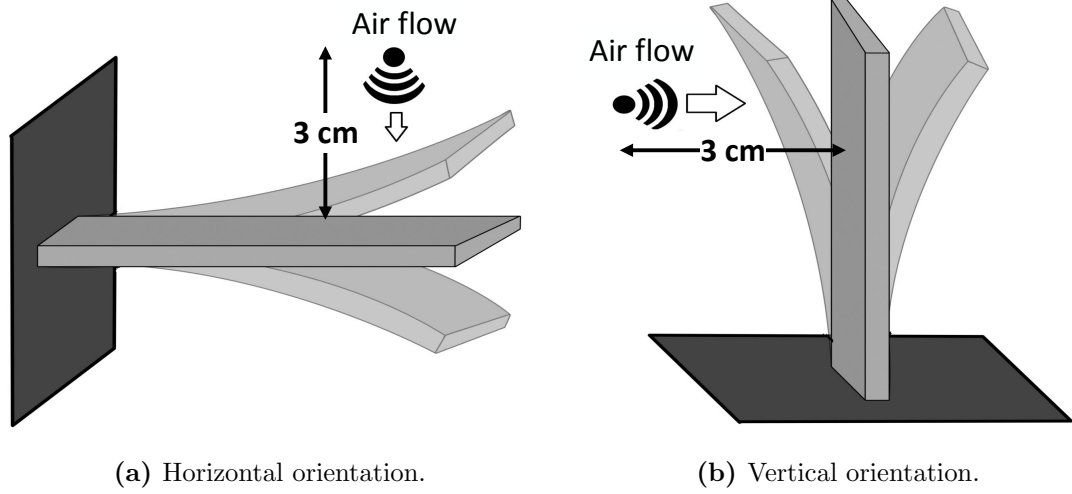
Figure 7.3: Horizontal and vertical orientations of the VEH data logger.

likely to be configured to maximise power from human activity. The entire procedure is implemented using MATLAB and SIMULINK.

Although, our prototype collects both VEH and accelerometer data at 1000 Hz sampling rate, most mobile devices restrict the accelerometer sampling rate to a maximum of 200 Hz in order to reduce power consumption [35]. Therefore, we downsampled our accelerometer sampling rate to 200 Hz to match the current availability of accelerometer sampling rate in mobile devices and to provide a fair comparison. In total, we have five different datasets. Three of them are VEH datasets for indirect scenario, and two direct scenario orientations (horizontal and vertical). The remaining two sets are accelerometer datasets for two sampling rates: 1000 Hz and 200 Hz. The accelerometer datasets are used for comparing the performance of accelerometer-based hotword detection with VEH-based hotword detection.

7.5.4 Hotword Training and Classification

The VEH data obtained in both indirect and direct scenarios were used to evaluate VEH-based hotword detection in comparison with accelerometer-based hotword detection. We refer to the original feature set (OFS) presented in Table 4.3 of Chapter

4 as the considered features set for VEH-based hotword detention, which was also considered previously in [35] for hotword detection from accelerometer data. As discussed previously, the table shows single axis features, which are extracted from the single axis signals of VEH, in both direct and indirect scenarios, and each axis of the accelerometer signal separately. Besides the single axis features, the table shows multiaxis features extracted from the combination of the three axes of the accelerometer signal. Because all hotwords were completed within 2 seconds, we used a time window of 2 seconds to extract the features.

Like the authors in [35], we chose Decision Tree (DT) classifier, a simple, yet powerful and popular tree-based tool for classification and prediction [77]. In the DT classifier, the classification process starts at the root of the tree and grows sequentially until reaching a leaf node. The focus of the tree-growing algorithm is testing and selecting the feature with the most inhomogeneous class distribution, based on its information gain (IG), explained in Chapter 3. A well-known algorithm, which has been widely used for building decision trees over the years, is C4.5 [78]. In this algorithm, pruning is used to optimise the size of the tree, without reducing predictive accuracy. A tree that is too large risks overfitting the training data and poorly generalizing to new samples. A small tree might not capture important structural information about the sample space [79].

In all usage scenarios, we evaluate two types of hotword detection, speaker-independent and speaker-dependent. In the speaker-dependent case, the classification process is applied on the data collected from each individual participant. In the speaker-independent hotword detection, all of the data gathered from the eight participants were first mixed and then fed to the classifier. In both cases, a 10-fold cross validation scheme [85] is used to get the results. In this scheme, the original data set is randomly divided into 10 equally sized subsets, where 9 of them are used for training and one subset is used for testing. This is repeated 10 times (the folds) and then the average of the results is reported.

7.6   Results

In this section, we present the results of our hotword detection study using piezo-electric VEH. We present results for the indirect usage scenario, followed by the direct scenario. For both scenarios, we analyse the results for speaker-independent and speaker-dependent detections. The results of VEH-based hotword detection is compared with accelerometer-based detection. We also investigate speaker identification using piezoelectric VEH and compare it to accelerometer-based identification. Finally, we analyse the effect of speech direction relative to the piezoelectric beam on the performance of hotword detection. In all of our results, we use the total accuracy as our evaluation metric. The total accuracy is calculated using Eq. 7.1 as a percentage.

$$Accuracy = \frac{TP + TN}{N} \times 100(\%), \tag{7.1}$$

where TP is the number of instances where speaking the hotword is correctly recognized as speaking the hotword, TN is the number of instances where speaking the non-hotword is correctly recognized as speaking the non-hotword, and N is the total number of instances.

7.6.1   Indirect Vibrations

Recall, that in this scenario, VEH is expected to capture only *ambient* vibrations caused by the speech. Figure 7.4(a) shows the triaxial accelerometer output signals sampled at 1000 Hz, which represent these ambient vibrations. We see that there are no or negligible vibrations when the user remains silent (the top graph). However, the presence of ambient vibration is clearly captured in the next four graphs. These results are in line with [35], which showed that human speech can be detected by accelerometers.

As explained in Section 7.5, accelerometer traces can be used to estimate the power that may be potentially harvested by VEH. Figure 7.4(b) shows estimated traces of power if VEH was used to harvest ambient vibrations caused by speech.
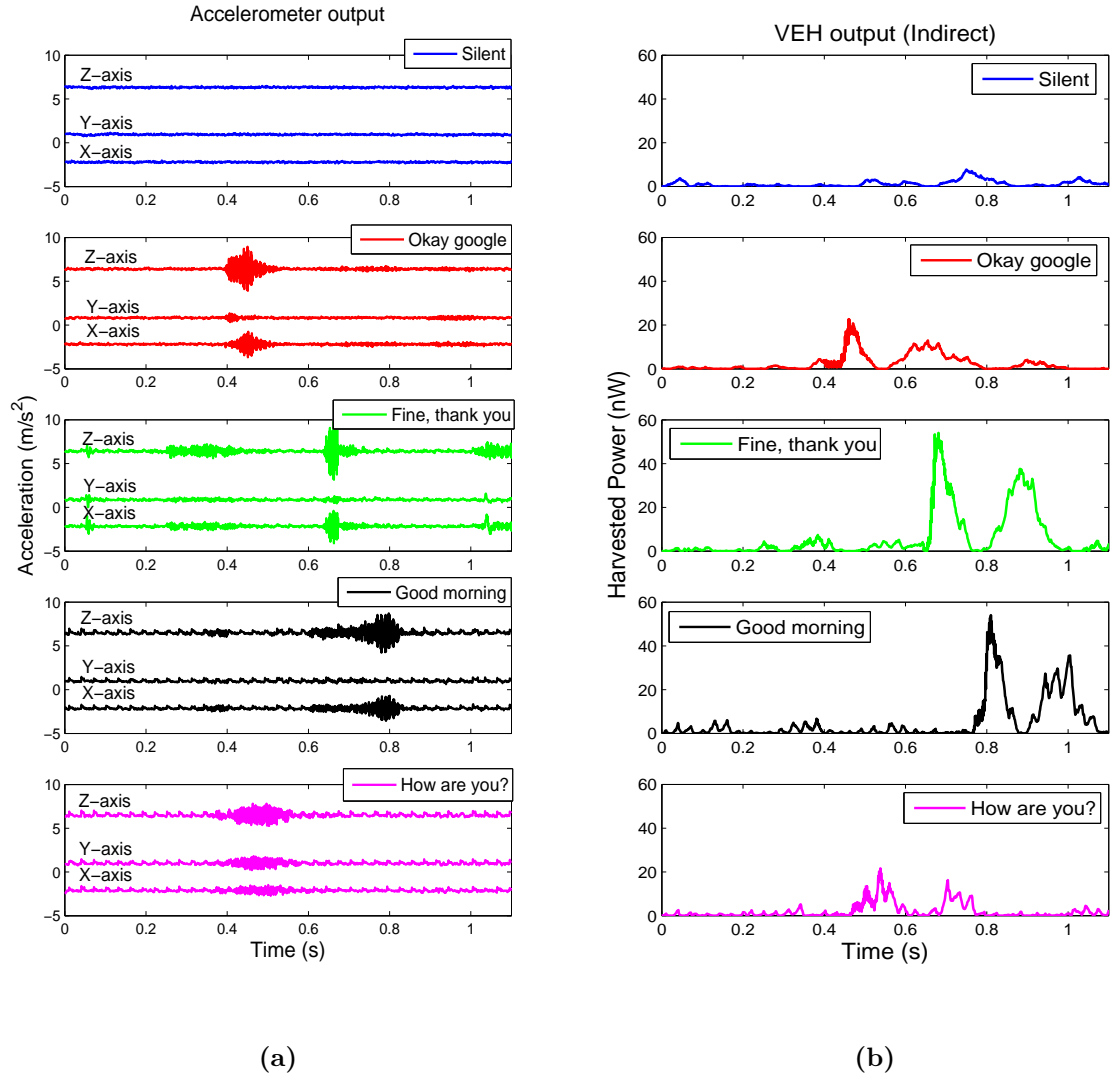
Figure 7.4: Ambient vibrations captured by the internal accelerometer: (a) raw acceleration data and (b) VEH power estimated from acceleration data using the mass-spring model.

We can see that the amount of power that could be harvested from such ambient vibrations is very low, in the order of tens of nW. However, we are not really interested in the amount of power generated by speech, but rather the patterns of power generation that could be used to detect hotwords. In this regard, we see that the power amplitudes for all four phrases are certainly higher than *silence* and that they all exhibit different power patterns. This implies that the indirect usage scenario may be able to detect hotwords with some success.

To formally assess the discriminating capacity of the patterns of VEH power generation for hotword detection, we use the information gain theoretic analysis
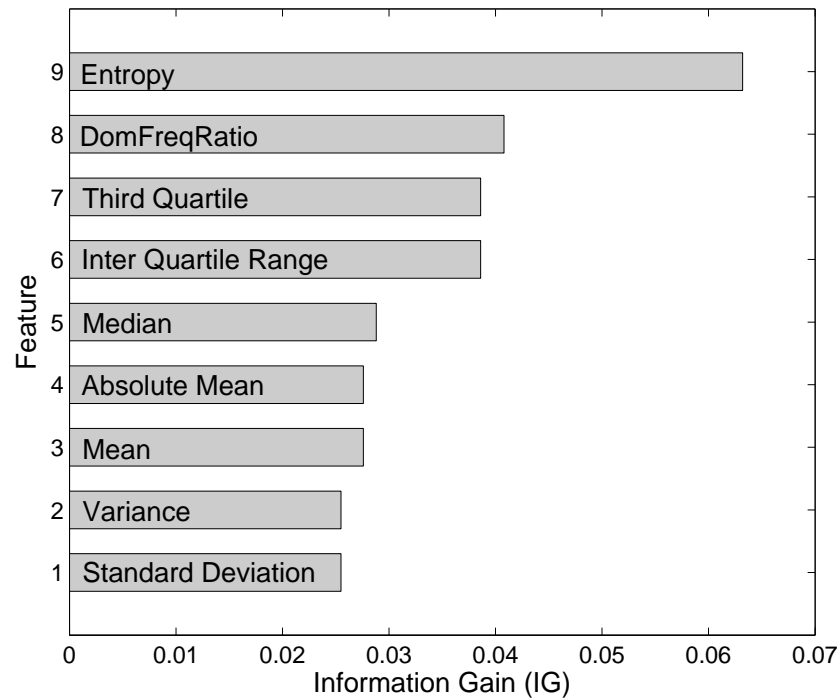
Figure 7.5: Information gain of VEH power signals for the first nine features used for hotword detection.

explained in Section 7.5.4. IG is a measure that determines how useful a given feature is for discriminating between the classes to be learned. Figure 7.5 shows the IG of VEH power signals for the first nine features used for hotword detection. Indeed, this analysis shows that many features provide positive gains, giving evidence that even these low power signals contain information to detect hotwords.

Table 7.2 shows the hotword detection accuracy results for indirect VEH. We find that for speaker-independent, VEH can detect hotwords with 54% accuracy, which means that users would have to repeat the hotword about once to pet the voice control system into the command mode. However, the accuracy improved to 63% with speaker-dependent training.

To see how these results compare to hotword detection using the triaxial accelerometer itself, we conducted the training and classification with the acceleration data collected at 1000 Hz and sub-sampled at 200 Hz. Table 7.3 shows the hotword detection results that could be achieved using the accelerometer. Once more, we found that speaker-dependent outperform speaker-independent, but we find that

Table 7.2: Accuracies (%) of hotword detection for indirect VEH.

Speaker Independent		**54.38**
Speaker Dependent	F1	53.33
	F2	63.33
	F3	46.67
	F4	56.67
	M1	78.33
	M2	66.67
	M3	70.00
	M4	75.00
	Average	**63.75**

Table 7.3: Accuracies (%) of hotword detection for accelerometer.

Accelerometer Sampling Rate		200 Hz	1000 Hz
Speaker Independent		**76.04**	**83.13**
Speaker Dependent	F1	81.67	83.33
	F2	83.33	83.33
	F3	86.67	95
	F4	85	87.33
	M1	96.67	96.67
	M2	93.33	98.33
	M3	90	85
	M4	80	95
	Average	**87.08**	**90.5**

accelerometer achieves much higher accuracies than VEH. For example, even with 200 Hz, accelerometer can achieve accuracies of 76% and 87%, respectively, for speaker independent and speaker-dependent detections. The better performance of accelerometer compared to VEH can be explained by the 3-dimensional information available in the accelerometer (VEH has only 1-dimensional power data). However, VEH performance can be improved by harnessing voice vibrations more directly as examined in the following section.

7.6.2 Direct Vibrations

In this subsection, we examine the benefit of capturing voice vibrations more directly from the user. As explained in Section 7.5, with this scenario, we conduct the training and classification using the AC voltage signal collected directly from
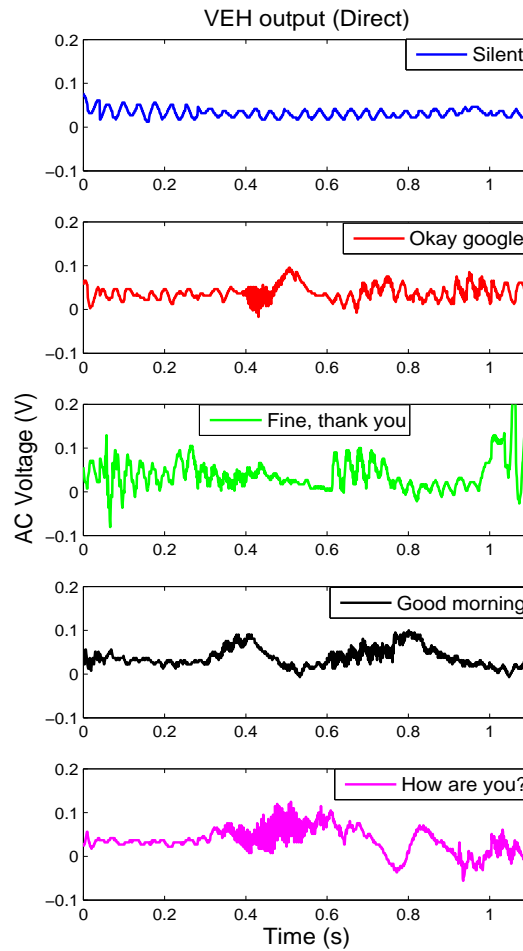
Figure 7.6: VEH output signals for the direct scenario.

the piezoelectric beam in our VEH data logger. Figure 7.6 shows the patterns of AC voltage for silence and when the four phrases are spoken. We see that voltage produced by silence is significantly lower than those produced by voice. We also notice that silence has a more periodic voltage pattern, which captures the background (noise) vibrations, while the voltage is markedly biased in the positive direction when phrases are spoken. This is expected because, in this scenario, sound waves continuously hit directly on one surface of the piezoelectric beam causing it to vibrate asymmetrically around the neutral position.

Table 7.4 presents accuracies when VEH AC Voltage is used for hotword detection with the subject speaking directly to a flat surface of the piezoelectric beam.

Table 7.4: Accuracies (%) of hotword detection for direct VEH.

Speaker Independent		**73.04**
Speaker Dependent	F1	81.67
	F2	76.67
	F3	88.33
	F4	88.33
	M1	96.67
	M2	85.00
	M3	75.00
	M4	93.33
	Average	**85.63**

Compared to the ambient vibration examined in the previous subsection, we see marked improvement in the performance. With direct vibration capture, VEH can detect hotwords with accuracies of 73% and 85%, respectively, for speaker-dependent and speaker-independent detections, which are now comparable to accelerometer-based results with 200 Hz sampling.

7.6.3   Speaker Identification

Previous work [35] has noted that an accelerometer can be used to distinguish a voice from others, which can be useful for user authentication applications. Therefore, in this subsection, we investigate VEH AC Voltage for speaker identification. To do so, we perform a multiclass classification by considering the data of each of the eight participants as a separate class. Table 7.5 shows the confusion matrix when VEH AC Voltage is used for speaker identification with the subject speaking directly to a flat surface of the piezoelectric beam. The results of the accelerometer-based identification are shown in parenthesis for comparison purpose. The results show that the accelerometer outperforms VEH for speaker identification. The overall accuracy of VEH-based speaker identification is 56.87% compared to 85.83% for accelerometer-based identification. This reveals that VEH-based speaker identification still has room for improvement which we consider as possible future work.

Table 7.5: Confusion matrix of VEH-based speaker identification. Results of accelerometer-based identification are shown in parenthesis for comparison.

		Classified as							
		F1	F2	F3	F4	M1	M2	M3	M4
Actual User	F1	41 (50)	7 (0)	1 (0)	2 (0)	1 (6)	4 (3)	2 (0)	2 (1)
	F2	8 (1)	26 (55)	5 (2)	0 (1)	1 (0)	7 (0)	10 (0)	3 (1)
	F3	4 (0)	6 (2)	29 (51)	6 (7)	2 (0)	1 (0)	9 (0)	3 (0)
	F4	1 (0)	1 (3)	6 (4)	33 (49)	2 (0)	5 (3)	5 (1)	7 (0)
	M1	2 (6)	0 (0)	2 (0)	2 (0)	47 (53)	0 (1)	7 (0)	0 (0)
	M2	4 (2)	8 (0)	0 (1)	4 (5)	2 (0)	34 (45)	6 (4)	2 (3)
	M3	2 (0)	3 (0)	4 (2)	4 (1)	7 (0)	3 (6)	34 (51)	3 (0)
	M4	6 (0)	4 (0)	5 (0)	4 (0)	0 (1)	5 (1)	7 (0)	29 (58)

Table 7.6: Accuracies (%) of hotword detection for vertically speaking to VEH.

Speaker Independent		**62.92**
	F1	88.33
	F2	80
	F3	83.33
	F4	65
Speaker Dependent	M1	90
	M2	80
	M3	56.67
	M4	83.33
	Average	**78.33**

7.6.4   Impact of VEH Orientation

Finally, we examine the impact of the orientation of the piezoelectric beam relative to the speaking or air flow direction. Table 7.6 shows the accuracy results when the subject is speaking vertically to the beam (see Section 7.5). Interestingly, although the distance between the subject and the beam is the same in both orientations, the vertical orientation degrades hotword detection performance. These results show that if a direct vibration usage scenario is planned for VEH-based hotword detection, VEH placement within the mobile device may have to be carefully designed.

7.7   Conclusion

Power consumption of microphone-based audio sensing for hotword detection is a major issue for enabling voice control in mobile devices. To combat battery constraints, next generation mobile devices may incorporate vibration energy harvesting (VEH) circuits to generate renewable energy from ambient vibrations. In this chapter, we investigated VEH as a potential new source of information for detecting hotwords, such as "OK Google", used by popular voice control applications to distinguish user commands from other conversations. Unlike existing sensors, such as microphones, gyroscopes, or accelerometers, our proposal enables pervasive voice control at minimum energy cost. The idea of using power signals of VEH to detect hotwords is based on the fact that human voice creates vibrations in the air, which could potentially be measured by the VEH hardware inside a mobile device.

Using experiments with a piezoelectric VEH device and real subjects, we have shown that hotwords can be detected from the power generation patterns of VEH circuits with up to 85% accuracy, which is comparable to accelerometer-based hotword detection. Our study has further revealed that the orientation of the VEH device relative to the speaking direction can have a major impact on the performance of VEH-based hotword detection.

Chapter 8

Conclusion and Future Work

This chapter highlights the key outcomes and conclusions of this dissertation, followed by a discussion of possible future directions of this research.

8.1 Conclusions and key outcomes

This thesis investigated the power requirements of accelerometer-based HAR, demonstrating the power limitation of kinetic energy harvesting (KEH) when it is used to power a wearable device. The research undertaken in this thesis demonstrated the effectiveness of using the generated KEH patterns for three main applications: human activity recognition, step counting, and hotword detection. The key outcomes and conclusions of this thesis are presented below.

- Our study revealed that, although accelerometers are considered low-power electronics in general, they can be the bottleneck of self-powered pervasive HAR. Accelerometers are usually considered low-power electronics drawing only about a few μW per sample per second (Hz). However, when used in kinetic-powered devices, accelerometer power requirements is considered relatively high compared to the total kinetic power available, which is also measured in μW.

- We proposed HARKE as a novel approach for HAR. The proposed HARKE

infers human activity directly from energy harvesting patterns, without using an accelerometer. By eliminating the accelerometer, a significant amount of the harvested power is saved.

- Using extensive data collected from a commercially available piezoelectric energy harvester (PEH), we demonstrated the potential effectiveness of using generated KEH patterns as a new source of information for human activity recognition (HAR). We showed that the generated KEH signals changes to clearly distinguishable patterns when the user changes activities.

- Although we have shown that good HAR accuracies are possible for many common activities when HARKE is adopted, we have also found that the kinetic power signal cannot distinguish very similar activities, such as going up and down the stairs, with high accuracy. For such cases, an accelerometer has a clear advantage with its triaxial measurement capability, which provides more detailed (multi-dimensional) motion information, leading to high recognition accuracy.

- We introduced a new framework based on Bayesian Decision Theory that guarantees energy neutrality for HARKE. Our framework uses a capacitor to store incoming energy harvested from a PEH for a fixed-length time window and then uses all the stored energy to transmit an unmodulated signal, called an *activity pulse*. Because different activities generate power at different rates, the transmission and receiving signal strengths also differ. Thus, those signal strengths can be used to classify the activities. Energy neutrality is guaranteed because the transmission power of the activity pulse uses only the amount of energy harnessed in the last time window, and no additional energy is required to power sensing or classification components in the wearable device.

- We conducted the first study investigating the viability of step detection using piezoelectric energy harvesting signals. We demonstrated that, like acceleration, power traces also exhibit distinctive peaks for steps. We demonstrated that widely used peak detection algorithms can detect steps from PEH power generation patterns with an accuracy of 96% when the device is attached to

the waist. However, more experimentation is still needed to study the effect of different device placement.

- We demonstrated that VEH generated patterns can potentially be used as a new source of information for detecting hotwords, such as "OK Google", used by popular voice control applications to distinguish user commands from other conversations. Unlike existing sensors, such as microphones, gyroscopes, or accelerometers, VEH enables pervasive voice control at a minimum energy cost. We have shown that hotwords can be detected from the power generation patterns of VEH circuits with up to 85% accuracy, which is comparable to accelerometer-based hotword detection.

- Our study of VEH-based hotword detection has further revealed that the orientation of a VEH device relative to speaking direction can have affect the performance of VEH-based hotword detection. This finding may serve as an important input to the design of next generation energy-harvesting mobile devices.

8.2 Future Work

Some of the future research directions can be summarised as follows:

- The experimental analysis provided in this thesis was based on a single axis kinetic energy harvester. However, exploring the possibility of using multi-dimensional (multi-axial) kinetic energy harvesters may lead to more accurate HAR, especially in the case of distinguishing very similar activities, such as going up and down stairs. Using multi-dimensional (multi-axial) kinetic energy harvesters which allow the generation of three output signals, one for each axis, will enable more advanced training of the classifier, similar to HAR based on a triaxial accelerometer.

- We analysed HAR accuracy when the accelerometer and the energy harvester are used in a *mutually exclusive* manner. A logical future direction is to

consider a hybrid system where a triaxial accelerometer is sampled at a low sampling rate (low power consumption), but the classifier is trained using both the accelerometer samples and the KEH samples, thus enabling very accurate HAR with low power consumption. The hybrid system combines the advantages of both signals to realise a more flexible HAR with a goal to achieve a better accuracy-power trade-off than that which is possible with the mutually exclusive method.

- Harvesting energy from multiple sources, such as kinetic, thermal, and light, is a recent trend to maximize the amount of power generation to cover the power requirements. This would be another source for improving the accuracy of HAR. For example, human body temperature may change for different activities. We suspect that new thermal energy harvesting circuits may be able to detect this change in the output signal, so thermal energy harvesting may be used to improve the accuracy of HAR.

- Studying the relationship between the form factor (size) of the energy harvester and the recognition accuracy of HAR is a valid future direction. It is known that reducing the form factor of the harvester minimizes the amount of power that can be generated. However, it is not known how this may affect the recognition accuracy of HAR. It is also interesting to study how nanoscale energy harvesting would affect both the output power and the recognition accuracy. Exploring new materials such as graphene would also be very interesting.

- Power generation from a VEH in a wearable can be predicted using activity switching probabilities because activities influence power generation. This can lead to accurate power generation predictions, which may be useful in designing more robust wireless communication systems for such devices.

- Using energy harvesting signals as a novel source of information may be applied in a wide range of applications for sensing and tracking human health. For example, it may be possible to identify a "walking signature" of a person that could help realise various applications including user authentication or detecting abnormal walking behaviour. Structural health monitoring, such as

bridges, buildings, or trains, might also be an interesting future application.

Bibliography

[1] The 2015 Revision of World Population Prospects. `http://esa.un.org/unpd/wpp/publications/files/key_findings_wpp_2015.pdf`. Accessed on 27 November, 2015.

[2] Growing older (AIHW) - Australian Institute of Health and Welfare. `http://www.aihw.gov.au/australias-welfare/2015/growing-older/`. Accessed on 27 November, 2015.

[3] An Aging Nation: The Older Population in the United States. `https://www.census.gov/prod/2014pubs/p25-1140.pdf`. Accessed on 27 November, 2015.

[4] How much does Australia spend on health care? `http://www.aihw.gov.au/WorkArea/DownloadAsset.aspx?id=60129547594`. Accessed on 27 November, 2015.

[5] Venet Osmani, Sasitharan Balasubramaniam, and Dmitri Botvich. Human activity recognition in pervasive health-care: Supporting efficient remote collaboration. *Journal of Network and Computer Applications*, 31(4):628 – 655, 2008.

[6] Octav Chipara, Chenyang Lu, Thomas C. Bailey, and Gruia-Catalin Roman. Reliable clinical monitoring using wireless sensor networks: Experiences in a step-down hospital unit. In *Proceedings of the 8th ACM Conference on Embedded Networked Sensor Systems*, SenSys '10, 2010.

[7] Fahd Albinali, Stephen Intille, William Haskell, and Mary Rosenberger. Using wearable activity type detection to improve physical activity energy expendi-

ture estimation. In *Proceedings of the 12th ACM International Conference on Ubiquitous Computing*, Ubicomp '10, 2010.

[8] Bernd Tessendorf, Andreas Bulling, Daniel Roggen, Thomas Stiefmeier, Manuela Feilner, Peter Derleth, and Gerhard Trster. Recognition of hearing needs from body and eye movements to improve hearing instruments. In *Proceedings of Prevasive*, 2011.

[9] Thomas Wyss and Urs Mder. Recognition of military-specifi c physical activities with body-fixed sensors. *MILITARY MEDICINE*, 175(11):858–864, 2010.

[10] K. Altun and B. Barshan. Pedestrian dead reckoning employing simultaneous activity recognition cues. *Measurement Science and Technology*, 23(2):1–20, February, 2012.

[11] Sara Khalifa, Mahbub Hassan, and Aruna Seneviratne. Adaptive pedestrian activity classification for indoor dead reckoning systems. In *International Conference on Indoor Positioning and Indoor Navigation(IPIN13)*, Montbéliard-Belfort, France, Oct 2013.

[12] K. Wongpatikaseree, M. Ikeda, M. Buranarach, T. Supnithi, A.O. Lim, and Yasuo Tan. Activity recognition using context-aware infrastructure ontology in smart home domain. In *Seventh International Conference on Knowledge, Information and Creativity Support Systems (KICSS)*, Nov 2012.

[13] Geetika Singla, Diane J. Cook, and Maureen Schmitter-Edgecombe. Recognizing independent and joint activities among multiple residents in smart environments. *Journal of ambient intelligence and humanized computing*, 1(1):5763, 2010.

[14] W. He, Y. Guo, C. Gao, and X. Li. Recognition of human activities with wearable sensors. *EURASIP Journal on Advances in Signal Processing*, 2012.

[15] Robert Bodor, Bennett Jackson, Nikolaos Papanikolopoulos, and Human Tracking. Vision-based human tracking and activity recognition. In *Proc. of the 11th Mediterranean Conf. on Control and Automation*, 2003.

[16] Ronald Poppe. A survey on vision-based human action recognition. *Image and Vision Computing*, 28(6):976 – 990, 2010.

[17] Paul D Mitcheson, Eric M Yeatman, G Kondala Rao, Andrew S Holmes, and Tim C Green. Energy harvesting from human and machine motion for wireless electronic devices. *Proc. of the IEEE*, 96(9):1457–1486, 2008.

[18] Jaeseok Yun, Shwetak N Patel, Matthew S Reynolds, and Gregory D Abowd. Design and performance of an optimal inertial power harvester for human-powered devices. *Mobile Computing, IEEE Transactions on*, 10(5):669–683, 2011.

[19] Maria Gorlatova, John Sarik, Guy Grebla, Mina Cong, Ioannis Kymissis, and Gil Zussman. Movers and shakers: Kinetic energy harvesting for the internet of things. In *Proc. of ACM SIGMETRICS*, pages 407–419, 2014.

[20] O.D. Lara and M.A. Labrador. A survey on human activity recognition using wearable sensors. *IEEE Communications on Surveys and Tutorials*, 15(3):1192–1209, 2013.

[21] M.C. Hamilton. Recent advances in energy harvesting technology and techniques. In *IECON 2012 - 38th Annual Conference on IEEE Industrial Electronics Society*, Oct 2012.

[22] Niell Elvin and Alper Erturk. *Advances in Energy Harvesting Methods.* Springer Link, 2013.

[23] D. Lee, G. Dulai, and Vassili Karanassios. Survey of energy harvesting and energy scavenging approaches for on-site powering of wireless sensor- and microinstrument-networks. In *Proc. SPIE 8728, Energy Harvesting and Storage: Materials, Devices, and Applications*, May 28, 2013.

[24] Jeremy Bickerstaffe. Energy harvesting. `http://www.sagentia.com/resources/white-papers/2011/energy-harvesting.aspx`. Accessed on 27 November, 2015.

[25] Felix Bsching, Ulf Kulau, Matthias Gietzelt, and Lars Wolf. Comparison and validation of capacitive accelerometers for health care applications. *Computer Methods and Programs in Biomedicine*, 106(2):79 – 88, 2012.

[26] Zhixian Yan, Vigneshwaran Subbaraju, Dipanjan Chakraborty, Archan Misra, and Karl Aberer. Energy-efficient continuous activity recognition on mobile phones: An activity-adaptive approach. In *Proceedings of the 16th Annual International Symposium on Wearable Computers (ISWC)*, Newcastle, UK, 18-22 June 2012.

[27] Harvey Weinberg. Minimizing power consumption of imems accelerometers. In *Applications AN-601, Analog Devices*, 2002.

[28] Nishkam Ravi, Nikhil Dandekar, Preetham Mysore, and Michael L Littman. Activity recognition from accelerometer data. In *AAAI*, volume 5, pages 1541–1546, 2005.

[29] Shuangquan Wang, Jie Yang, Ningjiang Chen, Xin Chen, and Qinfeng Zhang. Human activity recognition with user-free accelerometers in the sensor networks. In *Neural Networks and Brain, 2005. ICNN&B'05. International Conference on*, volume 2, pages 1212–1217. IEEE, 2005.

[30] Jennifer R Kwapisz, Gary M Weiss, and Samuel A Moore. Activity recognition using cell phone accelerometers. *ACM SigKDD Explorations Newsletter*, 12(2):74–82, 2011.

[31] Adil Mehmood Khan, Young-Koo Lee, and T-S Kim. Accelerometer signal-based human activity recognition using augmented autoregressive model coefficients and artificial neural nets. In *Proc. 30th Annual International Conference of the IEEE Engineering in Medicine and Biology Society*, Vancouver, Canada, Aug 2008.

[32] Xin Qi, Matthew Keally, Gang Zhou, Yantao Li, and Zhen Ren. Adasense: Adapting sampling rates for activity recognition in body sensor networks. In *In Proc. IEEE 19th Real-Time and Embedded Technology and Applications Symposium (RTAS)*, Montbéliard-Belfort, France, 2013.

[33] Alberto Olivares, Juan M Grriz, Gonzalo Olivares, Javier Ramrez, and Peter Glsektter. A study of vibration-based energy harvesting in activities of daily living. In *Proc. 4th International Conference on Pervasive Computing Technologies for Healthcare (PervasiveHealth)*, Munchen Germany, Mar 2010.

[34] Y. Michalevsky, D. Boneh, and G. Nakibly. Gyrophone: Recognizing speech from gyroscope signals. In *23rd USENIX Security Symposium (USENIX Security 14)*, San Diego, CA, Aug. 2014.

[35] Li Zhang, Parth H. Pathak, Muchen Wu, Yixin Zhao, and Prasant Mohapatra. Accelword: Energy efficient hotword detection through accelerometer. In *MobiSys15*, Florence, Italy, 18–22 May, 2015.

[36] Muhammad Shoaib, Stephan Bosch, Ozlem Durmaz Incel, Hans Scholten, and Paul J.M. Havinga. A survey of online activity recognition using mobile phones. *Sensors*, 15(1), 2015.

[37] Karen Henricksen, Jadwiga Indulska, and Andry Rakotonirainy. Using context and preferences to implement self-adapting pervasive computing applications. *Software: Practice and Experience*, 36(11-12):1307–1330, 2006.

[38] Claudio Bettini, Oliver Brdiczka, Karen Henricksen, Jadwiga Indulska, Daniela Nicklas, Anand Ranganathan, and Daniele Riboni. A survey of context modelling and reasoning techniques. *Pervasive and Mobile Computing*, 6(2):161 – 180, 2010.

[39] S.C. Mukhopadhyay. Wearable sensors for human activity monitoring: A review. *Sensors Journal, IEEE*, 15(3):1321–1330, March 2015.

[40] Wearable technology 2015-2025: Technologies, markets, forecasts. `http://www.idtechex.com/research/reports/wearable-technology-2015-2025-technologies-markets-forecasts-000427.asp?viewopt=showall`.

[41] L. Bao and S. S. Intille. Activity recognition from user-annotated acceleration data. *Pervasive Computing*, 3001:1–17, 2004.

[42] Jonghun Baek, Geehyuk Lee, Wonbae Park, and Byoung-Ju Yun. Accelerometer signal processing for user activity detection. In *Knowledge-Based Intelligent Information and Engineering Systems*, volume 3215 of *Lecture notes in Computer Science*, pages 610–617. Springer Berlin / Heidelberg, 2004.

[43] Kerem Altun, Billur Barshan, and Orkun Tunçel. Comparative study on classifying human activities with miniature inertial and magnetic sensors. *Pattern Recognition*, 43(10):3605–3620, 2010.

[44] Jennifer R. Kwapisz, Gary M. Weiss, and Samuel A. Moore. Activity recognition using cell phone accelerometers. *ACM SIGKDD Explorations Newsletter*, 12(2):74–82, 2010.

[45] D. Gusenbauer, C. Isert, and J. Krösche. Self-contained indoor positioning on off-the-shelf mobile devices. In *"International Conference on Indoor Positioning and Indoor Navigation (IPIN10)*, Zürich, Switzerland, 15–17 Septemper 2010.

[46] Avinash Parnandi, Ken Le, Pradeep Vaghela, Aalaya Kolli, Karthik Dantu, Sameera Poduri, and Gaurav S. Sukhatme. Coarse in-building localization with smartphones. In *Mobile Computing, Applications, and Services*, volume 35 of *Lecture Notes of the Institute for Computer Sciences, Social Informatics and Telecommunications Engineering*, pages 343–354. Springer Berlin / Heidelberg, 2010.

[47] M.A. Ayu, T. Mantoro, A.F.A. Matin, and S.S.O. Basamh. Recognizing user activity based on accelerometer data from a mobile phone. In *Proceedings of the IEEE International Symposium on Computers and Informatics (ISCI 2011)*, Kuala Lumpur, Malaysia, 20-23 March 2011.

[48] Sara Khalifa, Mahbub Hassan, and Aruna Seneviratne. Adaptive pedestrian activity classification for indoor dead reckoning systems. In *International Conference on Indoor Positioning and Indoor Navigation (IPIN13)*, Montbéliard-Belfort, France, 28-31 October 2013.

[49] Piero Zappi, Clemens Lombriser, Thomas Stiefmeier, Elisabetta Farella, Daniel Roggen, Luca Benini, and Gerhard Trster. Activity recognition from on-body sensors: Accuracy-power trade-off by dynamic sensor selection. In *European Conference on Wireless Sensor Networks (EWSN)*, Bologna, Italy, 30 Jaunary-1 February 2008.

[50] R.J.M. Vullers, R. van Schaijk, I. Doms, C. Van Hoof, and R. Mertens. Micropower energy harvesting. *Solid-State Electronics*, 53(7):684 – 693, 2009.

[51] Texas Instruments, Energy Harvesting. `http://www.ti.com/corp/docs/landing/cc430/graphics/slyy018_20081031.pdf`. Accessed on 27 November, 2015.

[52] Helios Vocca and Francesco Cottone. Kinetic energy harvesting. 2014.

[53] P.D. Mitcheson, E.M. Yeatman, G.K. Rao, A.S. Holmes, and T.C. Green. Energy harvesting from human and machine motion for wireless electronic devices. *Proceedings of the IEEE*, 96(9):1457–1486, Sept 2008.

[54] Burkhard Habbe. Thermal Energy Harvesting Infinite Clean Power for Wireless Sensor Networks. `http://archive.treasury.gov.au/igr/igr2010/Overview/pdf/IGR_2010_Overview.pdf`. Accessed on 27 November, 2015.

[55] Guodong Xu, Yang Yang, Yixin Zhou, and Jing Liu. Wearable thermal energy harvester powered by human foot. *Frontiers in Energy*, 7(1):26–38, 2013.

[56] Adamu Murtala Zungeru, Li-Minn Ang, S. R. S. Prabaharan, and Kah Phooi Seng. Radio frequency energy harvesting and management for wireless sensor networks. *CoRR*, abs/1208.4439, 2012.

[57] P. Nintanavongsa, U. Muncuk, D.R. Lewis, and K.R. Chowdhury. Design optimization and implementation for rf energy harvesting circuits. *Emerging and Selected Topics in Circuits and Systems, IEEE Journal on*, 2(1):24–33, March 2012.

[58] Yuan Rao, Shuo Cheng, and David P Arnold. An energy harvesting system for passively generating power from human activities. *Journal of Micromechanics and Microengineering*, 23(11), 2013.

[59] Henry A. Sodano, Daniel J. Inman, and Gyuhae Park. Comparison of piezo-electric energy harvesting devices for recharging batteries. *Journal of Intelligent Material Systems and Structures*, 16(10):799–807, 2005.

[60] HeungSoo Kim, Joo-Hyong Kim, and Jaehwan Kim. A review of piezoelectric energy harvesting based on vibration. *International Journal of Precision Engineering and Manufacturing*, 12(6):1129–1141, 2011.

[61] S H Chae, S Ju, Y Choi, S Jun, S M Park, S Lee, H W Lee, and C-H Ji. Electromagnetic vibration energy harvester using springless proof mass and ferrofluid as a lubricant. *Journal of Physics: Conference Series*, 476(1):012013, 2013.

[62] S. Boisseau, G. Despesse, and B. Ahmed Seddik. Electrostatic conversion for vibration energy harvesting.

[63] Elie Lefeuvre, Adrien Badel, Claude Richard, Lionel Petit, and D Guyomar. A comparison between several vibration-powered piezoelectric generators for standalone systems. *Sensors and Actuators*, 126(2):405–416, 2006.

[64] Maria Gorlatova, John Sarik, Guy Grebla, Mina Cong, Ioannis Kymissis, and Gil Zussman. Movers and shakers: Kinetic energy harvesting for the internet of things. *ACM SIGMETRICS Performance Evaluation Review*, 42(1):407–419, June 2014.

[65] Subir Biswas and Muhannad Quwaider. Modeling energy harvesting sensors using accelerometer in body sensor networks. In *8th International Conference on Body Area Networks (BODYNETS)*, October 2013.

[66] Jaeseok Yun, Shwetak Patel, Matt Reynolds, and Gregory Abowd. A quantitative investigation of inertial power harvesting for human-powered devices. In *Proceedings of the 10th International Conference on Ubiquitous Computing*, UbiComp '08, Seoul, Korea, 21-24 September 2008.

[67] S. Boisseau, B G. Despesse, and Ahmed Seddik. Electrostatic conversion for vibration energy harvesting. 2012.

[68] Mahbub Hassan. A performance model of pedestrian dead reckoning with activity-based location updates. In *IEEE International Conference on Networks (ICON)*, Singapore, 12-14 December, 2012.

[69] Du Tran and Alexander Sorokin. Human activity recognition with metric learning. In *Computer Vision–ECCV 2008*, pages 548–561. Springer, 2008.

[70] Kui Jia and Dit-Yan Yeung. Human action recognition using local spatio-temporal discriminant embedding. In *IEEE Conference on Computer Vision and Pattern Recognition (CVPR)*, Anchorage, Alaska, USA, 23-28 June, 2008.

[71] Sara Khalifa. Inertial Kinetic Energy Harvesting Model. http://www.mathworks.com/matlabcentral/fileexchange/53585-inertial-kinetic-energy-harvesting-model.

[72] Xiubo Geng, Tie-Yan Liu, Tao Qin, and Hang Li. Feature selection for ranking. In *Proceedings of the 30th annual international ACM SIGIR conference on Research and development in information retrieval*, Amsterdam, The Netherlands, 23-27 July 2007.

[73] ADS7042. `http://www.ti.com/lit/ds/symlink/ads7042.pdf`. Accessed: 2015-04-20.

[74] Zhaohui Zheng. Feature selection for text categorization on imbalanced data. *ACM SIGKDD Explorations Newsletter*, 6(1):80–89, 2004.

[75] T. Mitchell. *Machine Learning*. McGraw-Hill, New York, 1997.

[76] Mark A. Hall. *Correlation-based feature selection for machine learning*. PhD thesis, Department of Computer Science, University of Waikato, Hamilton, New Zealand, 1998.

[77] J. Parkka, M. Ermes, P. Korpipaa, J. Mantyjarvi, J. Peltola, and I. Korhonen. Activity classification using realistic data from wearable sensors. *Information Technology in Biomedicine, IEEE Transactions on*, 10(1):119–128, 2006.

[78] J. Ross Quinlan. *C4.5: programs for machine learning.* Morgan Kaufmann Publishers Inc, San Francisco, CA, USA, 1993.

[79] Yishay Mansour. Pessimistic decision tree pruning based on tree size. In *Proceedings of the Fourteenth International Conference on Machine Learning.* Morgan Kaufmann, 1997.

[80] David W. Aha, Dennis Kibler, and Marc K. Albert. Instance-based learning algorithms. *Machine Learning*, 6(1):37–66, 1991.

[81] S.K. Pal and S. Mitra. Multilayer perceptron, fuzzy sets, and classification. *IEEE Transactions on Neural Networks*, 3(5):683 –697, 1992.

[82] Lutz Prechelt. A quantitative study of experimental evaluations of neural network learning algorithms: Current research practice. *Neural Networks*, 9(3):457 – 462, 1996.

[83] Mevlut Ture, Imran Kurt, A. Turhan Kurum, and Kazim Ozdamar. Comparing classification techniques for predicting essential hypertension. *Expert Systems with Applications*, 29(3):583 – 588, 2005.

[84] George John and Pat Langley. Estimating continuous distributions in bayesian classifiers. In *Proceedings of the Eleventh Conference on Uncertainty in Artificial Intelligence.* Morgan Kaufmann, 1995.

[85] Satyen Kale, Ravi Kumar, and Sergei Vassilvitskii. Cross-validation and mean-square stability. In *Proceedings of the 25th International Conference on Supercomputing*, Loews Ventana Canyon Resort, Tucson, Arizona, 31 May - 4 June 2011.

[86] Marco Altini, Julien Penders, Ruud Vullers, and Oliver Amft. Estimating energy expenditure using body-worn accelerometers: a comparison of methods, sensors number and positioning. *Biomedical and Health Informatics, IEEE Journal of*, 19(1):219–226, 2015.

[87] Jonathan Lester, Carl Hartung, Laura Pina, Ryan Libby, Gaetano Borriello, and Glen Duncan. Validated caloric expenditure estimation using a single body-worn sensor. In *Proc. of ACM UbiComp*, pages 225–234, 2009.

[88] Fahd Albinali, Stephen Intille, William Haskell, and Mary Rosenberger. Using wearable activity type detection to improve physical activity energy expenditure estimation. In *Proc. of ACM UbiComp*, pages 311–320, 2010.

[89] Sara Khalifa, Mahbub Hassan, and Aruna Seneviratne. Pervasive self-powered human activity recognition without the accelerometer. In *Proc. of IEEE PerCom*, 2015.

[90] James O Berger. *Statistical decision theory and Bayesian analysis.* Springer Science & Business Media, 2013.

[91] Andreas Krause, Matthias Ihmig, Edward Rankin, Derek Leong, Smriti Gupta, Daniel Siewiorek, Asim Smailagic, Michael Deisher, and Uttam Sengupta. Trading off prediction accuracy and power consumption for context-aware wearable computing. In *Proc. of IEEE ISWC*, pages 20–26, 2005.

[92] Zhixian Yan, Vigneshwaran Subbaraju, Dipanjan Chakraborty, Archan Misra, and Karl Aberer. Energy-efficient continuous activity recognition on mobile phones: An activity-adaptive approach. In *Proc. of IEEE ISWC*, pages 17–24, 2012.

[93] Luca Palmerini, Laura Rocchi, Sabato Mellone, Franco Valzania, and Lorenzo Chiari. Feature selection for accelerometer-based posture analysis in parkinson's disease. *Information Technology in Biomedicine, IEEE Transactions on*, 15(3):481–490, 2011.

[94] Hassan Ghasemzadeh, Navid Amini, Ramyar Saeedi, and Majid Sarrafzadeh. Power-aware computing in wearable sensor networks: An optimal feature selection. *Mobile Computing, IEEE Transactions on*, 14(4):800–812, 2015.

[95] Sara Khalifa, Mahbub Hassan, Aruna Seneviratne, and Sajal K. Das. Energy harvesting wearables for activity-aware services. *Internet Computing, IEEE*, 20(5):2–10, 2015.

[96] Theodore S Rappaport et al. *Wireless communications: principles and practice*, volume 2. 1996.

[97] William Tranter, K Shanmugan, Theodore Rappaport, and Kurt Kosbar. *Principles of communication systems simulation with wireless applications*. Prentice Hall Press, 2003.

[98] Jiuqiang Xu, Wei Liu, Fenggao Lang, Yuanyuan Zhang, and Chenglong Wang. Distance measurement model based on rssi in wsn. *Wireless Sensor Network*, 2(08):606, 2010.

[99] G. M. Weiss and J. W. Lockhart. The impact of personalization on smartphone-based activity recognition. In *Proc. Activity Context Representation: Techniques and Languages Workshop (AAAI-2012)*, 2012.

[100] J. Juen, Qian Cheng, and B. Schatz. A natural walking monitor for pulmonary patients using mobile phones. *Biomedical and Health Informatics, IEEE Journal of*, 19(4):1399–1405, 2015.

[101] Nicole A Capela, Edward D Lemaire, and Natalie Baddour3. Novel algorithm for a smartphone-based 6-minute walk test application: algorithm, application development, and evaluation. *JOURNAL OF NEUROENGINEERING AND REHABILITATION*, 19(4):1399–1405, 2015.

[102] D. Gusenbauer, C. Isert, and J. Krösche. Self-contained indoor positioning on off-the-shelf mobile devices. In *International Conference on Indoor Positioning and Indoor Navigation (IPIN10)*, Zürich, Switzerland, 15-17 Septemper, 2010.

[103] Wonho Kang, Seongho Nam, Youngnam Han, and Sookjin Lee. Improved heading estimation for smartphone-based indoor positioning systems. In *2012 IEEE 23rd International Symposium on Personal Indoor and Mobile Radio Communications (PIMRC)*, September 2012.

[104] A.R. Pratama, Widyawan, and R. Hidayat. Smartphone-based pedestrian dead reckoning as an indoor positioning system. In *System Engineering and Technology (ICSET), 2012 International Conference on*, September 2012.

[105] Fan Li, Chunshui Zhao, Guanzhong Ding, Jian Gong, Chenxing Liu, and Feng Zhao. A reliable and accurate indoor localization method using phone inertial sensors. In *Proceedings of the 2012 ACM Conference on Ubiquitous Computing*, UbiComp '12, 2012.

[106] D. Pai, M. Malpani, I. Sasi, N. Aggarwal, and P.S. Mantripragada. Padati: A robust pedestrian dead reckoning system on smartphones. In *Trust, Security and Privacy in Computing and Communications (TrustCom), 2012 IEEE 11th International Conference on*, June 2012.

[107] S. Ayub, X. Zhou, S. Honary, A. Bahraminasab, and B. Honary. Indoor pedestrian displacement estimation using smart phone inertial sensors. *Int. J. Innovative Computing and Applications*, 4(1):35–42, 2012.

[108] A.R. Pratama, Widyawan, and R. Hidayat. Smartphone-based pedestrian dead reckoning as an indoor positioning system. In *International Conference on System Engineering and Technology (ICSET)*, Bandung, 11-12 Sept. 2012.

[109] Fan Li, Chunshui Zhao, Guanzhong Ding, Jian Gong, Chenxing Liu, and Feng Zhao. A reliable and accurate indoor localization method using phone inertial sensors. In *UbiComp 12*, Pittsburgh, USA, 5-8 Sept. 2012.

[110] Khaled Alanezi and Shivakant Mishra. Impact of smartphone position on sensor values and context discovery. Technical report, Department of Computer Science, University of Colorado Boulder, 2013.

[111] M.S Lee, S.H. Shin, and C.G. Park. Evaluation of a pedestrian walking status awareness algorithm for a pedestrian dead reckoning. In *Proceedings of the 23rd International Technical Meeting of the Satellite Division of the Institute of Navigation*, Portland, OR, 21-24 September 2010.

[112] S. H. Shin, M. S. Lee, C. G. Park, and Hyun Su Hong. Pedestrian dead reckoning system with phone location awareness algorithm. In *IEEE/ION Position Location and Navigation Symposium (PLANS)*, Indian Wells, CA, US, 4-6 May 2010.

[113] Sara Khalifa, Mahbub Hassan, and Aruna Seneviratne. Pervasive self-powered human activity recognition without the accelerometer. In *Proceedings of the International Conference on Pervasive Computing and Communication (PerCom)*, St. Louis, Missouri, USA, 23-27 March 2015.

[114] Sara Khalifa, Mahbub Hassan, Aruna Seneviratne, and Sajal K. Das. Energy harvesting wearables for activity-aware services. *IEEE Internet Computing*, 19(5):8–16, September/October 2015.

[115] Guohao Lan, Sara Khalifa, Mahbub Hassa, and Wen Hu. Estimating calorie expenditure from output voltage of piezoelectric energy harvester - an experimental feasibility study. In *Proceedings of the 10th EAI International Conference on Body Area Networks (BodyNets)*, Sydney, Australia, 2830 September 2015.

[116] S P Beeby, R N Torah, M J Tudor, P Glynne-Jones, T O'Donnell, C R Saha, and S Roy. A micro electromagnetic generator for vibration energy harvesting. *Journal of Micromechanics and Microengineering*, 17(7), 2007.

[117] R Torah, P Glynne-Jones, M Tudor, T O'Donnell, S Roy, and S Beeby. Self-powered autonomous wireless sensor node using vibration energy harvesting. *Measurement Science and Technology*, 19(12), 2008.

[118] P.D. Mitcheson, E.M. Yeatman, G.K. Rao, A.S. Holmes, and T.C. Green. Energy harvesting from human and machine motion for wireless electronic devices. *Proceedings of the IEEE*, 96(9):1457–1486, 2008.

[119] K Ylli, D Hoffmann, A Willmann, P Becker, B Folkmer, and Y Manoli. Energy harvesting from human motion: exploiting swing and shock excitations. *Smart Materials and Structures*, 24(2):025029, 2015.

[120] Apple siri. https://www.apple.com/ios/siri/. Accessed on 15 September, 2015.

[121] Google now. http://www.google.com/landing/now. Accessed on 15 September, 2015.

[122] Yu Zhong, T. V. Raman, Casey Burkhardt, Fadi Biadsy, and Jeffrey P. Bigham. Justspeak: Enabling universal voice control on android. In *Proceedings of the 11th Web for All Conference*, W4A '14, 2014.

[123] Nishkam Ravi, Nikhil Dandekar, Preetham Mysore, and Michael L.l Littman. Activity recognition from accelerometer data. In *Proceedings of the 17th conference on Innovative applications of artificial intelligence*, Pittsburgh, Pennsylvania, 9-13 July 2005.

[124] Jennifer R. Kwapisz, Gary M. Weiss, and Samuel A. Moore. Activity recognition using cell phone accelerometers. *ACM SIGKDD Explorations Newsletter*, 12(2):74–82, 2010.

[125] Akram Bayat, Marc Pomplun, and Duc A. Tran. A study on human activity recognition using accelerometer data from smartphones. *Procedia Computer Science*, 34:450 – 457, 2014.

[126] A. Matic, V. Osmani, and O. Mayora. Speech activity detection using accelerometer. In *Annual International Conference of the IEEE Engineering in Medicine and Biology Society (EMBC)*, 2012.

Appendix A

Acronyms